THE EFFECTS OF CREEP AND FATIGUE ON DAMAGE ACCUMULATION IN LIGAMENT

by

TIMOTHY DAVID SCHWAB

B.A.Sc., The University of British Columbia, 2003

A THESIS SUBMITTED IN PARTIAL FULFIMENT OF
THE REQUIREMENTS FOR THE DEGREE OF

MASTER OF APPLIED SCIENCE

in

THE FACULTY OF GRADUATE STUDIES

(Mechanical Engineering)

THE UNIVERSITY OF BRITISH COLUMBIA

January 2006

ABSTRACT

Ligaments are collagenous tissues that passively resist tensile forces to maintain joint stability and guide joint motion. When ligaments are damaged or are healing from an injury, they have increased laxity. Increased ligament laxity may cause increased joint laxity, which could lead to other musculo-skeletal complications. As damage is thought to influence ligament laxity, it is important to understand damage mechanisms and accumulation in ligament.

Ligaments can be damaged during loading and *in vivo* loads can be either constant (creep) or cyclic (fatigue); therefore, the effects of creep and fatigue on damage accumulation were investigated in ligament. Medial collateral ligaments were subject to *in vitro*, uniaxial creep or fatigue tensile loading. Testing was completed at three maximum stresses: 60%, 30% and 15% of the ultimate tensile strength. Some ligaments were loaded until rupture, and some did not rupture during loading. Behaviour of ligaments subjected to creep was compared to those subjected to fatigue at each stress level. Ligament behaviour was quantified with times-to-rupture, strain profiles, and stress-strain characteristics. Damage was confirmed with a stretch to failure for those ligaments that did not rupture in creep or fatigue.

Fatigue loading was more damaging than creep loading. Fatigue ligaments failed sooner than creep ligaments and the strain profiles differed between the two loading profiles. On a normalized time scale, creep ligaments experienced higher strains than fatigue ligaments. When time of loading was accounted for, fatigue ligaments failed sooner, which resulted in greater strains in fatigue than creep at specific time-points. Both creep and fatigue loading resulted in changes in stress-strain characteristics. Tangent modulus was used to track damage and inputted into a continuum damage mechanics model to predict time-to-rupture of creep and fatigue.

Results indicate that fatigue loading likely involves an additional damage mechanism not present in creep loading. In essence, fatigue loading involves both cycle-dependent and time-dependent damage, while creep loading only involves time-dependent damage. Therefore, loading condition (static versus cyclic) was found to affect damage accumulation in ligament. Information from this study furthers the current understanding of ligament damage accumulation.

TABLE OF CONTENTS

LIST OF TABLES

LIST OF FIGURES

GLOSSARY

Chord modulus: Change in stress per cycle divided by the change in strain per cycle

Cycle-dependent damage: Damage associated with the loading ramp

Effective stress: Force divided by the effective cross-sectional area (that contributing to load-bearing)

Failure Strain: Strain corresponding to either the ultimate tensile strength or residual strength during a single stretch to failure

Increase in strain: Strain accumulated in addition to the initial strain

Initial tangent modulus: Tangent modulus of the first loading ramp to the test stress

Initial strain: Strain resulting from the first loading ramp to the test stress

Linear-region: Region of the stress-strain curve with constant tangent modulus

Maximum tangent modulus: Largest tangent modulus recorded for each specimen during creep or fatigue loading

Modulus ratio: The ratio of tangent modulus at any time-point to the maximum tangent modulus

Nominal stress: Force divided by the fully intact (initial) cross-sectional area

Residual Strength: Maximum stress supported by each ligament during a single stretch to failure following a period of creep or fatigue loading

Strain-at-rupture: Strain recorded at the last time the ligament supported 99% of the test stress

Strain to 5 MPa: Strain at 5 MPa for each cycle minus the valley strain for the corresponding cycle

Steady state strain rate: The strain rate during secondary strain evaluated with the slope of a linear regression of the strain data

Tangent modulus: Slope of a linear regression fit to the upper 50% of the stress strain curve

Time-dependent damage: Damage associated with time at high load

Time-to-rupture: Total duration of creep or fatigue loading before ligament rupture

Toe-region: Region of the stress-strain curve with increasing tangent modulus

Ultimate tensile strength: Maximum stress supported by each ligament during a single stretch to failure

Valley strain: Minimum strain in each cycle

ACKNOWLEDGEMENTS

I would like to thank my supervisors Dr. Oxland and Dr. Thornton for their support and guidance. This work would not have been possible without their mentorship. Dr. Oxland provided valuable insight when critical decisions had to be made. Dr. Thornton was a constant resource and provided a wealth of insight into ligament behaviour and testing.

Many thanks to my family and Janis. I would not have been able to accomplish this (and many other things) without their support.

I would also like to thank the staff and students at the Division of Orthopaedic Engineering for their help and friendship. Thank you to NSERC, who provided funding for this project.

1.0 INTRODUCTION

Motivation for this work originates from the continued investigation into the properties of normal and healing ligaments (1,19,20,53,59-63). One major question remains to be answered: Why are healed ligaments more lax (stretched out) than normal ligaments? Ligament laxity may be affected by the interactions of damage and repair. However, a healing ligament is a very complex structure with aspects of normal ligament as well as some additional complications associated with scar tissue (53,63). An understanding of the interaction of damage and repair in normal ligament is required before the interaction of these mechanisms is understood in healing ligament. Both damage and repair are complicated issues and it is beneficial to first investigate them independently before studying their interactions. Damage in normal ligament is examined with mechanical evidence of damage to provide baseline knowledge for a much larger investigation of damage and repair. An understanding of ligament structure, function and mechanics is required to investigate ligament damage.

1.1 Ligament Structure, Function and Mechanics

Ligaments are discrete bands of connective tissue that connect articulating bones to one another, guide joint motion, maintain joint stability and resist tensile distraction (21,33). Some ligaments are thought to provide proprioception (4,33,55). Ligaments are composed of four main components that are arranged in a hierarchical fashion: collagen, proteoglycans, elastin and water (27).

Collagen molecules are the main load-bearing component in ligaments (44,68) and make up 70 to 80% of the dry weight of the tissue (21). They are predominantly type 1 collagen (21) and are about 340 nm in length. Collagen molecules connect to each other through crosslinks to form a helical chain (55). Groups of three crosslinked chains combine to make tropocollagen molecules, which in turn aggregate to form fibrils. Fibrils combine to create fibres, which then group together to form fascicles. Fascicles bundle together to create a ligament. It is unknown what length fibres are. It is suspected that they are continuous from origin to insertion (44,55), but it is

possible that some fibres are not continuous throughout the ligament. Discontinuous fibres are more prevalent in developing and healing ligaments (44).

Ligament fibres are predominantly aligned with the longitudinal (loading) axis of the ligament and are crimped in an unstressed state (33). Crimp is the 'waviness' or undulations associated with fibres (15,47). As ligaments are loaded, fibres straighten out. Some fibres straighten (become recruited into load bearing) before others. This is thought to contribute to the non-linearity of the ligament stress-strain response (28). In addition, fibre recruitment is affected by loading duration. A ligament subjected to a constant load over a long time period will recruit more fibres than one subjected to the same load for a shorter time (62). Whole ligament distribution of crimp is dependent on joint angle when a ligament is unstressed (62). For rabbit medial collateral ligament, crimp is evenly distributed across the ligament substance at 70° of flexion. Greater flexion causes reduced crimp (straightening of fibres) in the anterior of the ligament, while less flexion (extension) causes reduced crimp in the posterior of the ligament.

Fibres have potential to interact with each other by transmitting loads through the ground substance (composed mainly of proteoglycans) (68). Theoretically, a straightening fibre has potential to partially recruit surrounding fibres into load bearing by transmitting load through the proteoglycans. Load transmission results from shear forces induced in the ground substance (45,46,64), but the magnitude of load carried by the ground substance is likely much less than that carried by the fibres (as indicated by their relative moduli: 10^{-5} MPa versus 0.4 to 2 GPa, respectively (44)). Elastin is thought to help fibres return to their natural length when unloaded (21,68).

Water accounts for approximately two-thirds of the wet weight of a ligament (21). Viscoelastic properties of ligament are affected by water content through its interactions with proteoglycans (21,68) and perhaps tropocollagen molecules (55), influencing the time-dependent behaviour of fibre recruitment (62). In addition, it facilitates fascicle sliding and transports nutrients and wastes to and from fibroblasts (21).

Fibroblasts are the main type of cell within ligaments. With minimal internal vasculature (33), cells obtain nutrients from water within the ligament. Cells are linked together by cytoplasmic processes, which may assist in proprioception (33). Some evidence exists suggesting that

fibroblasts may be intimately attached to collagen fibres (29). If this is the case, then cell movement during loading could be used to indicate fibre alignment and stretching (50).

Ligament microstructure affects its mechanical behaviour (Figure 1). A typical stress-strain curve for a ligament is composed of two major regions: the toe- and linear-region. The toe-region, occurring at low stresses and strains, is characterized by an increasing tangent modulus (the slope of the stress-strain curve). The profile of the toe-region is likely affected by fibre crimp (50,62), fibre recruitment (50,62), fibre alignment (50), and axial fascicle rotation (50).

In rabbit MCL, the linear-region begins around 15% of the ultimate tensile strength and 5% strain when stretched at 20mm/min. The transition from toe-region to linear-region may vary depending on the loading rate and the ligament examined (24). Within the linear-region, the tangent modulus is fairly constant until rupture. Sources of stretching in the linear-region may be fibre or molecule stretching (50), fibre sliding (50) and perhaps lesser amounts of fibre recruitment (62).

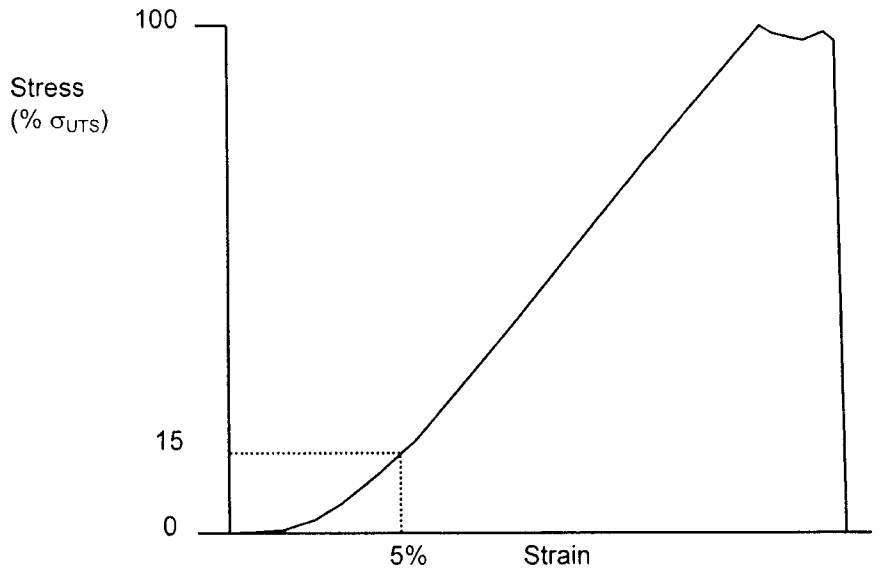

***Figure 1**: Schematic representation of a rabbit MCL stress-strain curve. The curve consists of two regions: a toe-region with increasing tangent modulus and a linear-region with constant tangent modulus. When stretched at 20 mm/min, the transition from toe- to linear-region occurs around 15% UTS and 5% strain.*

1.2 Knee Ligaments

Knee ligaments are often used to examine ligament behaviour because they have clear functional roles, they are easily accessible, and they have clinical relevance. There are four main knee ligaments: the anterior cruciate ligament (ACL), the posterior cruciate ligament (PCL), the medial collateral ligament (MCL) and the lateral collateral ligament (LCL). Figure 2 is a schematic diagram of the knee ligaments.

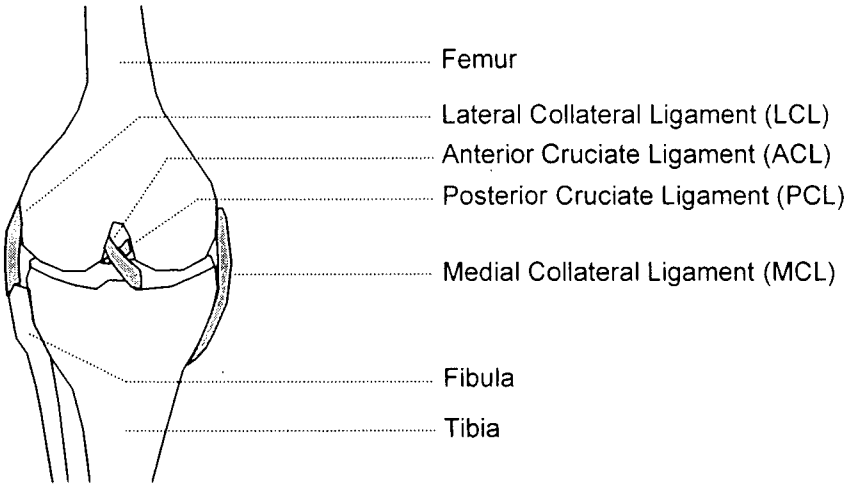

***Figure 2**: Schematic diagram of the knee ligaments showing the ACL, PCL, MCL, and LCL. The cruciate ligaments are both intra-articular, and the collateral ligaments are extra-articular. The schematic depicts a right knee.*

The cruciate ligaments are found within the joint (intra-articular) (33), while the collateral ligaments are found outside the joint capsule (extra-articular). The ACL originates from the posterior medial surface of the lateral femoral condyle and inserts to the anterior tibial plateau (33). The origin of the PCL is on the lateral face of the medial femoral condyle and its insertion is posterior and inferior to the tibial plateau.

The medial collateral ligament originates from the medial surface of the medial femoral condyle and inserts in the medial surface of the tibia inferior to the tibial plateau (21). The lateral collateral ligament originates at the lateral surface of the lateral femoral condyle and inserts on the lateral head of the fibula (21).

Knee ligaments have specific roles for maintaining knee stability by passively resisting certain forces and moments. All knee ligaments have both primary and secondary roles. Table 1 shows these primary and secondary roles.

***Table 1**: Primary and secondary roles of the knee ligaments (21).*

Ligament	Primary Role(s)	Secondary Role(s)
Medial Collateral Ligament	• Resist valgus bending • Resist external of rotation tibia	• Resist anterior translation of tibia
Anterior Cruciate Ligament	• Resist anterior translation of tibia	• Resist internal rotation of tibia
Posterior Cruciate Ligament	• Resist posterior translation of tibia	• Resist external rotation of tibia
Lateral Collateral Ligament	• Resist varus bending • Resist internal rotation of tibia	• Resist anterior and posterior translation of ligament

1.3 In Vivo Ligament Loading

In vivo loading of ligaments can be either constant or cyclic. Being a viscoelastic material, ligaments stretch out (creep) when exposed to a constant force. Whether exposed to constant loads or repetitive cyclic (fatigue) loads, ligaments can only resist tensile forces. As a result, cyclic loading will also produce a creep response in a ligament. This creep response may be responsible for increased joint laxity following repetitive loading (55).

Typical *in vivo* forces in knee ligaments result from both locomotion and sedentary periods. Walking and running both produce cyclic loads on ligaments. The loading frequencies during human walking and running are between 0.5 and 3 Hz (6,58).

In vivo stresses are thought to be within the toe-region and early portion of the linear-region of the stress-strain curve, between 15 and 25% UTS (36). Two methods have been used to estimate *in vivo* stresses: direct measurement and inverse dynamics. Holden et al. (26) measured *in vivo* stresses in goat ACL during walking and trotting using a pressure transducer. They found that the ACL stresses were less than 6% UTS. Rabbit biomechanics have been analyzed using 3D

motion capture and theoretical, inverse dynamic modeling (23). The model predicted ACL forces between 46 and 52 N. This corresponds to 20-23% UTS based on a UTS of 62 MPa and assuming a CSA of 3.55 mm^2 (72). Estimates of peak human ACL loads during walking span the range between 156 N to 1000 N (51), which corresponds to 9% to 57 % of the failure load (37). *In vivo* ACL strains have been estimated between 4 and 14%, but measurements are complicated by the uneven strain distribution along the ligament length (17).

While fatigue and creep loading can cause materials to rupture at stresses below the ultimate tensile strength, it is unlikely that ligaments would rupture due to low-stress loading encountered during physiologic loading. However, at higher stresses, creep and fatigue damage accumulation may affect ligament behaviour. When complementary structures of the joint are damaged, the remaining intact ligaments will likely experience higher than normal stresses.

The incidence (per 1000) of knee ligament injuries in the general population is highest for the ACL (between 0.3 and 0.57). The second most injured knee ligament is the MCL with incidences ranging between 0.24 and 0.26 injuries per 1000 people (38). Conservative treatment of ACL injuries has been shown to increase joint laxity (2,22). This likely causes additional load on the secondary restraints (2,22). An injured ACL will result in increased anterior tibial translation. The secondary restraint opposing anterior tibial translation is the MCL; therefore, an injured ACL will result in higher stresses in the MCL. In fact, patients with a combined ACL/MCL injuries had more laxity (as measure by tibial translation) than those with an isolated ACL injury (2). A combined ACL/MCL injury was observed to negatively affect MCL healing when compared to isolated MCL injury in a canine model (74). A computational model predicted that the MCL was the primary restraint to anterior tibial translation in an ACL deficient knee (52). The model calculated a three-fold increase in force on the MCL in an ACL deficient knee when compared to a normal knee during walking. It is reasonable to assume that an injury to a primary restraint will result in increased laxity and expose the secondary restraints to higher stresses. At high stresses, ligaments may be susceptible to damage from creep and fatigue loading. It is likely that damage of the secondary restraints will, in turn, result in additional joint laxity. Anderson (2) observed increased joint laxity in patients twelve months after injury when compared to joint laxity at the time of injury. Given that creep and fatigue loading may cause damage *in vivo*, it is important to understand how these mechanisms interact and cause damage within ligaments.

1.4 Mechanics

Principles from classical engineering mechanics are relevant to the current study. An introduction to creep, fatigue and damage is provided with specific emphasis on biologic tissue.

1.4.1 Creep

Slow, continuous deformation of a material subjected to a constant stress is termed creep (16). Typically, creep behaviour can be separated into three stages: primary, secondary and tertiary creep. The three stages of creep are shown in Figure 3. Primary creep (primary strain stage) exhibits a decreasing strain rate. The strain rate approaches a steady-state and will stay relatively constant for a period of time. The stage of steady-state strain rate is termed secondary creep (secondary strain stage). Tertiary creep (tertiary strain stage) involves an increasing strain rate and ends in fracture of the material. While commonly referred to as primary creep, secondary creep and tertiary creep, these stages are referred to by the more general terms of primary strain, secondary strain and tertiary strain, in this work, so they could be applied to non-zero fatigue tests.

Creep in metals is a concern at elevated temperatures (9) while creep in viscoelastic materials, like composites (57) and plastics (9), occurs at ambient temperatures. Viscoelastic tissues, like ligament (25,60-62), tendon (34,66), cartilage (29) and bone (8,18), are susceptible to creep at physiologic temperatures.

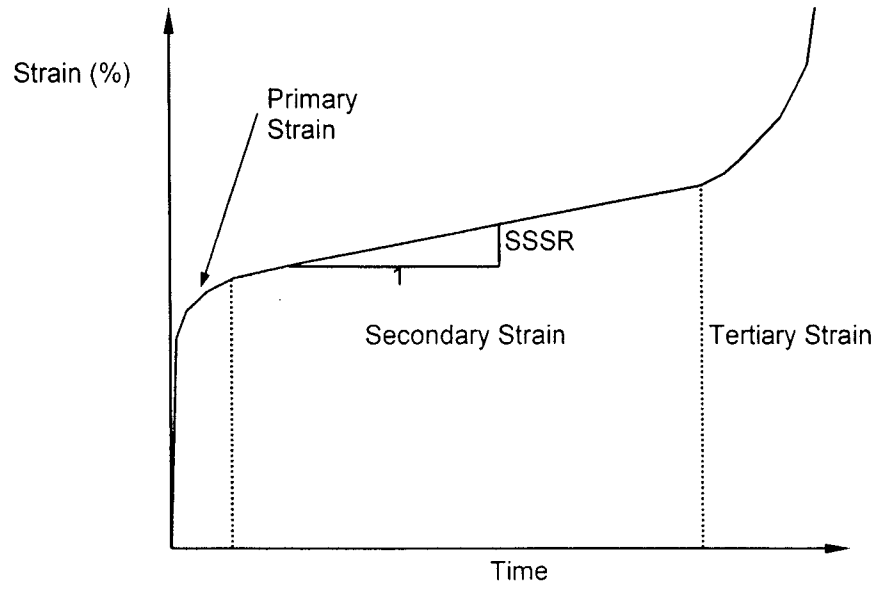

***Figure 3**: Schematic showing primary, secondary and tertiary strain. Steady-state strain rate (SSSR) is the strain rate during secondary strain.*

1.4.2 Fatigue

Fully-reversed fatigue loading creates an ideal stress profile for examining material properties. That is, applied stresses are both tensile and compressive, with a mean stress of zero. Fully-reversed loading ensures that the material behaviour is only a result of load cycling and does not involve creep mechanisms. Ligaments, as stated above, can only resist tensile loads so fully-reversed fatigue loading is not applicable. Therefore, the mean stress will be tensile and fatigue testing will also cause a creep response. Different techniques exist to quantify fatigue behaviour. A common technique involves creating fatigue life plots (9) where stress and fatigue life, usually quoted as cycles-to-failure, are plotted against each other. These plots can be used to predict times-to-failure. Fatigue failure in metals and brittle materials is thought to involve crack initiation and propagation. Fracture mechanics (crack propagation) can be used to predict catastrophic failure and, thus, lifetime of a material. While fracture models can be applied to ligaments (1), it may be more realistic to model diffuse damage in ligaments rather than crack propagation.

1.4.3 Damage

An alternate technique to analyze damage in a material is continuum damage mechanics (CDM). Continuum damage mechanics assumes that diffuse damage accumulates in a material, which reduces the effective cross-sectional area (CSA) and eventually causes failure (32). A material subjected to a nominal stress (σ_o, a stress based on the original cross-sectional area) will be damaged and the intact CSA will decrease. As the intact area decreases, the effective stress (σ_e, the stress that the intact material is subjected to) increases (32).

Different techniques can be applied to determine the damage state of a material. Lemaitre provides a comprehensive review in his book on damage mechanics (32). Damage can be related to cross-sectional area reduction through the following equation.

$$D = \left(1 - \frac{A}{A_o}\right) \tag{1}$$

where D is the damage and can vary between 0 and 1
A is the intact CSA
A_o is the initial CSA

As the equation implies, the best technique to determine damage is to directly measure the remaining area; however, this is not always practical. Other techniques have been used to quantify damage in materials. Changes in stiffness (or modulus) as an indicator of an area reduction. As intact area reduces, the stiffness will decrease as well. Changes in ultrasonic wave propagation can also be used to track damage. In some materials, micro-hardness or density changes can signify damage accumulation. Acoustic emission can also be used to show damage (5,81). Sounds created when damage occurs can be recorded to show increases in damage rate and pinpoint where damage is occurring, but can not describe the damage state of the material. Electrical resistance can also be used to track damage. Two additional techniques involve material plasticity response and tertiary creep response (32). Continuum damage mechanics has been used to study biologic tissues (notably bone (10) and tendon (66,67,75)), but has not been applied to creep and fatigue in ligaments. Continuum damage mechanics are applied to ligament in the present study.

1.5 Creep, Fatigue and Damage in Relevant Materials

To the author's knowledge, creep and fatigue interactions and influences on ligament damage have not been previously investigated. Insightful information can be found in literature on other relevant materials: bone, engineered composites and tendon. Techniques used to study bone and composites may be applied to study ligament, but proposed damage mechanisms are not directly applicable to ligament because of different microstructures. Tendon has a similar structure to ligament, so both techniques used to study tendon damage, and proposed theories describing tendon damage can be applied to ligament work. In addition, previous investigations in ligament covering any aspects of damage are also relevant. The interactions of two possible mechanisms of damage, the time at high load and the loading ramp, are of particular importance for the present study. These mechanisms of damage give rise to two terms: time-dependent damage (time at high load) and cycle-dependent damage (loading ramp).

1.5.1 Bone

Early work involving creep, fatigue and CDM in cortical bone includes that of Caler and Carter (8), who recognized the importance of studying creep and fatigue damage in biologic tissue. Bone can resist both tensile and compressive loads so they performed creep and fatigue tests (0.02 and 2 Hz) in both tension and compression. Zero-tension, zero-compression and tension-compression (with a non-zero mean tensile load) fatigue tests were completed. Creep tests yielded strain behaviour and time-to-failure. For comparison, strain behaviour, time-to-failure and cycles-to-failure were analyzed for fatigue. Power law regressions were used to relate time-to-failure and normalized stress (stress divided by the specimen's predetermined modulus). No differences were found between tensile creep and compressive creep time-to-failure. Fatigue data was also fit with power law regressions. In both zero-tension and zero-compression fatigue tests, time was a better predictor of failure than cycles. In a previous study, Carter and Caler (10) created a CDM model based on creep data, assuming a constant damage rate that varied with stress. This model was used to predict fatigue life. The model worked well when comparing tensile creep to zero-tension fatigue, but did not work well for fatigue tests involving compression. This led Caler and Carter to speculate that different damage mechanisms exist in

tension and compression and that creep (time-dependent) and fatigue (cycle-dependent) have significant interaction that affect damage accumulation. The results of Caler and Carter seem to imply that tensile damage in bone is dominated by creep mechanisms (as highlighted by their CDM model), while compressive damage is also influenced by fatigue damage mechanisms.

Other investigators have examined creep and fatigue interactions in trabecular bone (7,35). Bowman et al. (7) investigated trabecular bone behaviour when subjected to compressive creep and zero-compression fatigue. Numerous measurements were analyzed in their study including time-to-failure, cycles-to-failure, steady-state creep rate, hysteresis along the strain axis, and increase in cycle strain and strain at failure. The increase in cyclic strain magnitude can be used to approximate chord modulus changes. Chord modulus is calculated by dividing the total change in stress by the total change in strain for each loading cycle. If the stress change is constant for every cycle, then cycle strain is a fair reflection of the chord modulus. Cycles-to-failure data was related to normalized stress (stress divided by the specimen's predetermined modulus) using a power law regression. Steady-state strain rate was also related to normalized stress with a power law regression. Two relevant findings arise from the above study. First, creep strains at failure were approximately 5.2 times greater than fatigue strains at failure. This equality was used in conjunction with relations between steady-state strains and normalized stress and the relation between cycles-to-failure and normalized stress to predict "cycles-to-failure" for the creep data. Good agreement was seen between fatigue cycles-to-failure and the predicted cycles-to-failure based on creep data. Second, fatigue damage may result from a combination of creep damage and slow crack growth, implying that both creep and fatigue have different damage mechanisms that are not independent.

A recent study by the same group re-examined the interactions of creep and fatigue in trabecular bone (35). Creep relations from Bowman et al. (7) were used to predict upper and lower bounds for fatigue behaviour. A new set of fatigue data was collected. Time-to-failure and the translation of the minimum strain in each loading cycle (residual strains) were analyzed. Residual strains were greater for fatigue tests than the upper bound predicted by creep data. Time-to-failure of the fatigue tests were shorter than the lower bound predicted by creep data. This suggests that fatigue is more damaging than creep. Moore et al. (35) suggested that residual strains measured during fatigue testing resulted from diffuse damage and microcracking rather than a creep response. Moore et al. (35) also stated that creep may be significant in osteoporotic

bone where some trabecular struts have been resorbed. Clearly, the interactions of creep and fatigue in trabecular bone are difficult to quantify and they have yet to be fully understood.

Additional work investigating creep and fatigue in cortical bone has been completed. Cotton et al. (13) looked at strain characteristics of human cortical bone subjected to zero-tension fatigue. They compared steady-state strain rate of fatigue tests to published creep data (18) by integrating the previously published creep strain rate equation while accounting for a sinusoidally varying stress. Straight comparison of the two data sets revealed that the strain rate of the fatigue tests was only 5-9% of the steady-state strain rates seen in creep tests. Using the described integration of creep data, Cotton et al. showed fairly strong agreement between predicted strains and most of their experimental data. They concluded that creep mechanisms must be affecting the fatigue response, but acknowledged that other factors may be involved as well.

In a later work, Cotton et al. (12) compared different methods of predicting cycles-to-failure for zero-tension fatigue tests of cortical bone. While they did not compare creep and fatigue in this study, they did provide some insight into CDM modeling with respect to biologic tissue. They found that using normalized stress as a predictor for cycles-to-failure was not as good as using steady-state strain rate or damage rate to predict cycles-to-failure.

Zioupos and colleagues (79,80,82) have researched fatigue damage in different types of bone. One study (82) compared damage in bovine femur to that in less-mineralized deer antler. They used a continuum damage model to investigate fatigue damage accumulation in both materials. The damage model used the ratio of secant modulus at any given time to the initial elastic modulus as an indicator of damage. The model allowed for a non-constant damage rate. An interesting finding was that the damage rate for antler actually slowed down as the specimen became more damaged. This is contrary to bone behaviour where damage rate accelerated towards failure. Zioupos et al. speculate that the microstructure of antler is such that additional cracks are 'discouraged' from initiating. They also defined a damage target, which was used to indicate the damage at failure. Damage target was dependent on stress level, so they questioned the validity of defining failure as a set value of modulus reduction for all stress levels. This finding is intimately tied to the interactions of nominal and effective stress at failure (see methods section for further discussion on failure criteria). Zioupos et al. stated that they could not determine whether an endurance limit existed for bone and antler. Their methodology

provided insight into two of the intricacies associated with damage modeling: defining damage rate, and defining failure criteria.

Zioupos et al. (80) experimented with both human and bovine bone in zero-tension fatigue. They performed tests at 0.5 and 5 Hz to determine if cycles-to-failure or time-to-failure was important for tensile fatigue loading. The major finding confirmed Caler and Carter's finding that zero-tension fatigue damage is governed by time-to-failure rather than cycles-to-failure.

Results from bone studies indicate that creep and fatigue damage may result from different and not entirely separable mechanisms. Damage modeling techniques used in the above studies provide insight into difficulties and assumptions related to continuum damage mechanics and the interactions of creep and fatigue.

1.5.2 Engineering Composites

Poursartip et al. (42) studied fatigue damage accumulation in a quasi-isotropic carbon fibre composite laminate. Damage was monitored using Young's modulus. Laminate modulus reduction was directly related to matrix delamination (area reduction) by measuring intact area on C-scans. Total delamination was observed at $0.65*E/E_0$, where E was the Young's modulus at a given time and E_0 was the maximum Young's modulus during loading. The maximum modulus was chosen to account for initial specimen stiffening. Modulus ratio was linearly related to damage using the C-scans and resulted in the following equation for damage rate as a function of modulus ratio change.

$$\frac{dD}{dN} = -2.857 \cdot \left(\frac{1}{E_o} \cdot \frac{dE}{dN} \right) \tag{2}$$

where D was damage

E was the Young's modulus

E_o was the maximum Young's modulus during loading

N was the number of cycles

Poursartip et al. modeled damage to the matrix and defined failure as the time when only the 0° plies carried the load. They acknowledged that an additional damage parameter could be established to model damage accumulation in the 0° plies, but it was not required as functional failure was reached using the model above. The above model was also written in terms of applied stress range by relating the modulus ratio at failure to the maximum stress divided by the tensile strength. In other words, the modulus ratio at failure indicated an area reduction which causes an effective stress equal to the tensile strength.

A coupled viscoelastic-damage model was created for randomly reinforced swirl mat composite subjected to fatigue loading (56). Damage was measured with increase in compliance (inverse of modulus) and permanent strain. To incorporate damage into the viscoelastic model, the time-varying nature of damage was simplified by only varying damage with maximum stress, not time. This approximation was thought to be acceptable as the time-dependent nature of damage becomes important only during tertiary creep. Damage was assumed to occur at the peak stresses of each cycle. The model was used to predict strain of the composite when subjected to cyclic loading. Smith and Weitsman (57) used a similar approach to model creep viscoelastic-damage behaviour in swirl mat composites in a later study.

As with studies in bone, the above work in composites provided technical insight into damage modeling. Of particular importance was the finding of Poursartip et al. that modulus ratio was not necessarily equivalent to an area reduction. In the case of the composite tested, area reduction and modulus reduction were related linearly, but this relation is likely affected by the microstructure of the material.

1.5.3 Tendon

Creep rupture of wallaby tail tendons has been investigated using *in vitro* testing (66). Creep tests were performed at stresses ranging between 20 MPa and 80 MPa, which correspond to 14% and 55% of the yield stress. Tendon behaviour was modeled using continuum damage mechanics with tangent modulus as the damage indicator. However, tangent modulus cannot be extracted from a pure creep test; therefore, tendons were unloaded and reloaded with 2 sinusoidal

oscillations at specified strain levels. Wang and Ker (66) directly related stiffness ratio to an effective cross-sectional area reduction. They defined the damage at rupture to be equal to an area reduction resulting in an effective stress equal to the yield stress; therefore, damage at rupture is a function of the nominal stress and yield stress (yield stress was used in the same way other damage theories use UTS). Damage rate for intact material was assumed to be constant for a given stress level and approximated using the initial damage rate for a given nominal stress. During loading, the effective stress increased, and therefore, the damage rate increased as well. The initial damage rate was determined using steady-state strain rate and a relation between strain and stiffness ratio. The damage rate equation was integrated and used to predict creep time-to-failure. The agreement between experimental data and theoretical predictions showed that time-dependent damage could be modeled with CDM.

In an accompanying paper, Wang et al. (67) investigated fatigue rupture of wallaby tail tendons. Tendons were subjected to sinusoidal loading from 11.5 MPa to a maximum stress between 20 MPa and 80 MPa. Fatigue loading was completed at 1.1, 2.1, 5.3, 10 and 50 Hz. The damage model created from their creep study was applied with an oscillating stress to predict time-to-failure for fatigue tests. The prediction overestimated time-to-failure for fatigue. In addition, higher frequency fatigue tests failed sooner than lower frequency tests. Another finding that was not explicitly addressed when comparing creep and fatigue was that creep tests with the same stress as the maximum stress in fatigue tests appeared to have similar times-to-failure. This qualitative conclusion is based on visual comparison of their data (see Figures 37 and 38). Wang et al. also found a linear relation between 'extra strain' and modulus reduction. The CDM model developed with creep data was used to predict the time-to-failure of fatigue loading, but it overestimated the time-to-failure.

Schechtman and Bader (48) investigated fatigue behaviour of human extensor digitorum longus tendons using a zero-tension square-wave. Both magnitude and frequency were simultaneously varied. Stresses varied between 10% and 90% UTS and frequencies varied from 1 to 4 Hz. Low stress tests were performed at high frequencies and high stress tests were performed at low frequencies. The square wave used during testing kept the loading rate constant for all frequencies. In an ideal case, frequency would increase the number of loading cycles without affecting the time-at-high-load. Time-to-failure was fit with a log-normal relation and a simple damage model was applied. The Palmgren-Minor rule was used to model the interactions of

damage and healing. The model included assumptions that the damage and healing rates were constant. A more sophisticated model would have involved the time-dependent nature of damage and healing, as the Palmgren-Minor rule might not be fully applicable to damage modeling (79).

An additional investigation into the fatigue behaviour of human extensor digitorum longus was performed by Schechtman and Bader (49). More emphasis was given to damage accumulation and changes in material behaviour resulting from partial damage than in their previous study. Three parameters were used to indicate the damage state in the material: dynamic modulus ratio, tangent modulus ratio, and the ratio of residual strength to UTS. All three indicators could be used to track damage, but the residual strength/UTS ratio was less than the dynamic modulus (loss and storage moduli) and tangent modulus ratios. The authors speculated that the discrepancy may have resulted from different microstructural behaviour influencing UTS and modulus. They also suggested that strain would not be a reliable indicator of damage. Recently, damage in human extensor digitorum longus was modeled using linear elastic fracture mechanics (1). The data was provided by Schechtman, and Paris' law was applied to predict number of cycles-to-failure. Predictions worked well for higher stresses, but deviated from the data at low stresses (10 and 20% UTS).

Interactions of fatigue and creep were investigated in human Achilles tendon (75). Tendons were subjected to both creep and fatigue at maximum stresses between 30 and 80 MPa. The minimum stress during cyclic loading was 10 MPa. Cyclic loading resulted in increased hysteresis, extended toe-region, and decreased secant modulus. Initial strain was a better predictor of time-to-failure than nominal stress for both creep and fatigue tests. This counter-intuitive result may be explained by the large variation of specimen UTS or potential errors in cross-sectional area measurement. Creep and fatigue interaction were modeled using initial strain data and a constant damage rate, which was the inverse of time-to-failure (similar to Carter and Caler (10)). The authors concluded that both creep and fatigue have separate damage mechanisms, but fatigue and creep damage could not be delineated in cyclic loading. Fatigue loading caused rupture sooner than the time predicted using creep data.

In summary, damage in tendon is affected by loading environment, with fatigue being more damaging than creep. Fatigue damage likely includes both time- and cycle-dependent damage as

shown by time-dependent damage models that over predict time-to-rupture of fatigue loading. As with bone and composites, the techniques and models used to study damage accumulation are applicable to ligament research.

1.5.4 Ligament

Azangwe et al. (5) used acoustic emission to track damage evolution in rabbit ACLs subjected to a single stretch to failure. Knowledge from composite literature aided in the characterization of the acoustic emission signals. They determined an acoustic waveform that corresponded to fibre rupture, and found very little evidence of damage at stresses below the ultimate tensile strength. This led the authors to speculate that loading to stresses below the UTS would not result in permanent damage and no residual deformations would be recorded if the load was removed. This theory contradicts work completed by Provenzano et al. (43), Panjabi and coworkers (39-41) and Yahia et al. (77) who found that damage was present at stresses below the ultimate tensile strength.

Structural and cellular damage has been characterized in rat MCL (43). Ligaments were exposed to varying levels of strain to induce a partial failure. Structural damage was determined by the amount of permanent strain recorded after waiting a period of time equivalent to 300 times the loading duration. Cellular damage was established by staining for both live and necrotic cells and counting the pixels for each stain. Cell damage was approximated by the area of necrotic stain divided by the total stained area, and they found that cellular damage occurred at lower strains than structural damage. Structural damage was only seen after strains above 5.14%, indicating a structural damage threshold. Toe-region, tangent modulus and UTS were not affected by subfailure stretching below 5.14%. No threshold was determined for cellular damage because necrotic stain was found in controls not subjected to a partial failure. The authors speculated that structural damage may arise from fibre rupture or protease degradation of the extra-cellular matrix (resulting from cell death). They also suggested that cellular damage may be influenced by localized damage to a greater extent than the structural damage parameter.

Panjabi et al. (40) also investigated the effect of subfailure injury on ligament. Relaxation was measured before and after a stretch to 80% of the failure displacement. Control specimens showed no change in relaxation force between the first and second relaxations, however, those subjected to the subfailure stretch showed a 50% decrease in relaxation stress. An earlier work by Panjabi et al. (41) showed that a stretch to 80% failure displacement resulted in an elongated toe-region and a higher tangent stiffness, but it did not affect the deformation, load, or energy to failure. The authors speculated that the subfailure injury may have caused damage to crosslinks or individual fibres. Both studies provide further evidence that subfailure stretch can cause ligament damage. Recent work by Panjabi and Courtney (39) found that a high-speed stretch to 80% of the failure displacement resulted in decreased energy absorbed to failure, increased toe- and linear-region displacements, increased failure displacements and increased stress relaxation.

Yahia et al. (76) used scanning electron microscopy to evaluate fibre ruptures in rabbit MCL stretched to and held at 10%, 15% and 20% strain. They saw elimination of crimp and some fibre ruptures (1 to 3 μm in diameter) at 10% strain. At 15% strain, greater numbers of fibre ruptures were observed. At 20% strain, ruptured fibre bundles were observed to be knotted or coiled. They concluded that significant microruptures occur far below the ultimate load of ligament.

Recent work by Thornton et al. (62) investigated rabbit medial collateral ligaments subjected to creep. Ligaments were preconditioned with 30 cycles at 1 Hz, and then they were loaded to the creep stress and held at a constant force. Creep stresses were 4.1, 7.1, 14 and 28 MPa (about 4.2, 7.4, 14.7 and 29.4% UTS, respectively). Ligaments subjected to 4.1, 14 and 28 MPa were frozen with liquid nitrogen while still under load at two time-points: at the start of static creep or at the end of static creep (20 minutes). The authors observed that ligaments strained during both cyclic (preconditioning) and static loading. Strain accumulated during cyclic and static loading at 28 MPa was greater than at other stresses. Cyclic strain at 14 MPa was greater than that at 4.1 and 7.1 MPa. No differences were seen in static creep strain for 4.1, 7.1 and 14 MPa. At 4.1 and 7.1 MPa, no differences in either cyclic or static strain were observed. Cyclic preconditioning revealed a stiffening of ligaments reflected by an increasing tangent modulus and some discontinuities were observed at 28 MPa. Crimp decreased at all stress levels after initial loading indicating fibre recruitment. Additional fibre recruitment occurred when the load was sustained for 20 minutes. Fibre recruitment was greater at higher stresses. Those ligaments with a

discontinuity during cyclic loading had more crimped fibres than those without a discontinuity (at the same stress level), indicating potential recoil of ruptured fibres. This study showed that fibre recruitment likely affects the creep response of ligament and there is an associated insensitivity to creep stress within the toe-region. Fibre recruitment was shown to minimize the effect of damage in ligament by transferring load to surrounding fibres after a fibre rupture occurred.

As the above studies indicate, ligaments exposed to stresses above the normal physiologic range are susceptible to damage. Damage can be caused by single traumatic episodes as highlighted by the partial failure studies (39-41,43,76). Work by Thornton et al. (62) showed that damage can be caused from repetitive loading at low linear-region stresses (28 MPa). The above studies also show that damage will affect the strain response of ligaments, as characterized by permanent strain, increased toe-region strain, or decreased modulus. However, the effects of long-term cyclic or static loading on ligament damage have yet to be determined.

1.6 Objectives

Ligaments subjected to static and cyclic loads may be susceptible to damage. Accelerated damage may occur when complementary joint structures are injured because intact ligament loading may be increased above the normal physiologic level. Damage in intact ligaments may cause a further increase in laxity and create a chronically unstable joint as suggested by Panjabi et al. (41). Figure 4 is a graphical representation of this idea.

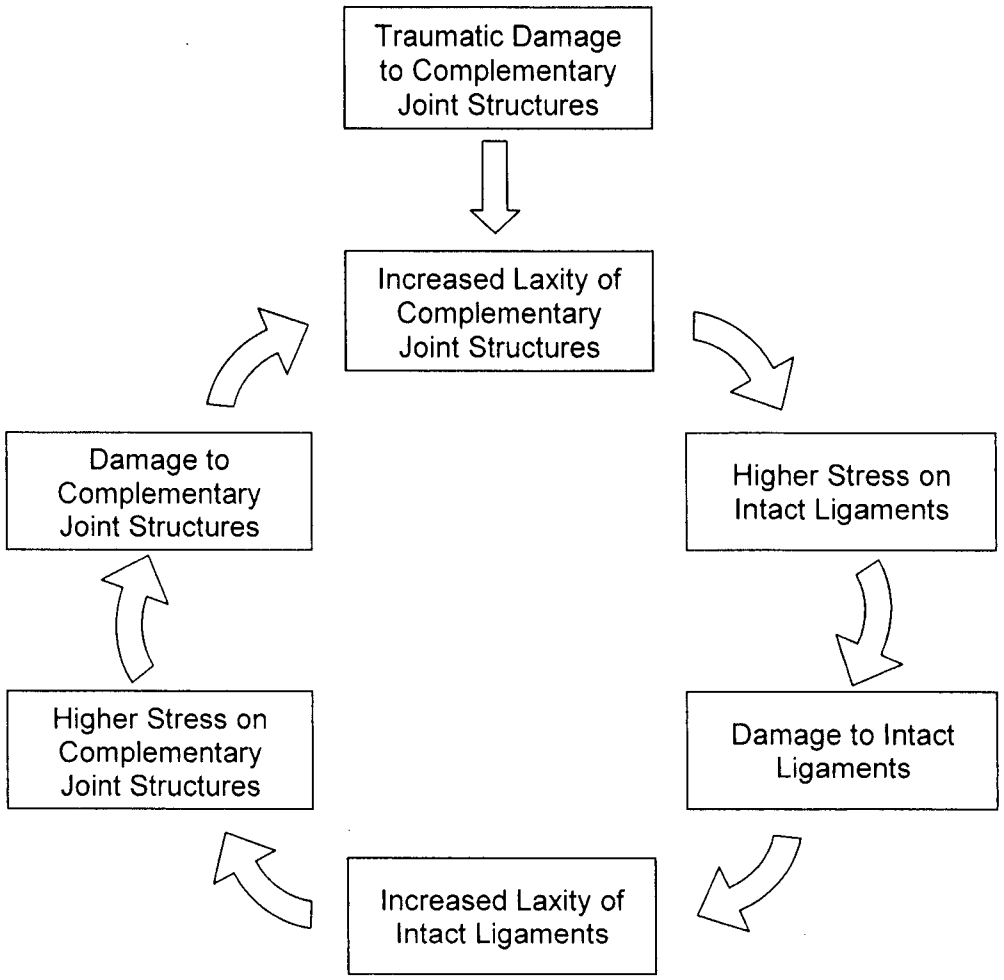

Figure 4: *Schematic showing the cycle of damage. Initial damage in a complementary joint structure may be induced by a traumatic event and followed by an increased laxity. In this state, intact ligaments may be subjected to higher than normal in vivo stresses, become damaged and have increased laxity. In turn, additional laxity may cause higher stress and additional damage in remaining complementary joint structures.*

Studying damage evolution in ligaments subjected to cyclic fatigue and static creep has clinical relevance and it is also important as a baseline for future studies with healing ligaments. Baseline knowledge provides insight into the interactions of creep and fatigue resulting from non-zero tensile fatigue loading. Fatigue may involve additional damage mechanisms that do not occur in creep. To elucidate these mechanisms, mechanical evidence is required for both loading conditions. Mechanical evidence of damage can be linked to the functional role of ligaments. If a ligament becomes damaged and, as a result, it has a different mechanical behaviour, then its

ability to perform its functional role may be compromised. With the above in mind, the major purpose of this study was to answer the following major question:

1. Does loading condition (static creep or cyclic fatigue) alter damage accumulation in rabbit medial collateral ligament as measured by changes in mechanical behaviour?

It was hypothesized that damage would influence the time-to-rupture, strain profile, stress-strain characteristics and residual strength. Time-to-rupture was the duration of ligament loading. Strain profile was the behaviour of strain as a function of time, which includes the progression through primary, secondary and tertiary strain. Stress-strain characteristics included valley strain translation, toe-region strain and linear-region tangent modulus. Residual strength was characterized by changes in ligament behaviour following a period of loading. The preceding damage measures formed the basis of specific sub-questions that were posed to help answer the first major purpose:

1a. Does creep or fatigue result in an earlier time-to-rupture?
1b. Do the strain profiles differ between creep and fatigue?
1c. Does creep or fatigue cause changes in stress-strain characteristics?
1d. Can residual strength and strain be used to confirm damage from creep and fatigue?

A secondary purpose of the study was to model the damage behaviour of creep and fatigue using continuum damage mechanics. Theoretical modeling was used to give insight into the contributions of creep and fatigue to damage. The following question was posed to address the secondary purpose.

2. Can fatigue time-to-rupture be predicted with a continuum damage model of creep behaviour?

In summary, the study consisted of two major objectives highlighted by questions 1 and 2 above. It was hypothesized that cyclic loading would be more damaging than static loading and this damage would be reflected by an earlier time-to-rupture, greater strains for a given loading duration, and earlier changes in stress-strain characteristics. Residual strength and strain were expected to mirror damage accumulated by both creep and fatigue loading. Fatigue time-to-

rupture was hypothesized to be over-predicted by the continuum damage model, indicating that fatigue has an additional damage mechanism that is not present in creep.

2.0 METHODS

This study was approved by the Animal Care Committee at the University of British Columbia. Rabbit MCL was used to investigate creep and fatigue ligament mechanics *in vitro*. The rabbit MCL model has been used by many researchers in the past (14,20,25,59,72,76) because its structure and physiologic response is similar to human (3). All rabbit hindlimbs were frozen at -20°C with all muscle intact and gauze wrapped around the knee joint. This method of storage was shown to have no effect on rabbit MCL strength, strain and energy at failure (73). Specimens came from skeletally mature (12.1 ± 0.3 months old) female Burgunder rabbits.

2.1 Specimen Preparation

All rabbit hindlimbs were prepared in the same manner. Figure 5 shows the grips and an intact knee joint after potting. Hindlimbs were dissected with a standardized technique to isolate the collateral ligaments, cruciate ligaments and the menisci. Following dissection, the tibia was potted in the top grip using dental stone (Tru-Stone, Heraeus Kulzer Inc, Armonk, NY), with the insertion of the MCL 10 mm from the edge of the mount. The top grip was mounted on a servo-hydraulic materials testing system (Dynamight, 8841, Instron, Canton, MA) that was equipped with a ±1000 N load cell (accuracy of ±0.5% of reading down to 1% full scale, temperature compensated between 15°C and 71°C). A load cell calibration certificate is provided in Appendix A. The actuator displacement was measured with a linear variable differential transformer (LVDT). The LVDT had a resolution of 0.025 mm and an accuracy of 0.25 mm. Validation of displacement measurements is provided in Appendix B. Once fixed to the actuator, the knee joint was allowed to hang at approximately 70° of flexion. A joint angle of 70° of flexion has been shown to create uniform fibre crimp throughout the MCL midsubstance (62). Load was then zeroed to account for the weight of the specimen and the femur was potted in the bottom grip using dental stone, with the origin 10 mm from the edge of the mount. Knee ligaments were kept hydrated using 0.85% saline (Oxoid, Basingstoke, UK) during potting.

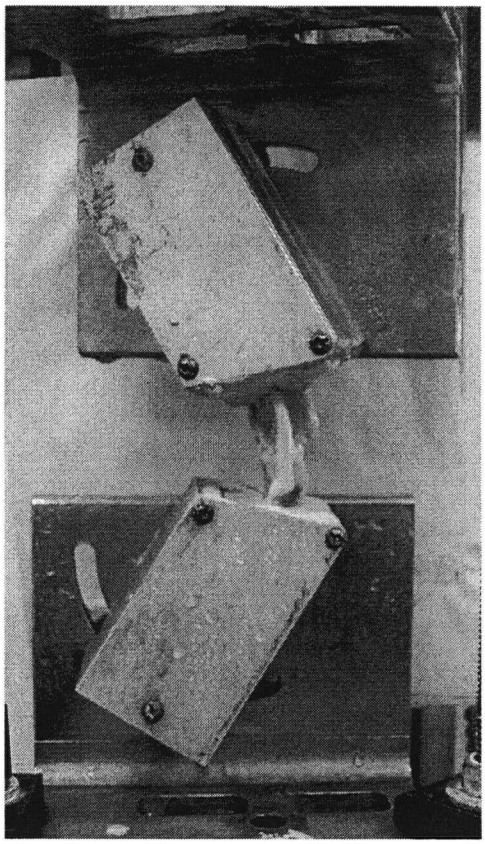

***Figure 5**: Intact knee joint mounted on the materials testing system prior to isolation of the MCL. Slight rotation of the grips about the vertical axis was required to align the MCL with the actuator.*

Two compression-tension cycles were performed from -5 N to +2 N at 1 mm/min, ending at 0 N. Historically, compression-tension cycles have been used to measure joint laxity (61). In addition, the compression-tension cycles ensured the grip system was secure and the dental stone was dry. Further dissection isolated the MCL and an additional set of compression-tension cycles were performed, ending at 1 N, to define the *ligament zero* position. Three measurements of MCL length were made using Vernier calipers (resolution of 0.05 mm). Initial ligament length was defined as the average of these three measurements. Ligament load was increased to 5 N to measure the cross-sectional area (CSA) using a dual caliper approach (25). Five newtons of force was required to open the joint space enough to insert the calipers for measurements and is comparable to previous work (53,54,59-63). Two digital calipers (resolution of 0.01 mm) were used to simultaneously measure MCL width and thickness of the midsubstance. Measurements were made three times and the averages were used to calculate the cross-sectional area, assuming a rectangular cross-section. Woo et al. (70) have shown that this is an acceptable method of determining the CSA of rabbit MCL. Following CSA measurement, ligaments were

returned to the *ligament zero* position and a custom environmental chamber was installed. Details of the environment chamber are provided in Appendix C.

The environment chamber was used to control both temperature and humidity. Temperature has been shown to affect both ligaments (31,71) and tendons (65). A test temperature of 37°C was selected because it is within the recommended temperature window (33°C to 37°C) suggested by Woo et al. (71) and it allows for comparison to earlier tests performed on the rabbit MCL (59,60,62,63). Maintaining a relative humidity of 99% has been shown to maintain the physiologic water content of rabbit ligaments (69).

After chamber conditions stabilized at 37°C and 99% relative humidity, compression-tension cycles were repeated, again ending at 1 N, to re-establish *ligament zero*. Position was recorded and load was zeroed before testing was initiated.

2.2 Experimental Groups

Forty-six MCLs were divided into three groups: single stretch to failure (n=5), fatigue (n=18) and creep (n=23). Figure 6 is a flow chart showing all test groups and subject numbers. Three stresses were investigated in fatigue and creep: a high linear-region stress (60% UTS), a low linear-region stress (30% UTS), and the toe- to linear-region transition stress (15% UTS). These stress levels are shown on a stress-strain schematic in Figure 7. Some MCLs were paired between different groups (4 pairs between 30% fatigue and 30% creep, 4 pairs between 15% fatigue and 15% creep, and 1 pair between 30% creep and 15% creep).

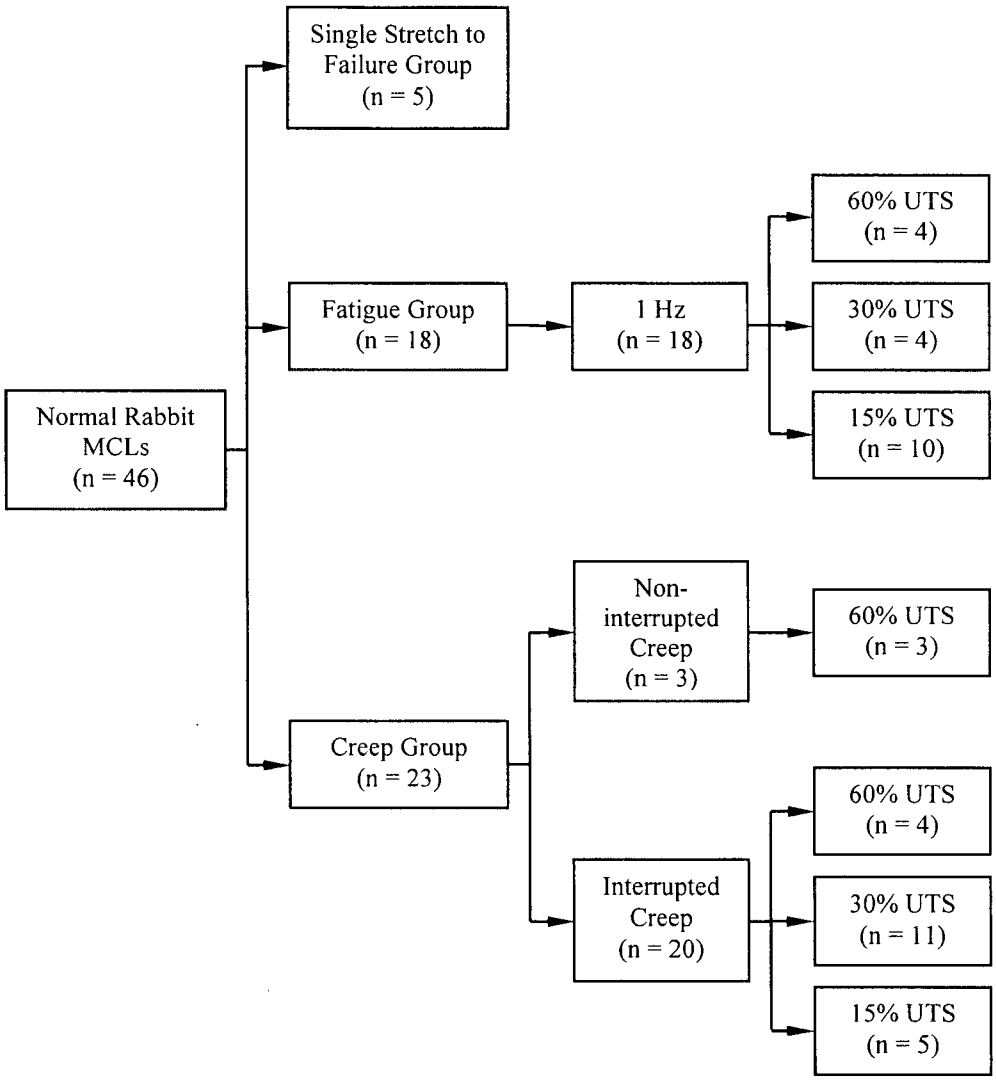

***Figure 6**: Flowchart showing test groups and the number of specimens allotted to each group.*

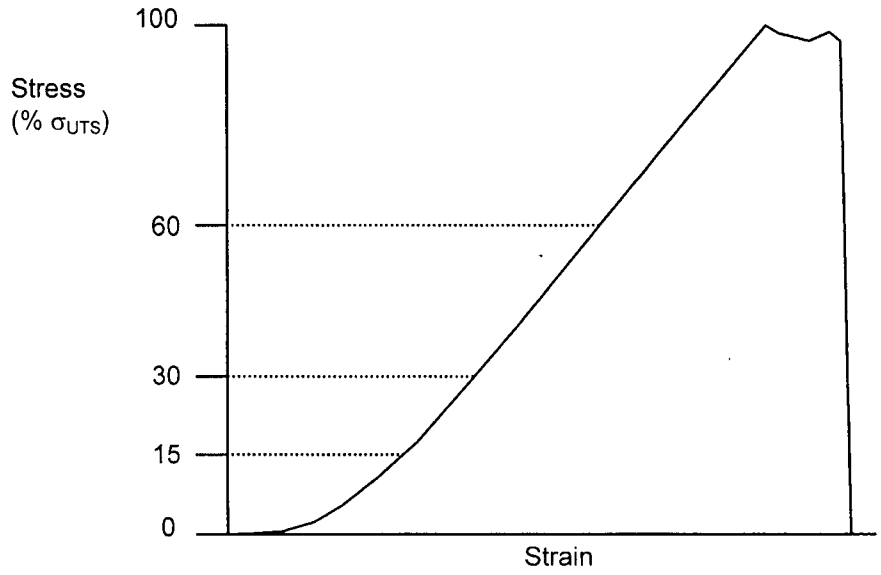

***Figure** 7: Schematic of a ligament stress-strain curve (based on a 20 mm/min elongation) highlighting the stress levels tested in creep and fatigue loading: the high linear-region stress, 60% UTS; the low linear-region stress, 30%; and the toe-to linear-region transition stress, 15% UTS.*

2.2.1 Single Stretch to Failure Group

Ultimate tensile strength (UTS) was determined to normalize stress levels for the fatigue and creep groups. The single stretch to failure protocol is shown schematically in Figure 8. Five ligaments were preconditioned with 30 cycles of 1 Hz sinusoidal loading from 1 N to a force corresponding to approximately 4.8 MPa. This stress was 5% of the expected UTS, based on data from another species of rabbit (5% of 95.4 MPa (60)). Preconditioning was performed to remove some viscoelastic variation, but was completed at a low stress to avoid any potential damage (43). Following preconditioning, ligaments were elongated to failure at 20 mm/min.

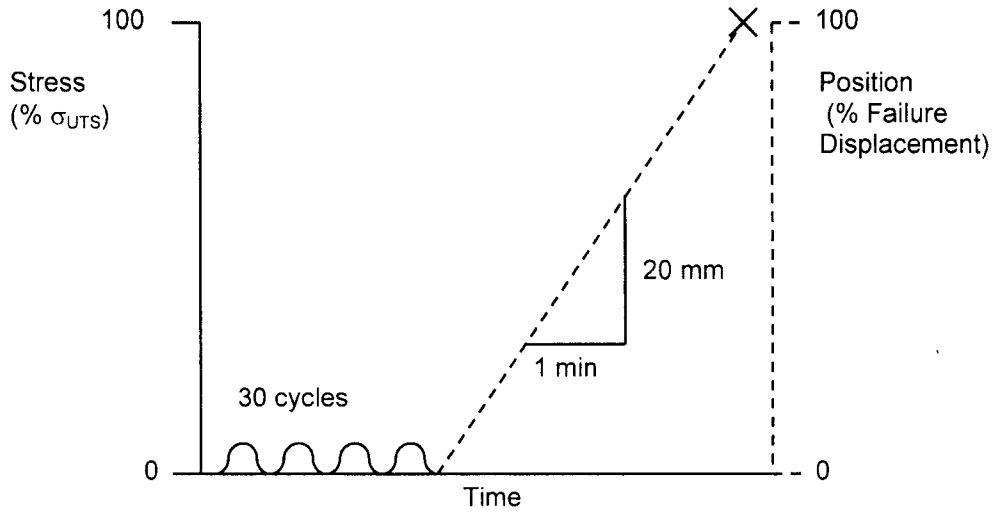

***Figure 8**: Schematic diagram showing the single stretch to failure protocol. The left ordinate, stress, applies to the preconditioning and the right ordinate, position, applies to the ramp to failure.*

2.2.2 Fatigue Group

Fatigue specimens were divided into 3 groups with maximum stresses (peak of cycle) equal to 60% UTS (n=4), 30% UTS (n=4) or 15% UTS (n=10). The fatigue protocol is shown in Figure 9. Each ligament was preconditioned with 30 cycles at 1 Hz from 1 N to 5% of the MCL UTS (4.9 MPa, determined with data from the single stretch to failure group). Following preconditioning, ligaments were cycled with sinusoidal loading at 1 Hz from 1 N to a force corresponding to the maximum stress. A minimum load of 1 N may better represent physiologic loading than a minimum of 0 N because ligaments are known to have an *in situ* force that is present in the neutral position (68). In addition, a minimum load of 1 N provided better actuator response than a minimum load of 0 N. MCLs were either cycled until a predetermined time (24, 48, or 72 hours), or until rupture. Ligaments that did not rupture during loading were subjected to an hour hold at 1 N, then to the single stretch to failure protocol to provide residual strength data (see Section 2.3.1.7). Censor-times (24, 48 and 72 hours) were selected to provide varying levels of damage caused from fatigue loading for residual strength testing.

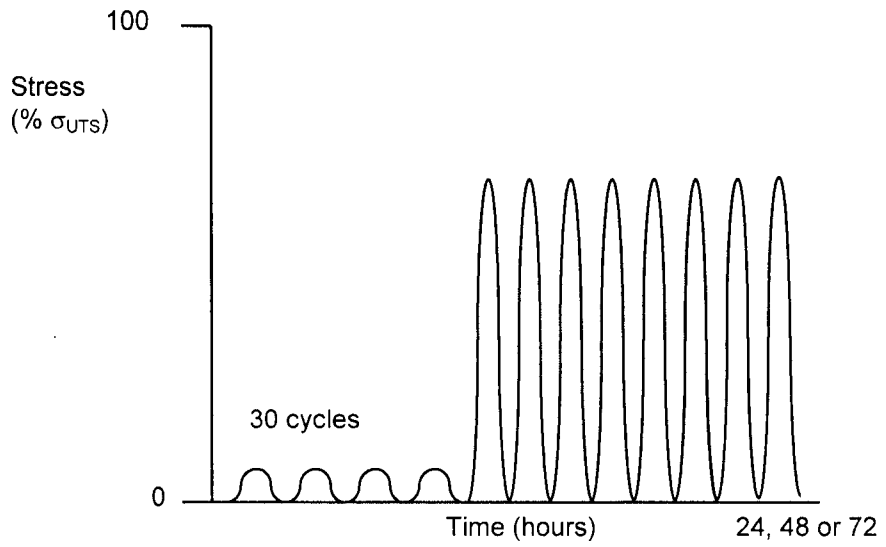

***Figure 9**: Schematic representation of fatigue protocol: 30 cycles of preconditioning followed by 24, 48 or 72 hours of 1 Hz sinusoidal loading.*

2.2.3 Creep Group

Creep specimens were similarly divided into 3 groups with different creep stresses: 60% UTS (n=7), 30% UTS (n=11) and 15% UTS (n=5). The ligaments subjected to a creep stress of 60% UTS were further divided into two groups: non-interrupted creep (n=3, Figure 10(a)) and interrupted creep (n=4, Figure 10(b)). The creep tests performed at creep stresses equal to 30% UTS and 15% UTS were all interrupted creep tests.

Non-interrupted creep ligaments were preconditioned the same as the fatigue tests, then loaded to a force corresponding to the creep stress using a half sine wave at 1 Hz. The creep stress was held constant for a predetermined time (24 hours) or until rupture. Ligaments that did not rupture during loading were subjected to one hour hold at 1 N, followed by the single stretch to failure protocol.

Interrupted creep tests were carried out in a similar fashion to the non-interrupted creep tests except they were periodically unloaded to 1 N and reloaded to the test stress using a sine wave at 1 Hz. Interruptions were performed to provide a way of determining tangent modulus throughout

the creep testing. These interruptions were completed at pre-selected times shown in Table 2. A maximum of 21 unloads occurred in the interrupted creep tests, so specific times varied depending on overall test duration.

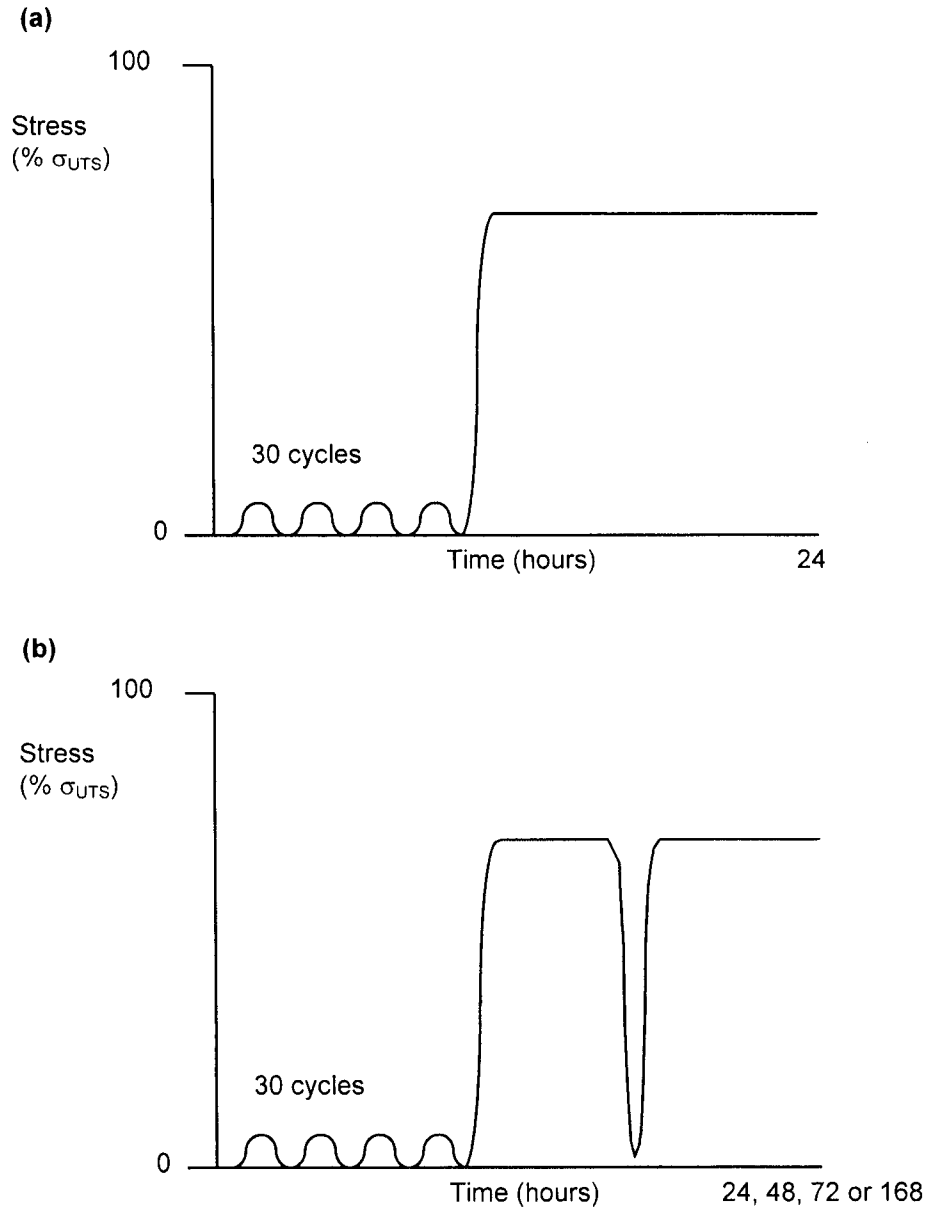

***Figure 10**: Schematic representation of creep protocols: 30 cycles of preconditioning followed by 24, 48 or 72 hours of (a) non-interrupted creep and (b) interrupted creep.*

***Table 2**: Timing of unloading/reloading for interrupted creep tests with respect to overall loading duration. Bold numbers indicate unloading/reloading times common to all test durations.*

	Time of Unloading/Reloading (hours)				
Unload Number	24 hour Test	48 hour Test	72 hour Test	120 hour Test	168 hour Test
1	**0.8**	**0.8**	**0.8**	**0.8**	**0.8**
2	1.7	**2.5**	**2.5**	**2.5**	**2.5**
3	**2.5**	**4.2**	**4.2**	**4.2**	**4.2**
4	3.3	6.7	7.9	10.4	12.9
5	**4.2**	9.2	11.7	16.7	21.7
6	5.4	11.7	15.4	22.9	30.4
7	6.7	14.2	19.2	29.2	39.2
8	7.9	16.7	22.9	35.4	47.9
9	9.2	19.2	26.7	41.7	56.7
10	10.4	21.7	30.4	47.9	65.4
11	11.7	24.2	34.2	54.2	74.2
12	12.9	26.7	37.9	60.4	82.9
13	14.2	29.2	41.7	66.7	91.7
14	15.4	31.7	45.4	72.9	100.4
15	16.7	34.2	49.2	79.2	109.2
16	17.9	36.7	52.9	85.4	117.9
17	19.2	39.2	56.7	91.7	126.7
18	20.4	41.7	60.4	97.9	135.4
19	21.7	44.2	64.2	104.2	144.2
20	22.9	46.7	67.9	110.4	152.9
21	24.0	48.0	72.0	120.0	168.0

2.3 Analysis

2.3.1 Experimental Measurements

Load and displacement data were recorded at 25 Hz. Actuator displacement was used to determine ligament strains. Data analysis was completed using custom Matlab code (The Mathworks Inc, Natick, MA), Excel spreadsheets (Microsoft Corporation, Mississauga, ONT), MathCAD (Mathsoft Engineering & Education Inc., Cambridge MA) and SAS (SAS Institute Inc, Cary, NC).

2.3.1.1 Ultimate Tensile Strength

Ligament stress was calculated by dividing the force data by the CSA measured after establishing *ligament zero*. The ultimate tensile strength was the maximum ligament stress observed during a single stretch to failure.

2.3.1.2 Time-to-Rupture and Strain-at-Rupture

Time-to-rupture was the duration of creep or fatigue loading until complete ligament rupture, starting at the beginning of the initial ramp to the test stress (after preconditioning). Rupture was defined as the last time that the ligament supported 99% of the maximum test stress (Figure 11). Time-to-rupture data was fitted with a power curve to define a relation between time-to-rupture and applied stress (as a percent UTS).

$$T_{rupture} = U \cdot \left(\frac{\sigma_o}{\sigma_{UTS}} \cdot 100 \right)^V \qquad (3)$$

where U and V are constants determined by the regression

Comparisons of times-to-rupture were made between fatigue and creep at each stress level and between non-interrupted and interrupted creep at 60% UTS. Strain-at-rupture was the strain recorded at the time of rupture (Figure 11). Comparisons of strain-at-rupture were made between all groups (60% fatigue, 30% fatigue, 15% fatigue, 60% creep, 30% creep, and 15% creep).

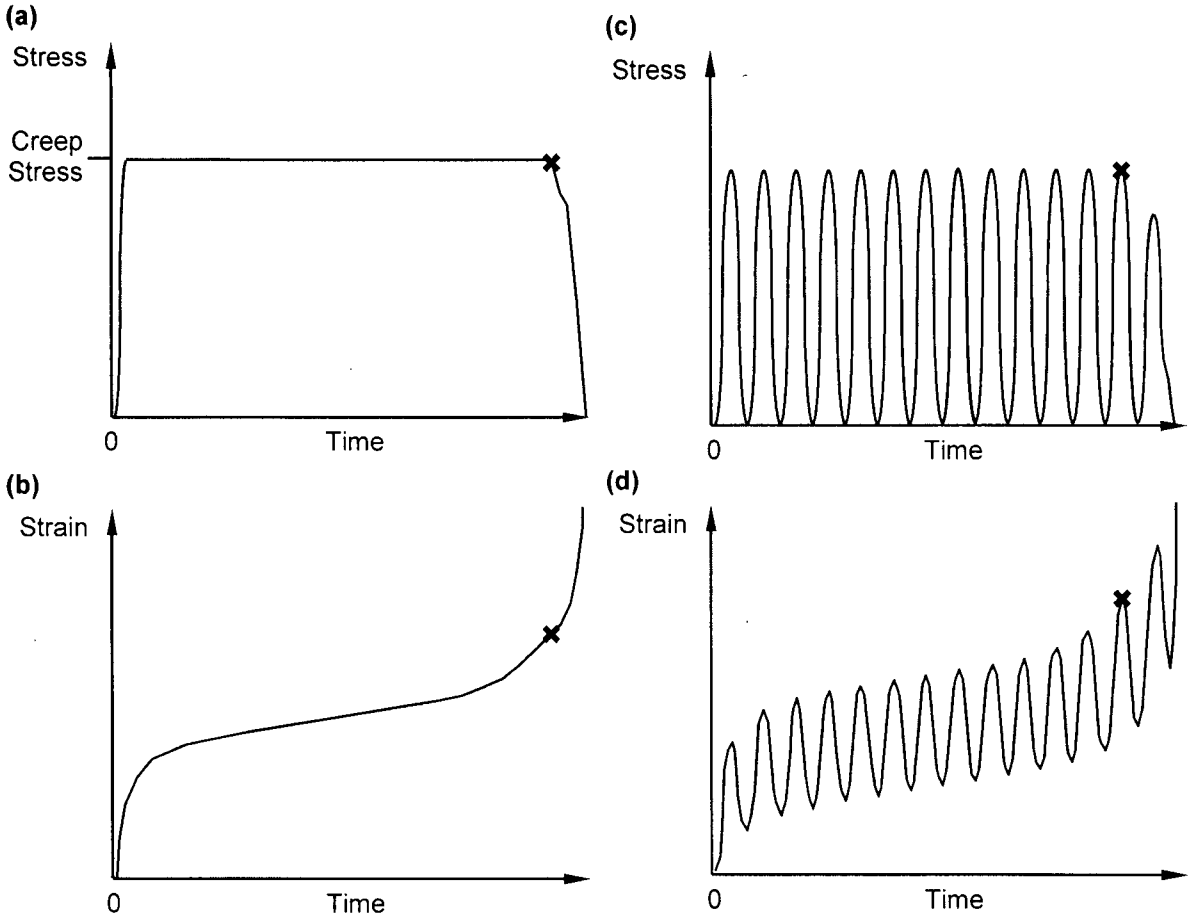

***Figure 11**: Schematic diagrams showing the definition of time-to-rupture for creep, (a) and (b), and fatigue, (c) and (d). Time-to-rupture was defined as the duration of loading until the specimen could not support 99% of the maximum test stress. Time-to-rupture is marked with an X-mark. Time-to-rupture was defined using a stress-time curve, (a) or (c), not a strain-time curve, (b) or (d). Time-to-rupture did not necessarily correspond to the last cycle of fatigue loading. Strain-at-rupture is shown with an X-mark in (b) and (d).*

2.3.1.3 Increase in Strain

The strain when the ligament was initially loaded to the maximum test stress (60% UTS, 30% UTS or 15% UTS) was defined as the initial strain (Figure 12(a)). Increase in strain was the additional strain recorded after the initial strain (Figure 12(b)). Increase in strain was analyzed at specific time-points: 0.8 hours, 4.2 hours, and 24.0 hours. The first time-point, 0.8 hours, was chosen because it was the time-point immediately before the first unloading and reloading of the

interrupted creep tests. Twenty-four hours of loading showed long term behaviour of creep and fatigue and 4.2 hours was an intermediate time common to all interrupted creep tests.

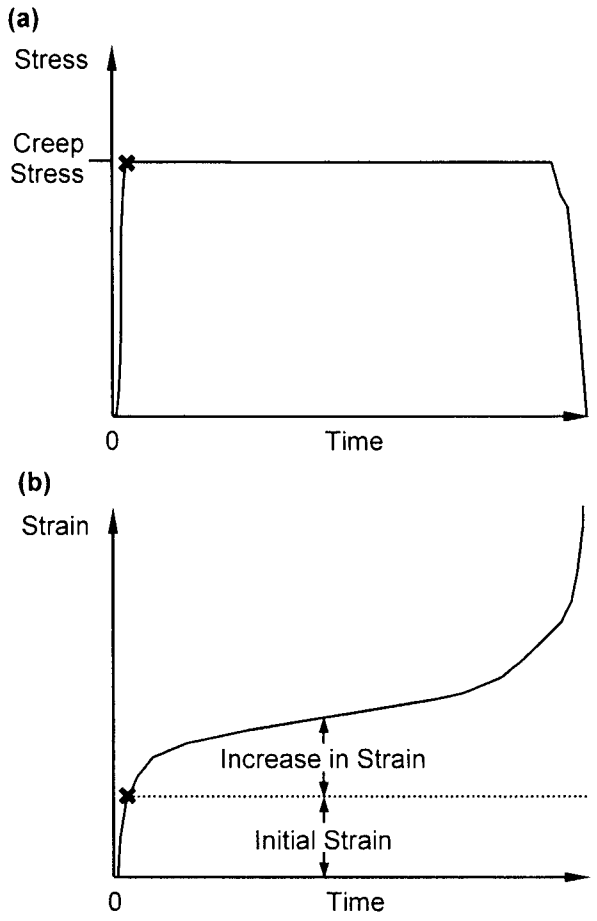

***Figure 12**: Schematic diagram defining increase in strain. (a) Stress versus time showing the point where initial strain is calculated. (b) Strain versus time showing the initial strain and the increase in strain (strain change above the dotted line).*

In addition to the time-points above, three normalized time-points were used to analyze increase in strain: 20%, 70% and 100% of the time-to-rupture (Figure 13). Twenty-percent and seventy-percent of the time-to-rupture were selected because these two time-points occurred after the transition to secondary strain and before the transition to tertiary strain, respectively. Only ligaments that ruptured during creep or fatigue loading were included in the analysis at normalized time-points. The above analysis performed at normalized time-points was also used to compare increase in strain for interrupted and non-interrupted creep tests.

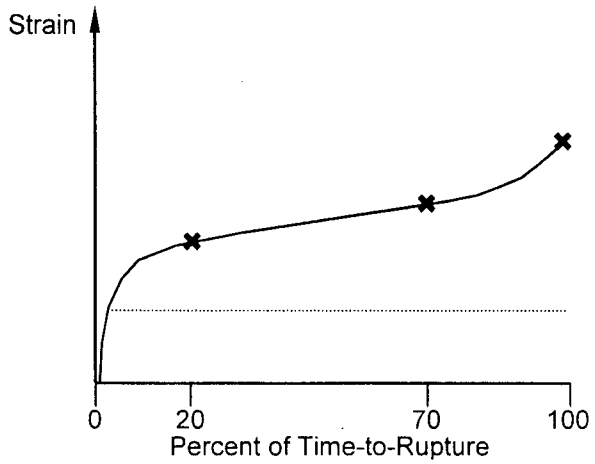

***Figure 13**: Schematic showing normalized time-points, 20%, 70% and 100% of the time-to-rupture, used to analyze increase in strain (strain accumulated after the initial strain shown by the dotted line).*

2.3.1.4 Steady-State Strain Rate

Steady-state strain rates were determined by fitting a line to the strain data (peak strain data for fatigue tests) between 20% and 70% of the time-to-rupture. If a specimen did not reach the tertiary creep stage, the strain data was fit between 20% and 99% of the loading. Both regions ensured that the steady-state strain rate (the slope of the linear fit) was calculated during secondary strain stage. Steady-state strain rates during fatigue and creep were compared at each stress level.

2.3.1.5 Tangent Modulus

Stress-strain curves were analyzed for all loading/unloading cycles (unloading/loading for the interrupted creep tests). Tangent modulus (E) was determined by a linear regression of the upper 50% of the loading portion of each stress strain curve ($r^2 > 0.999$, Figure 14). The initial tangent modulus (E_i) was calculated using the initial ramp to the test stress. In both creep and fatigue, the initial ramp was a half sine wave at 1 Hz. Maximum tangent modulus (E_{max}) was the largest tangent modulus recorded during loading. Both initial modulus and maximum modulus for

fatigue and creep were compared at each stress level. Modulus ratio was the tangent modulus at a time-point divided by the maximum tangent modulus (E/E_{max}). The last recorded modulus ratio prior to rupture ($E_{rupture}/E_{max}$) was analyzed for specimens that ruptured during creep or fatigue loading. Modulus ratios prior to rupture of creep and fatigue were compared at each stress level.

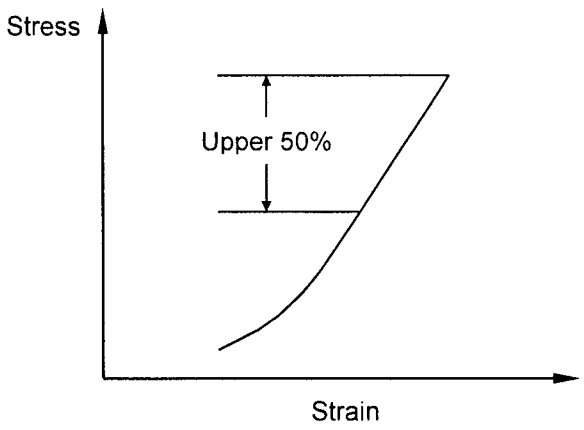

***Figure 14**: Schematic representation of the region used to calculate tangent modulus. Tangent modulus was calculated with the loading portion of the curve.*

2.3.1.6 Strain to 5 MPa

Valley strain was the minimum strain of each cycle (Figure 15). Strain to 5 MPa was the strain corresponding to a stress of 5 MPa in the loading portion of a cycle minus the valley strain in the same cycle. Total cycle strain was the peak strain in a given cycle minus the valley strain in the same cycle. Initial strain to 5 MPa was the strain to 5 MPa calculated for the first loading cycle (valley strain approximated by strain at 1 N for creep and fatigue).

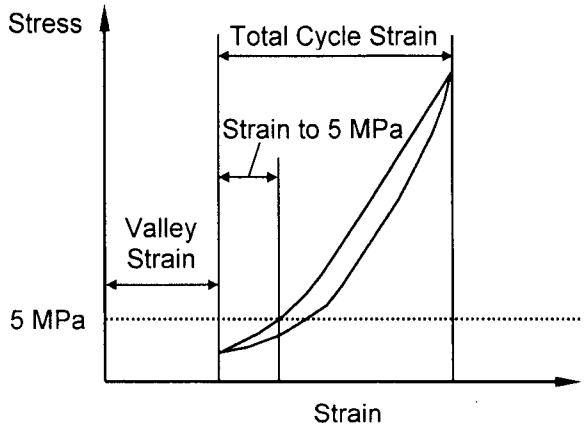

***Figure 15**: Schematic representation of a stress-strain curve for one cycle of loading highlighting valley strain, strain to 5 MPa, and total cycle strain.*

Strain to 5 MPa was used to approximate a *toe-region strain* because it was the highest stress still within the toe-region at all three stress levels. *Toe-region strain* (approximated by strain to 5 MPa) as a percentage of total cycle strain was compared between creep and fatigue at 60% UTS and 30% UTS at three normalized time-points: 0% of time-to-rupture (initial loading ramp), 20% of the time-to-rupture and 70% of the time-to-rupture. *Toe-region strain* for creep tests could not be calculated at exactly 20% and 70% of the time-to-rupture because the unloading/reloading cycles did not necessarily correspond to these values. As such, the values were approximated using linear interpolation.

In addition, *toe-region strain* as a percentage total cycle strain was compared within groups to determine if the values changed during loading. Values were compared at 0%, 20% and 70% time-to-rupture within each group. Monitoring changes over time provided information on how *toe-region strain* (estimated by strain to 5 MPa) and linear-region strain (total cycle strain minus *toe-region strain*) change with respect to one another during loading.

2.3.1.7 Residual Strength Analysis

Residual strength, failure strain, tangent modulus and strain at 10 MPa were calculated for ligaments that did not rupture during creep or fatigue loading. Residual strength was defined as

the maximum strength of ligaments after they had undergone creep or fatigue loading. This was determined by subjecting the ligaments to the single stretch to failure protocol. Failure strain was the strain recorded at the same time-point where the residual strength was determined. The term 'failure strain' applied to residual strength tests, whereas the term 'strain-at-rupture' applied to creep and fatigue loading. Tangent modulus was calculated with a linear regression of the upper 50% of the stress-strain curve. Strain at 10 MPa was recorded for residual strength tests to assess toe-region changes. Ten MPa was toward the end of the toe-region for 20 mm/min loading ramp, whereas 5 MPa was the maximum stress within the toe-region during creep and fatigue of all stresses tested. Similarly, UTS, failure strain, tangent modulus and strain at 10MPa was calculated for ligaments in the single stretch to failure group.

Ligaments included in the residual strength were separated into two categories: Group 1, ligaments without previous damage (those that had a modulus ratio greater than 0.97 at the end of creep or fatigue loading, n = 10); and Group 2, ligaments with previous damage (those that had a modulus ratio less than 0.97 at the end of creep or fatigue loading, n = 7). Both groups were compared to data from the single stretch to failure group (Group 3, n = 5).

2.3.2 Statistics

Four different statistical tests were used to compare creep and fatigue with respect to time-to-rupture, increase in strain, steady-state strain rate, strain to 5 MPa, residual strength, failure strain, tangent modulus, and strain at 10 MPa. Selection of the proper test followed a simple sequence of steps highlighted by Figure 16.

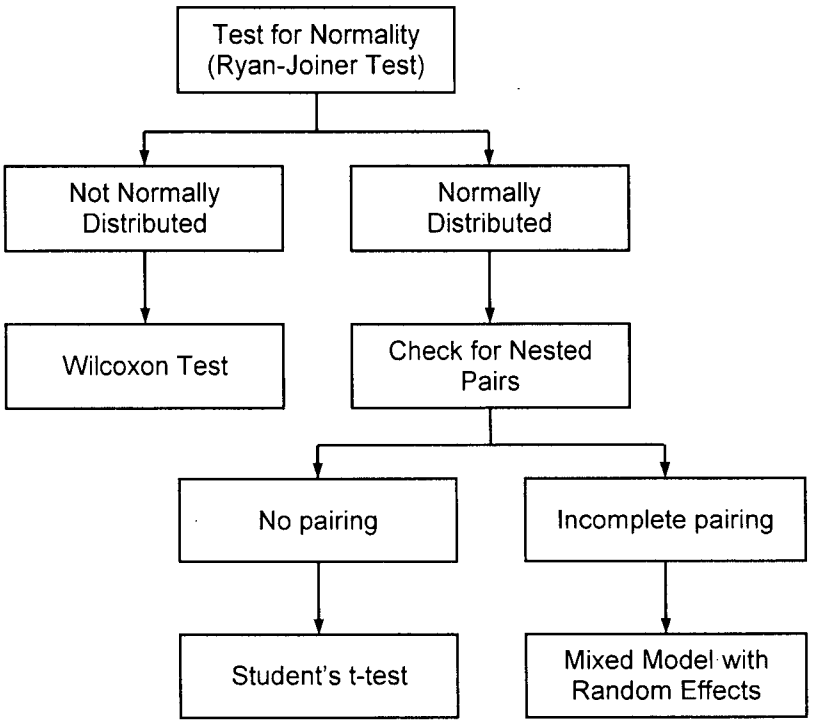

***Figure 16**: Sequence followed to determine the appropriate statistical test to perform for each data set. None of the non-parametric tests included partial pairing.*

The Ryan-Joiner test (similar to a Shapiro-Wilk test) involved creating a normal probability plot and testing the correlation between the data and expected values given a normal distribution. When the experimental data did not follow a normal distribution, then an exact Wilcoxon test was used to compare the data. There was no incomplete pairing present in the data analyzed with the Wilcoxon test. Normally distributed data was analyzed with either a Student's t-test or a mixed model. A student's t-test was used when no pairing was present between the two test groups.

When incomplete pairing was present and the data was normally distributed, a mixed model was used to analyze the data. The mixed model has the capabilities of an ANOVA analysis with the added ability of modeling two or more random effects. In the current study, there were two random effects modeled: random effects resulting from multiple sampling from the same subject (paired hindlimbs), and the random effects resulting from residual variances. The mixed model computes significance using restricted maximum likelihood. If no pairing was present, the data was normally distributed and the mixed model was still applied, the answer was identical to that provided by a Student's t-test.

Creep and fatigue were compared at each stress level. The effect of stress level on creep and fatigue individually was not analyzed. The difference between creep and fatigue was the primary outcome. The analysis of strain to 5 MPa was the only exception. This data was analyzed with repeated measures to investigate how each group (creep or fatigue) varied over time (a within group comparison). A summary of the statistical procedure used for each comparison is provided in Appendix D. The level of significance for all statistical tests was α=0.05.

2.3.3 Theoretical Modeling

Theoretical modeling of creep behaviour was undertaken to give more insight into the mechanisms of damage involved in both creep and fatigue. A continuum damage mechanics model was created to predict creep lifetime as a function of applied stress. The model used empirical input to model the time-dependent damage present during creep loading. The CDM model was verified against the creep data set and then used to predict fatigue lifetime based on time-dependent (creep) damage.

2.3.3.1 Continuum Damage Mechanics Model

The CDM model was based on a combination of continuum mechanics and two empirical relations. The first relation was between residual strength and modulus ratio. The second estimated initial damage rate using the rate of modulus ratio change during the early stage of damage.

2.3.3.1.1 Damage Equation

The CDM model relied on the assumption that damage resulted in a decrease in effective CSA and an increase in effective stress. This assumption was used to develop the following relation by Kachanov (described in (30)):

$$D = \left(1 - \frac{A}{A_o}\right) \tag{1}$$

where D was the damage

A was the intact cross-sectional area

A_o was the fully intact cross-sectional area

Equating forces applied to the material before and after damage created an expression to relate area decrease and effective stress.

$$F_{BeforeDamage} = F_{AfterDamage} \tag{4}$$

$$\sigma_o \cdot A_o = \sigma_{eff} A_{eff} \tag{5}$$

where F was the force applied to the material

σ_o was the nominal stress

σ_{eff} was the effective stress

Combining equation (1) and (5) resulted in the following.

$$D = \left(1 - \frac{\sigma_o}{\sigma_{eff}}\right) \tag{6}$$

The above equation has been used in other continuum damage models (30,66,82). An important task was to define a failure point. This was defined as a point when the cross-sectional area was reduced such that the effective stress equaled the ultimate tensile strength of the material (30,32,42,82).

$$\sigma_{eff} = \sigma_{UTS} \tag{7}$$

where σ_{UTS} was the ultimate tensile strength

The damage equation (6) was used with the above equality to define the damage level corresponding to rupture.

$$D_{rupture} = \left(1 - \frac{\sigma_o}{\sigma_{UTS}}\right) \tag{8}$$

where $D_{rupture}$ was the damage level at rupture

In this study, modulus ratio (E/E_{max}) was used as an indicator of damage. Previous studies have used a modulus ratio as a direct indicator of damage (42,66,82). In other words, modulus ratio was equated with CSA reduction ($E/E_{max} = A/A_o$). This required the assumption that damaged (ruptured) material no longer contributed to the strength of the structure. However, in ligaments, ruptured fibres may still be able to interact with intact fibres by transmitting loads through the ground substance. Therefore, it was beneficial to find a relation between area reduction (or effective stress) and modulus reduction without relying on this assumption.

The residual strengths of unruptured ligaments were used to find a relation between modulus ratio and effective stress using a power law regression.

$$RS = B\left(\frac{E_{final}}{E_{max}}\right)^C \tag{9}$$

where RS was the residual strength in MPa

E_{final}/E_{max} was the modulus ratio recorded just prior to the residual strength test

B and C were constants determined from the regression

The ratio of residual strength to the UTS was used to define the area reduction realized prior to the residual strength test. Equation (9) was substituted into the ratio to define CSA reduction as a function of modulus ratio.

$$\frac{RS}{\sigma_{UTS}} = \frac{A_{final}}{A_o} \tag{10}$$

$$\frac{B\left(\frac{E_{final}}{E_{\max}}\right)^C}{\sigma_{UTS}} = \frac{A_{final}}{A_o} \tag{11}$$

A generalized version of the above equation was substituted into the damage equation (equation (1)) and resulted in a relation between damage and modulus ratio.

$$D = 1 - \frac{B}{\sigma_{UTS}}\left(\frac{E}{E_{\max}}\right)^C \tag{12}$$

where D was the damage variable ranging from 0 to $D_{rupture}$

B and C were constants

E/E_{max} was the modulus ratio and σ_{UTS} is the ultimate tensile strength

σ_{UTS} was the ultimate tensile strength

2.3.3.1.2 Damage rate

Defining the damage rate was necessary to develop the continuum damage model. The second major assumption was made to define the damage rate: the damage rate of intact material was dependent on effective stress (this can be related to the current damage state, modulus ratio or CSA reduction). As damage accumulates, the effective stress on intact fibres increases; therefore, the damage rate will also increase. The initial damage rate was found as a function of nominal stress and was defined in a region with minor damage. Assuming the nominal stress and effective stress in this region are equivalent, the initial damage rate can be used to approximate

the damage rate as a function of effective stress. This approximation, written mathematically, was:

$$\dot{D}_o(\sigma_o) = \dot{D}(\sigma_{eff}) \tag{13}$$

where σ_o was the nominal stress

σ_{eff} was the effective stress

$\dot{D}_o$ was the initial damage rate as a function of nominal stress

$\dot{D}$ was the damage rate as a function of effective stress

To determine the damage rate ($\dot{D}$), an approximation for the initial damage rate was developed. Modulus ratio was used as an indicator of damage; therefore, it was logical to define damage rate with the modulus ratio rate-of-change. Wang and Ker (66) acknowledge this, but they had difficulty defining initial stiffness change and chose to model initial stiffness change by relating stiffness to strain. In the present study, the steady-state portion of the modulus ratio data was fit with a linear regression to determine the initial modulus rate-of-change. Figure 17 is a schematic showing the portion of the curve that was fit. A higher order polynomial curve fit did not change the results because the slope of the region was dominated by the first order value. To account for the potential of initial ligament stiffening during the testing, the region used to determine initial modulus rate-of-change started at the first point where modulus ratio increased to 98% and ended at the first point where modulus ratio decreased to 97%. If a test ruptured before the recorded modulus ratio decrease to 97%, then the last recorded modulus ratio point was used as the end of the region. Tests that were stopped before rupture and had a modulus ratio greater than 0.97 were excluded from the initial modulus ratio rate-of-change analysis.

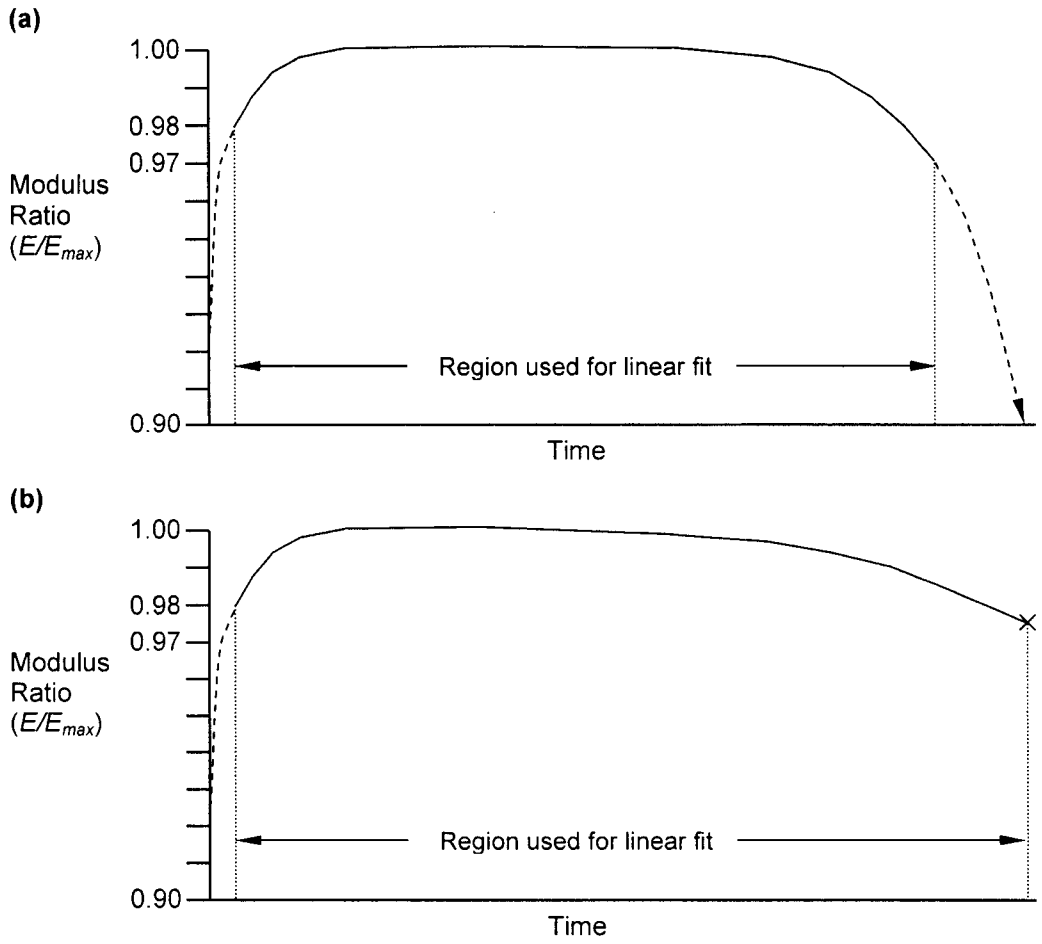

***Figure 17**: Schematic of modulus ratio versus time. Solid lines show the region fit with a linear regression and dashed lines show the portions of the curve not used to determine initial damage rate. Two cases are shown: (a) modulus ratio decreased to 97% before rupture and (b) modulus ratio did not decrease to 97% before rupture. Note that the images are not to scale, with the non-linearity greatly exaggerated. See the results section for typical modulus ratio plots.*

The slopes of the linear fits were used to approximate the initial modulus ratio rate-of-change. The initial modulus ratio rate-of-change was related to nominal stress using a power law regression. A power law relation gave the best fit to the experimental data.

$$\frac{d\left(\frac{E}{E_{\max}}\right)}{dt} = F\sigma_o{}^G \tag{14}$$

where F and G were constants determined by the regression

E/E_{max} was the modulus ratio and σ_{UTS} is the ultimate tensile strength

d/dt was the rate of change with respect to time

Combining the above with the derivative of equation (12) resulted in an expression for damage rate as a function of stress and modulus ratio.

$$\dot{D}_o = -\frac{B \cdot C}{\sigma_{UTS}} \cdot \left(\frac{E}{E_{\max}}\right)^{C-1} \cdot F\sigma_o{}^G \tag{15}$$

where B and C were constants

σ_{UTS} was the ultimate tensile strength

The above equation and equation (13) were used to define the damage rate as a function of modulus ratio and effective stress.

$$\dot{D} = -\frac{B \cdot C}{\sigma_{UTS}} \cdot \left(\frac{E}{E_{\max}}\right)^{C-1} \cdot F\sigma_{eff}{}^G \tag{16}$$

Both modulus ratio and effective stress were related to the damage state using equations (12) and (6), respectively. Equation (16) was re-written to give the final form of the damage rate equation:

$$\dot{D} = -\frac{F \cdot B \cdot C}{\sigma_{UTS}} \cdot \left(1 - D \cdot \frac{\sigma_{UTS}}{B}\right)^{\frac{C-1}{C}} \cdot \left(\frac{\sigma_o}{1-D}\right)^{G} \tag{17}$$

where $\dot{D}$ was the damage rate

F, B, C, and G were constants

σ_{UTS} was the ultimate tensile strength

σ_o was the nominal stress

D was the current state of damage in the material

2.3.3.1.3 Time-to-Rupture Prediction

The continuum damage model was used to predict time-to-rupture. Before loading, the damage was assumed to be zero. As described above, the damage at rupture ($D_{rupture}$) was 1- σ_o/σ_{UTS}. The damage rate equation can be integrated by separation of variables between zero and $D_{rupture}$ to predict time-to-rupture of creep loading based on the nominal stress.

$$T_{rupture} = -\frac{\sigma_{UTS}}{F \cdot B \cdot C} \cdot \int_0^{1-\frac{\sigma_0}{\sigma_{UTS}}} \left(1 - D \cdot \frac{\sigma_{UTS}}{B}\right)^{\frac{C}{C-1}} \cdot \left(\frac{\sigma_o}{1-D}\right)^{-G} dD \tag{18}$$

where $T_{rupture}$ was the predicted time-to-rupture

F, B, C, and G were constants determined from empirical data

σ_{UTS} was the ultimate tensile strength

σ_o was the nominal stress

D was the current state of damage in the material

Time-to-rupture for fatigue loading was also predicted with the continuum damage model. The constant nominal stress in equation (17) was replaced with a time varying stress as shown in the following equation.

$$\dot{D} = -\frac{F \cdot B \cdot C}{\sigma_{UTS}} \cdot \left(1 - D \cdot \frac{\sigma_{UTS}}{B}\right)^{\frac{C-1}{C}} \cdot \left(\frac{\frac{\sigma_{max}}{2} \cdot (1 + \sin(\pi \cdot f \cdot t)}{1 - D}\right)^{G} \quad (19)$$

where σ_{max} was the maximum stress

f was the frequency in Hz

t was the time in seconds

The addition of a time-dependent stress rendered the damage rate equation inseparable, so an alternate method was used to approximate time-to-rupture for fatigue loading. A 4th order Runge-Kutta approximation was used to compute the time required to reach $D_{rupture}$. The step size was 0.25 seconds. Fatigue time-to-rupture predictions were compared to fatigue experimental data.

2.3.3.1.4 Model Errors

A sensitivity analysis of the empirical inputs (*B*, *C*, *F*, and *G*) to the CDM model was performed to check the error in the prediction of time-to-rupture. Analysis was completed at 30% UTS nominal stress. Each constant was increased and decreased by 10% and the creep time-to-rupture was predicted using equation (18). To understand how much the constants B and C could reasonably vary, one data-point at a time was systematically removed from the residual strength versus modulus ratio data set. Similarly, one data-point at a time was systematically removed from the initial rate of modulus ratio change versus time data set to observe how much the constants F and G were affected. The maximum and minimum values of the constants were recorded and inputted into equation (18) to estimate the reasonable error in the time-to-rupture prediction.

3.0 RESULTS

Experimental data acquired from creep and fatigue loading was analyzed to assess differences in times-to-rupture, strain profiles, and stress-strain characteristics. Residual strength provided evidence of damage and continuum damage theory was used to model the time-dependent damage during creep and fatigue. Data from the single stretch to failure group were used to calculate a UTS of 97.7 ± 12.6 MPa. This UTS was used to normalize stresses in creep and fatigue loading. Forty-one of the 46 ligaments failed in the midsubstance. The remainder failed in the midsubstance with minor femoral avulsion.

3.1 Time-to-Rupture

At 60% UTS, all of the fatigue and creep tests were loaded until rupture, except for one non-interrupted creep test that was censored (stopped) at 24 hours. Non-interrupted creep had significantly longer time-to-rupture than interrupted creep ($p = 0.034$), when the one censored time was considered to be ruptured (Figure 18). If the censored time was excluded from analysis, there was still a strong trend for the time-to-rupture for non-interrupted creep to be longer ($p = 0.064$). Non-interrupted creep tests were only performed at 60% UTS.

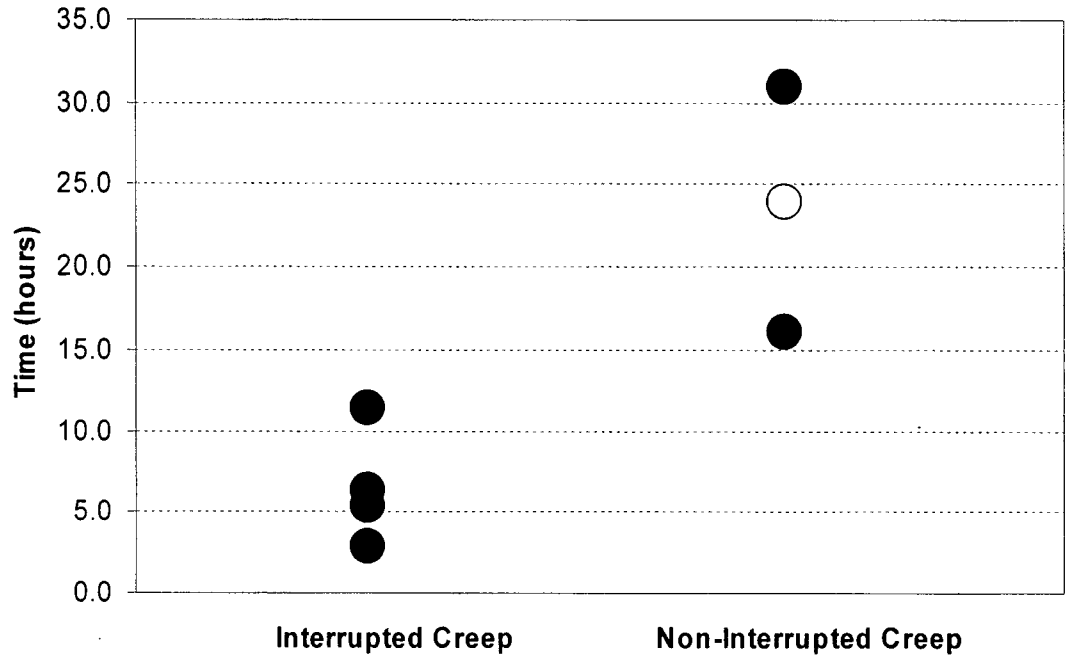

***Figure 18**: Time-to-rupture of interrupted and non-interrupted creep ligaments tested at 60% UTS. Solid circles indicate the ligament ruptured and a hollow circle indicates the ligament was still intact and the loading was stopped at that time.*

Time-to-rupture of interrupted creep (6.5 ± 3.5 hours) was greater than fatigue (0.55 ± 0.50 hours) at 60% UTS ($p = 0.043$). Similarly, time-to-rupture of all ruptured creep (12 ± 10 hours) was greater than fatigue at 60% UTS ($p = 0.041$). Non-interrupted creep also failure at greater times than fatigue ($p = 0.040$). The times-to-rupture and censor-times are summarized for all stress levels in Table 3 below.

***Table 3**: Total loading duration for each ligament. Paired ligaments are found on the same row, except in the case of the pair between 30% creep and 15% creep. Creep ligaments 9, 18 and 19 were not included in the residual strength analysis (see Section 3.4). Creep ligaments 9, 10, and 11 were non-interrupted tests.*

Stress Level (% UTS)	Fatigue Ligament	Time of Loading (hours)	Condition at End of Test	Creep Ligament	Time of Loading (hours)	Condition at End of Test
60	1	0.1	Ruptured	--	--	--
60	2	1.0	Ruptured	--	--	--
60	3	1.0	Ruptured	--	--	--
60	4	0.2	Ruptured	--	--	--
60	--	--	--	5	11.3	Ruptured
60	--	--	--	6	2.8	Ruptured
60	--	--	--	7	5.4	Ruptured
60	--	--	--	8	6.4	Ruptured
60	--	--	--	9	24.0	Censored
60	--	--	--	10	16.1	Ruptured
60	--	--	--	11	31.0	Ruptured
30	12	16.0	Ruptured	12	24.0	Censored
30	13	23.1	Ruptured	13	24.0	Censored
30	14	7.3	Ruptured	14	24.0	Censored
30	15	13.5	Ruptured	15	24.0	Censored
30	--	--	--	16	24.0	Censored
30	--	--	--	17	47.2	Ruptured
30	--	--	--	18	34.4	Censored
30	--	--	--	19	16.5	Censored
30	--	--	--	20	72.0	Censored
30	--	--	--	21	90.7	Ruptured
30	--	--	--	22	85.4	Ruptured
15	23	24.0	Censored	23	24.0	Censored
15	24	24.0	Censored	24	24.0	Censored
15	25	48.0	Censored	25	48.3	Censored
15	26	30.4	Ruptured	26	46.1	Ruptured
15	27	24.0	Censored	--	--	--
15	28	72.0	Censored	--	--	--
15	29	72.0	Censored	--	--	--
15	30	72.0	Censored	--	--	--
15	31	80.8	Ruptured	--	--	--
15	32	58.9	Ruptured	--	--	--
15	--	--	--	20	168	Censored

At 30% UTS, all the fatigue ligaments ruptured. Three interrupted creep ligaments ruptured and the remaining ligaments were censored at 24 hours (n = 5) or 72 hours (n = 1). Two additional tests, both 30% UTS creep, were unintentionally stopped during loading at 16.4 and 34.4 hours. Data from these tests were only analyzed up to these times. These two unintentionally stopped ligaments were not included in the residual strength analysis. Creep times-to-rupture (74 ± 24 hours) were greater than fatigue times-to-rupture (15 ± 6.5 hours) at 30% UTS, excluding censored data ($p = 0.004$). The maximum time-to-rupture for fatigue ligaments at 60% and 30%

UTS was smaller than all times-to-rupture or censor-times of the respective creep ligaments at 60% and 30% UTS (Figure 19).

At 15% UTS, three ligaments from fatigue and one from creep ruptured during loading. One ligament from each group ruptured at fairly early times ($Time_{fatigue}$ = 30.4 hours, $Time_{creep}$= 46.1 hours) and both of these were from the same animal. The remaining ligaments at 15% UTS were censored at 24 hours (fatigue, n = 2; creep, n = 2), 48 hours (fatigue, n = 1; creep, n = 1), 72 hours (fatigue, n = 3) or 168 hours (creep, n = 1). Time-to-rupture statistics were not completed at 15% UTS because only one creep ligament ruptured. One creep ligament was loaded for over 2 times the maximum recorded fatigue time-to-rupture without showing mechanical signs of damage. The complete set of time-to-rupture and censor-time data is shown in Figure 19.

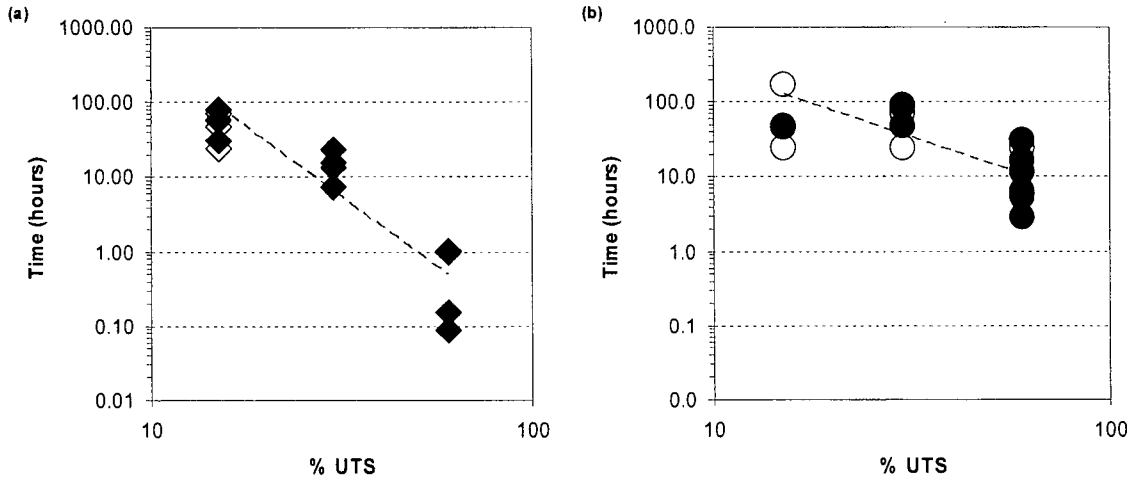

***Figure 19**: Time-to-rupture and censor-times for all tests in both (a) fatigue and (b) creep. Solid symbols indicate time of ligament rupture and hollow symbols indicate the time that ligaments were unloaded. Note that some data points may overlap. The dashed lines are power law curve fits of the ruptured data only.*

The time-to-rupture data for both creep and fatigue were fit with a power-law curve to relate between time-to-rupture and test stress normalized with the ultimate tensile strength. Coefficients were determined using a least squares approach.

$$T_{creep} = 1.54 \cdot 10^4 \cdot \left(\frac{\sigma_o}{\sigma_{UTS}} \cdot 100 \right)^{-1.78} \quad (3'a)$$

$$T_{fatigue} = 2.00 \cdot 10^6 \cdot \left(\frac{\sigma_o}{\sigma_{UTS}} \cdot 100 \right)^{-3.73} \quad (3'b)$$

Where T_{creep} and $T_{fatigue}$ are the times-to-rupture, in hours, for creep and fatigue, respectively, σ_o is the nominal stress and σ_{UTS} is the ultimate tensile strength. The r^2 for the creep fit was 0.52 and the r^2 for the fatigue fit was 0.83.

3.2 Strain Profiles

Strain profile comparisons were made using increase in strain, steady-state strain rate and strain at rupture. All data for the fatigue tests was generated using peak strains for each cycle. Initial strains were similar for creep and fatigue at each stress. Initial strains are shown in Table 4.

***Table 4**: Initial strain for creep and fatigue at 60%, 30% and 15% UTS. No statistical difference was detected between creep and fatigue at any stress. Data shown as mean ± standard deviation.*

Stress (% UTS)	Fatigue Initial Strain	Creep Initial Strain
60	0.0974 ± 0.0096	0.1016 ± 0.0179
30	0.0670 ± 0.0054	0.0686 ± 0.0076
15	0.0426 ± 0.0094	0.0451 ± 0.0086

In general, trends observed for increase in strain can be extrapolated to total strain because the initial strains for creep and fatigue were similar; however, increase in strain was used to eliminate the minor variation associated with initial strains.

3.2.1 Increase in strain

All ruptured ligaments exhibited three stages of strain: primary strain, secondary strain and tertiary strain. Censored ligaments were stopped in secondary strain or the beginnings of tertiary strain. Analysis was performed at specific time-points and normalized time-points. Typical increases in strain for creep and fatigue are shown at specific time-points (Figure 20) and normalized time-points (Figure 21). All increase in strain plots are provided in Appendix E.

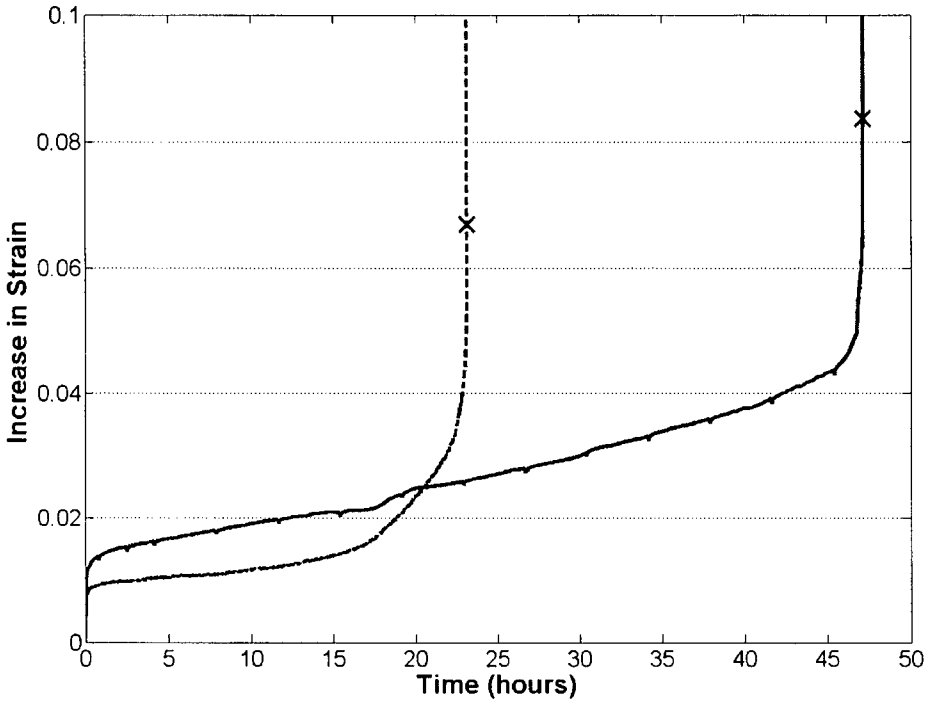

***Figure 20**: Typical increase in strain profiles at 30% UTS for fatigue (dashed line) and creep (solid line). The X-marks indicate the increase in strain-at-rupture.*

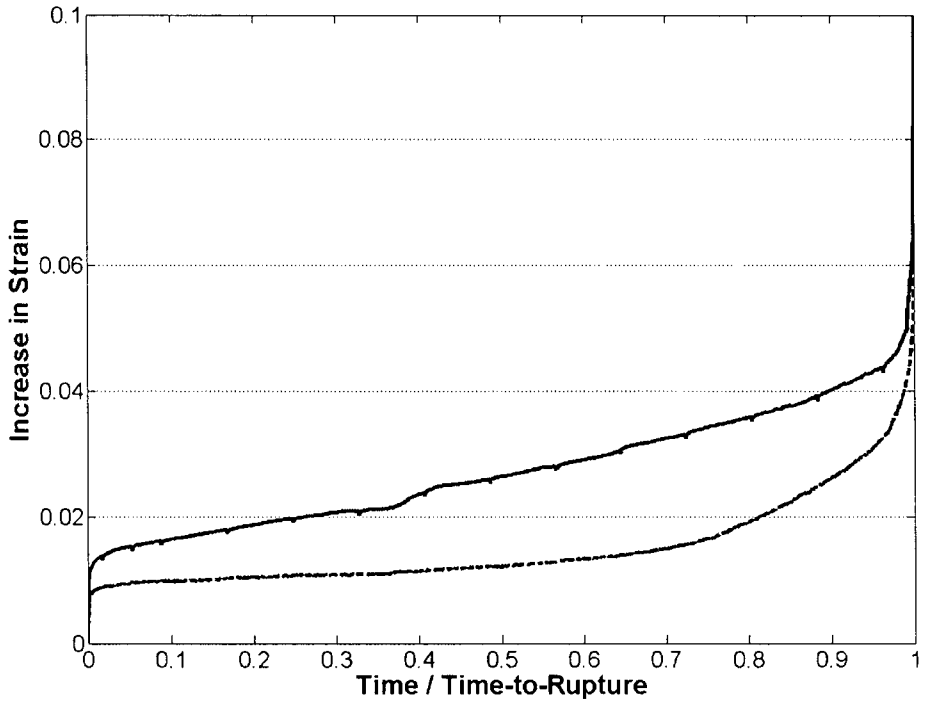

***Figure 21**: Typical increase in strain profiles at 30% UTS as a function of normalized time for creep (solid line) and fatigue (dashed line). The above specimens are the same as those plotted in Figure 19.*

At 60% UTS, increases in strain for interrupted and non-interrupted creep tests were compared at 20% of the time-to-rupture and at 70% of the time-to-rupture (Figure 22). One of the non-interrupted creep tests was excluded from the normalized time increase in strain analysis because it was not loaded to rupture. At 20%, 70% and 100% of the time-to-rupture, the increase in strain of interrupted creep was not different from non-interrupted creep. As a result, the non-interrupted and interrupted creep were combined together for creep and fatigue comparisons.

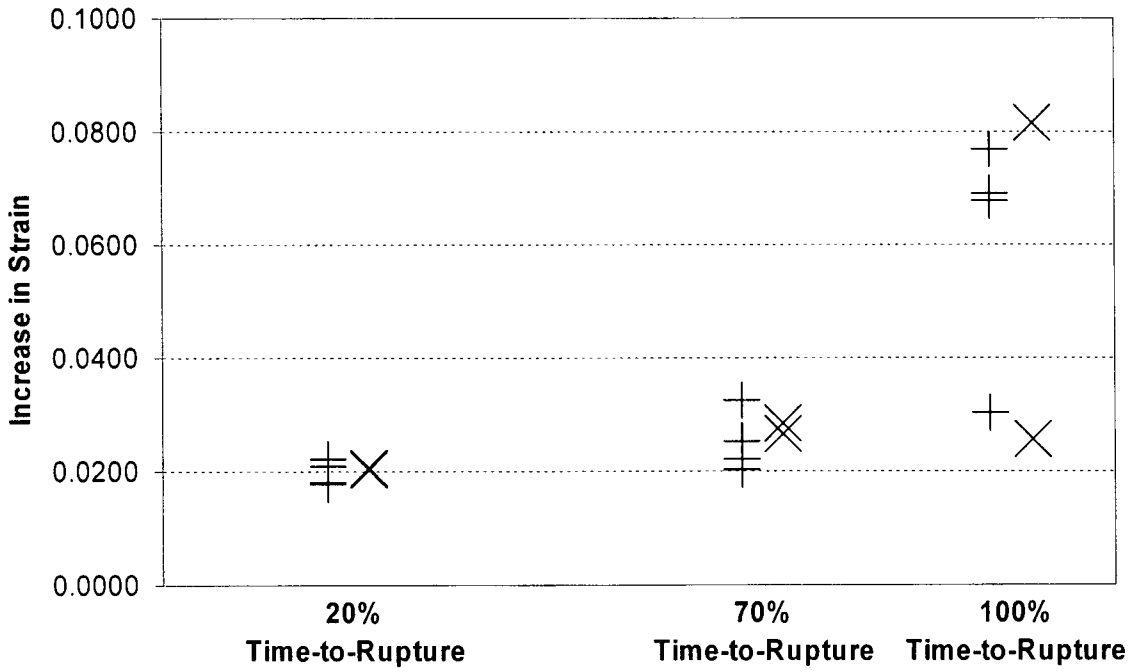

***Figure 22**: Increase in strain for interrupted creep (+) and non-interrupted creep (X) at 20% and 70% of time-to-rupture. Tests completed at 60% UTS.*

3.2.1.1 Increase in Strain at Specific Time-Points

At 60% UTS, increase in strain was greater for fatigue than creep after both 0.8 hours ($p = 0.014$) and 4.2 hours ($p = 0.038$, Figure 23(a)). Fatigue and creep increases in strain were similar at 24 hours. One fatigue specimen had a large discontinuity at 0.35 hours (see Appendix F). A discontinuity was defined as a large change in strain with no corresponding change in stress.

At 30% UTS, increase in strain was greater for creep than fatigue at 0.8 hours ($p = 0.042$, Figure 23(b)). After 4.2 hours, a trend for creep increase in strain to be greater than fatigue was detected, but it was not statistically significant ($p = 0.084$). At 24 hours, fatigue strain increases were greater than those of creep ($p < 0.001$).

At 15% UTS, creep strain increases were greater than fatigue strain increases at 0.8 hours ($p = 0.029$) and 4.2 hours ($p = 0.026$, Figure 23(c)). By 24 hours, creep and fatigue strain increases were similar at 15% UTS. The increase in strain at 15% UTS was almost an order of magnitude less than that at 60% UTS. At 30% and 15% UTS, the magnitude of the differences between creep and fatigue for increase in strain was small. An additional set of 60% fatigue data was collected but it was excluded from analysis because of apparatus malfunction resulting in very large increase in strain values (see Appendix G).

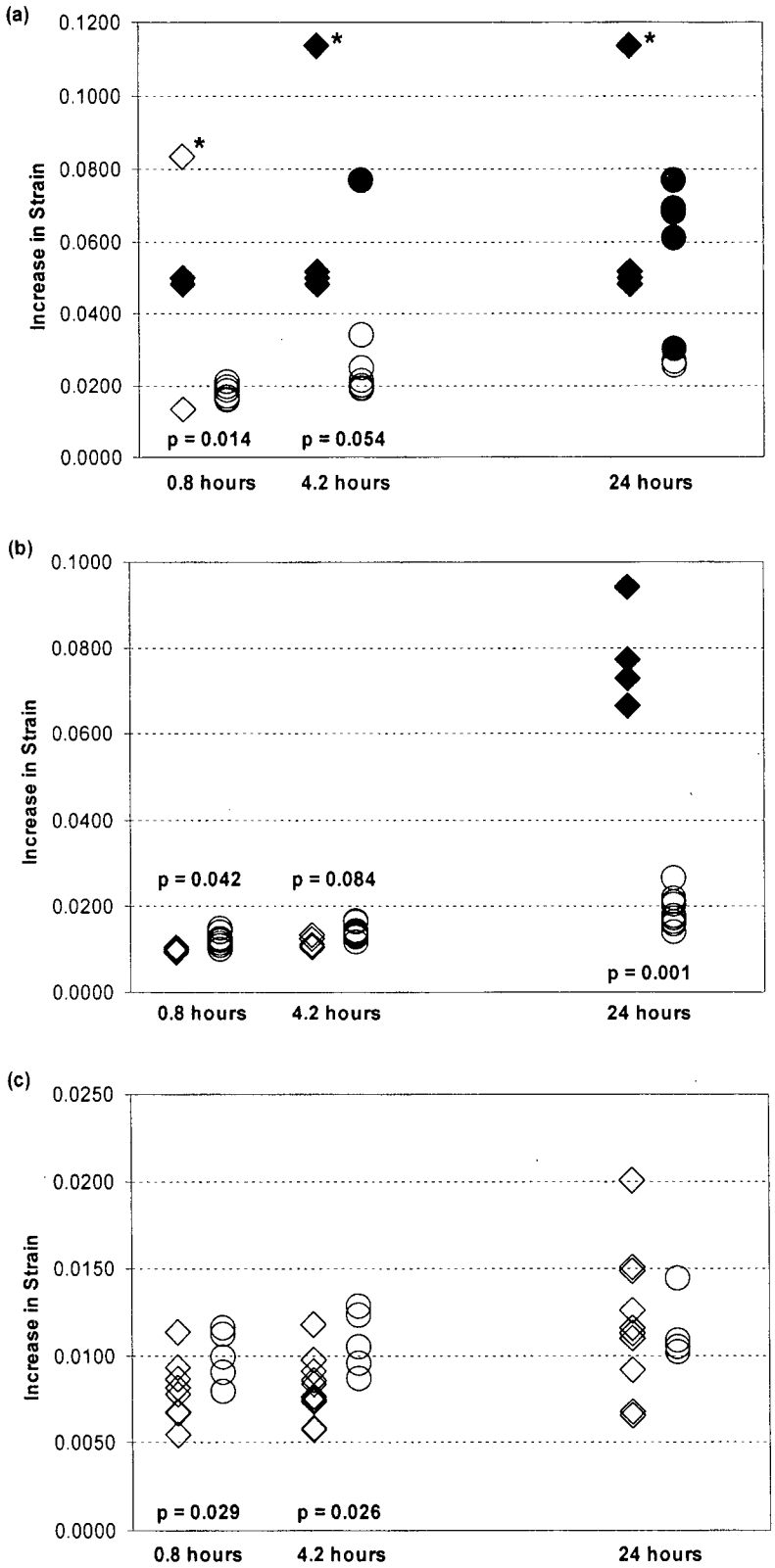

***Figure 23**: Increase in strain for fatigue (◆, ◇) and creep (●, ○) tests at (a) 60% UTS, (b) 30% UTS and (c) 15% UTS. Data is shown at three time-points: 0.8 hours, 4.2 hours and 24 hours. Solid symbols indicate that the ligament was ruptured at that time and hollow symbols indicate the ligament was still intact at that time. An asterisk (*) indicates the fatigue ligament at 60% UTS that had a large increase in strain discontinuity at 0.35 hours.*

In summary, at 0.8 hours fatigue increase in strain was greater than creep increase in strain at 60% UTS because two ligaments had ruptured and the remaining two were close to rupture (within 0.2 hours) and no creep ligaments had ruptured. Also at 0.8 hours, creep increase in strain was greater than fatigue increase in strain at 30% and 15% UTS. No ruptures occurred before 0.8 hours at 30% and 15% UTS.

At 4.2 hours, fatigue increase in strain at 60% UTS was greater than creep increase in strain because all four fatigue ligaments had ruptured while only one creep ligament ruptured. Creep increase in strain was still greater than fatigue increase in strain at 30% and 15% and no ruptures occurred before 4.2 hours at these two stresses.

At 24 hours and 60% UTS fatigue, increase in strain and creep increase in strain were the same because all ligaments (except one creep ligament) had ruptured. At 30% UTS, fatigue increase in strain was greater than creep increase in strain because all fatigue ligaments had ruptured and all creep ligaments were still intact. Fatigue and creep increases in strain were similar at 15% UTS. Both creep and fatigue (at 15% UTS) were in the secondary strain stage at 24 hours, so the increase in strain magnitudes were small.

3.2.1.2 Increase in Strain at Normalized Time-Points

Increase in strain was also analyzed on a normalized time scale (Figure 24). In general, increase in strain was larger for creep than fatigue at a given normalized time-point. Once again, the normalized time-point analysis only included specimens that ruptured. Not enough specimens ruptured in creep at 15% UTS to perform statistical analysis, so only 60% UTS and 30% UTS were analyzed.

At 20% of the time-to-rupture, increase in strain during creep was greater than increase in strain for fatigue. This was true at both 30% UTS ($p = 0.001$) and 60% UTS ($p < 0.001$). At 70% of the time-to-rupture and 30% UTS, increase in strain was greater for creep when compared to fatigue ($p = 0.034$). However, at 70% of the time-to-rupture and 60% UTS, increase in strain

was similar between creep and fatigue. At 100% of the time-to-rupture, creep and fatigue increases in strain were not different at either 60% or 30% UTS.

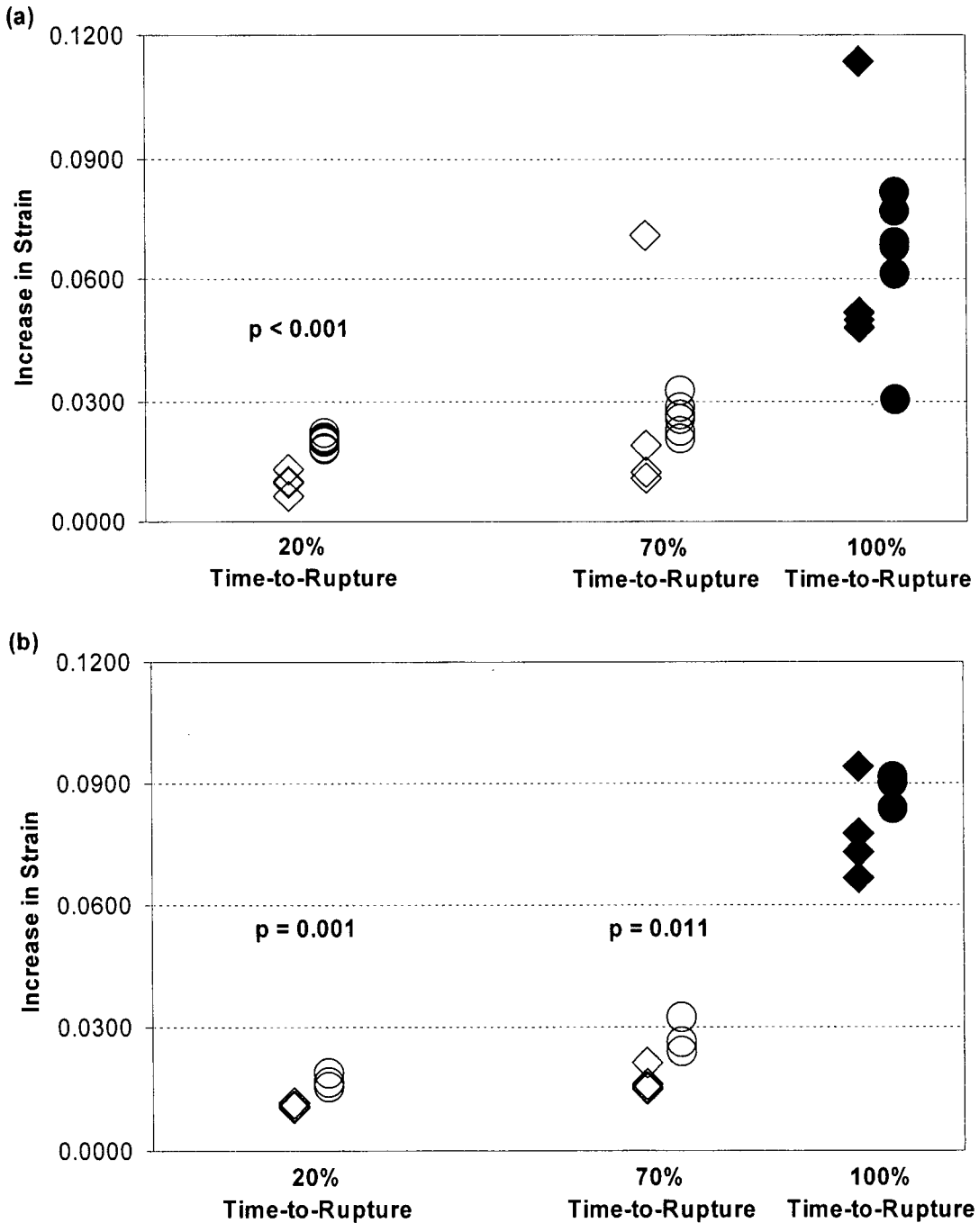

***Figure 24**: Increase in strain for fatigue (◆, ◇) and creep (●, ○) tests at (a) 60% UTS, and (b) 30% UTS. Data is shown at two normalized time-points: 20% of time-to-rupture, 70% of time-to-rupture and 100% of time-to-rupture. The first two normalized time-points occurred after the end of primary strain and before the beginning of tertiary strain. Solid symbols indicate that the ligament was ruptured and hollow symbols indicate the ligament was still intact.*

3.2.2 Steady-State Strain Rate

At all stress levels, fatigue steady-state strain rates showed a trend to be greater or was significantly greater that those resulting from creep loading (Figure 25). At 60% UTS fatigue steady-state strain was 26 ± 17 μ/sec while creep was 0.36 ± 0.34 μ/sec ($p = 0.008$). At 30% UTS, creep steady-state strain rate (0.063 ± 0.040 μ/sec) was less than fatigue (0.27 ± 0.15 μ/sec, $p = 0.013$). Tests performed at 15% UTS followed the same trend as above with fatigue (0.067 ± 0.056 μ/sec) larger than creep (0.013 ± 0.0077 μ/sec, $p = 0.074$).

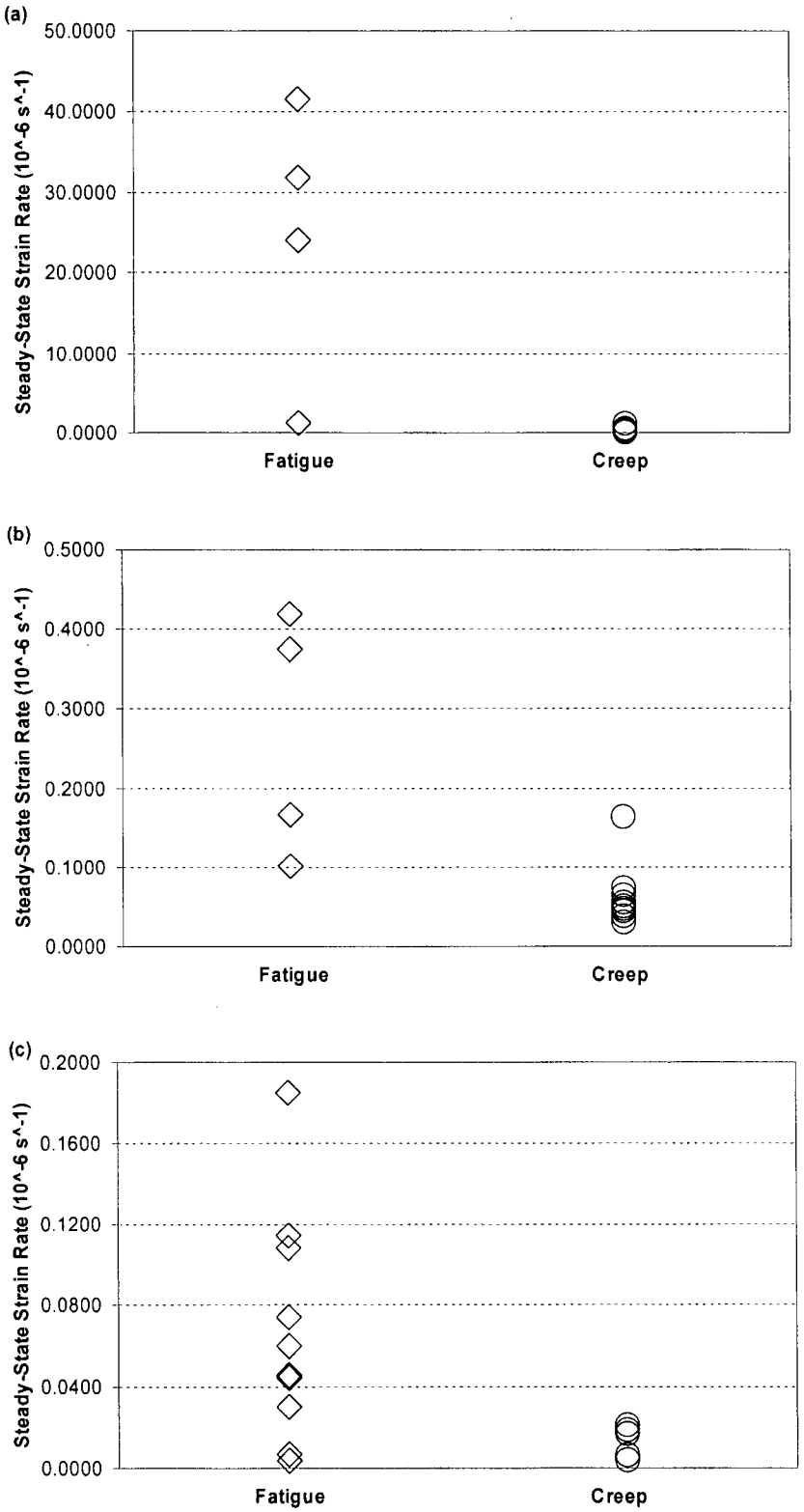

Figure 25: *Steady-state strain rate (measured in micro-strain/s) for fatigue and creep at (a) 60% UTS, (b) 30% UTS and (c) 15% UTS.*

3.2.3 Strain-at-Rupture

Creep and fatigue strains-at-rupture were also compared and no significant differences were detected between any groups (Figure 26). Average strains-at-rupture for 60%, 30% and 15% UTS fatigue loading were 0.167 ± 0.028, 0.146 ± 0.016, and 0.146 ± 0.012, respectively. Strains-at-rupture for 60%, 30% and 15% UTS creep tests were 0.168 ± 0.034, 0.148 ± 0.006, and 0.187 respectively. For continuity, strain-at-rupture was simply the addition of initial strain (Table 4 above) and increase in strain at 100% of the time-to-rupture (Figure 23 above).

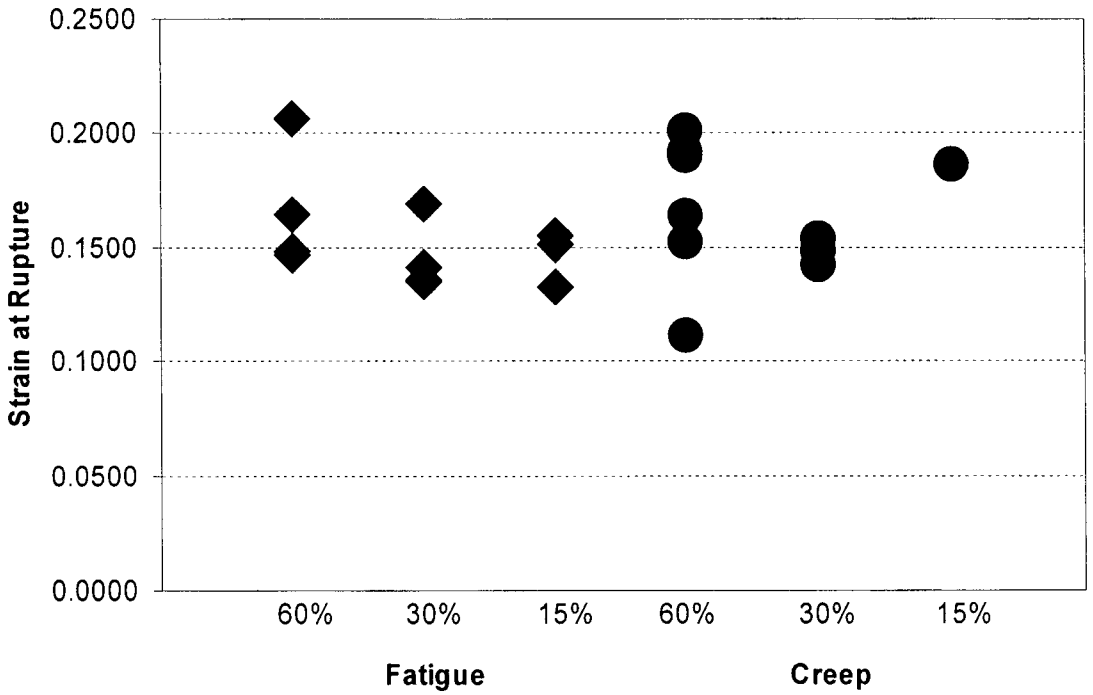

***Figure 26**: Strain-at-rupture for fatigue and creep at all stress levels: 60% UTS, 30% UTS and 15% UTS. No significant differences were detected for any group.*

3.3 Stress-Strain Characteristics

Two time-dependent changes in stress-strain characteristics were monitored during testing: tangent modulus, and strain to 5 MPa.

3.3.1 Tangent Modulus

No differences were seen for initial tangent modulus between creep and fatigue at 60%, 30% and 15% UTS (Table 5). In addition, no differences were found for maximum tangent modulus between creep and fatigue at all stress levels. Creep and fatigue were different when comparing the last recorded tangent modulus prior to rupture ($E_{rupture}/E_{max}$, Figure 27). At 60% and 30% UTS, the modulus ratio prior to rupture during fatigue loading was less than that observed during creep loading ($p < 0.001$ and $p = 0.066$, respectively). The analysis of modulus ratio prior to rupture only included specimens that ruptured and was not performed for 15% UTS because of insufficient numbers. The differences observed prior to rupture arose from the inability of the creep protocol to capture the modulus ratio just prior to rupture. The unloading/reloading cycles occurred at set times that were typically not very close to the time of rupture (see Tables 2 and 3). One 30% UTS creep test was unloaded and reloaded 10 seconds before rupture. In this case, the modulus ratio prior to rupture was 0.54, which was similar to those of fatigue at 30% UTS.

***Table 5**: Initial tangent modulus, maximum tangent modulus and modulus ratio prior to rupture for all stress levels (60%, 30% and 15% UTS). Data is shown as mean ± standard deviation. * indicates significant difference between creep and fatigue at the same stress.*

Stress Level (%UTS)	Initial Tangent Modulus (E_i, MPa)		Maximum Tangent Modulus (E_{max}, MPa)		Modulus Ratio Prior to Rupture ($E_{rupture}/E_{max}$)	
	Creep	Fatigue	Creep	Fatigue	Creep	Fatigue
60	811 ± 86	778± 92	887 ± 106	854 ± 112	0.96 ± 0.03	0.66 ± 0.03*
30	717 ± 62	674 ± 43	783 ± 69	735 ± 40	0.70 ± 0.14	0.51 ± 0.07*
15	598 ± 47	586 ± 76	649 ± 65	645 ± 82	--	0.45 ± 0.12

The calculated tangent modulus tended to have small fluctuations that had a typical range of 20 MPa for all stress levels. The fluctuations appear most evident for the 15% UTS fatigue tests because 20 MPa was a larger percentage of the modulus values observed at this stress level (Figure 27). One 15% UTS creep ligament was loaded for 168 hours with no sign of modulus ratio reduction. A complete set of modulus ratio plots is provided in Appendix H.

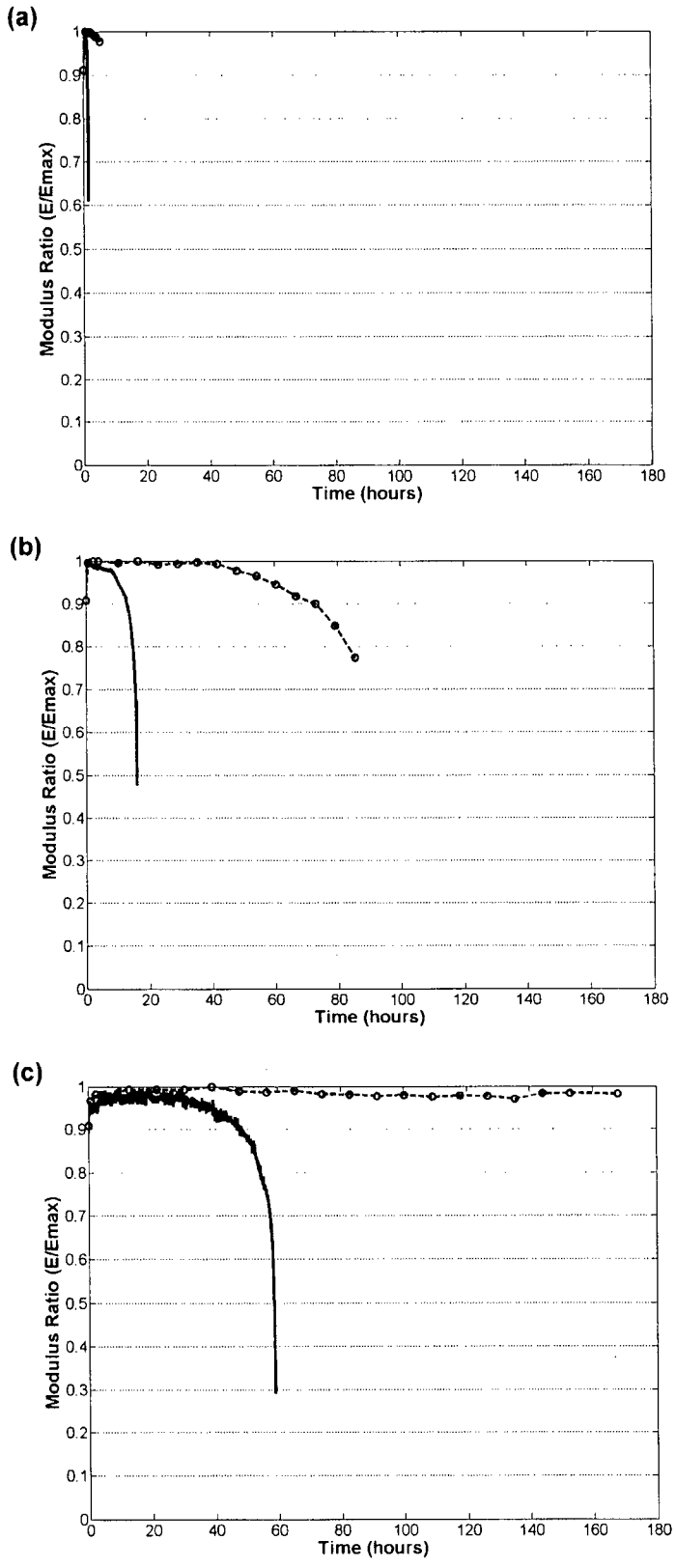

***Figure 27**: Typical modulus ratio plots comparing creep (circles and dashed lines) and fatigue (solid lines) for (a) 60% UTS, (b) 30% UTS and (c) 15% UTS. The circles indicate times when interrupted creep tests were unloaded and reloaded to determine modulus values. All graphs are plotted to the same scale.*

3.3.2 Strain to 5 MPa

There were no differences seen in initial strain to 5 MPa as a percentage of total cycle strain between creep and fatigue at all stresses (Figure 28). In general, strain to 5 MPa as a percentage of total cycle strain initially decreased and then stayed relatively constant for the duration of creep and fatigue loading. Three time points were examined within each group to assess changes over time: 0% time-to-rupture, 20% time-to-rupture, and 70% time-to-rupture (100% time-to-rupture was not analyzed because the creep protocol did not capture this time-point). Results are shown in Table 6.

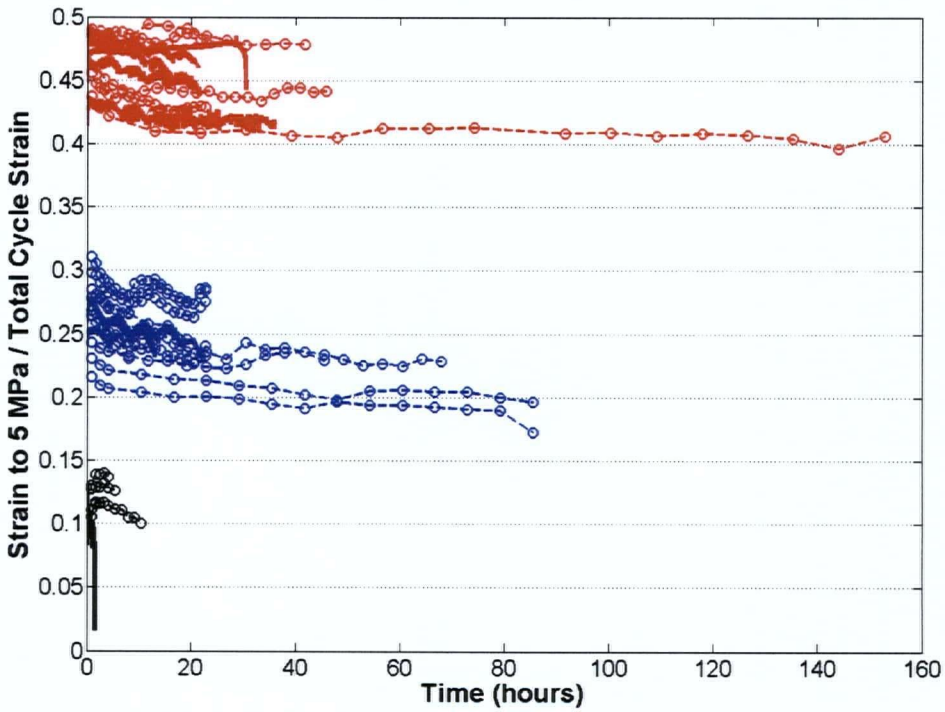

***Figure 28**: Toe-region strains as a percentage of total cycle strain versus time for creep (dashed lines) and fatigue (solid lines). All three stress levels are included on the graph: 60% UTS (black), 30% UTS (blue) and 15% UTS (red).*

***Table 6**: Strain to 5 MPa as a percentage total cycle strain for 0%, 20%, and 70% time-to-rupture. Data is presented as mean ± standard deviation. An asterisk (*) indicates a statistically significant difference between a value and 0% time to rupture for the same group. A square (■) indicates a statistically significant difference between 20% and 70% within the same group.*

Group	0% Time-to-Rupture	20% Time-to-Rupture	70% Time-to-Rupture
Fatigue 60% UTS	0.19 ± 0.01	0.10 ± 0.01*	0.10 ± 0.01*
Creep 60% UTS	0.18 ± 0.02	0.13 ± 0.01*	0.12 ± 0.02*
Fatigue 30% UTS	0.29 ± 0.01	0.26 ± 0.01*	0.25 ± 0.01*■
Creep 30% UTS	0.30 ± 0.03	0.22 ± 0.03*	0.21 ± 0.02*■
Fatigue 15% UTS	0.49 ± 0.01	0.45 ± 0.02	0.44 ± 0.03

No formal comparisons were made across stress levels, but inspection of Figure 27 and Table 6 show that the strain to 5 MPa accounted for a larger part of the total cycle strain for lower stresses.

3.3.3 Modulus Ratio and Increase in Strain

Modulus ratio was graphically compared to increase in strain (Figure 29). Fatigue data at all stress levels had three regions characterized by the modulus ratio: (1) region of increasing modulus ratio, (2) region of constant modulus ratio, and (3) region of decreasing modulus ratio. In the first region, modulus ratio and increase in strain had a non-linear relation where both increase in strain and modulus ratio increased. In the second region, increase in strain continued to increase, but modulus ratio maintained a value close to unity. Typically, the change in increase in strain in region 2 ranged from 0.005 to 0.100. In the last region, modulus ratio began to decrease until rupture while increase in strain continued to rise. Region 3 showed a fairly linear relation between modulus ratio and increase in strain. The fatigue test with a discontinuity at 60% is evident in Figure 29(a) where the third region is disrupted with a large change in strain (without a corresponding change in stress) while the modulus stayed constant. Creep data showed regions 2 and 3, but not region 1. Presumably, the first unloading/reloading cycle (at 0.8 hours) was after the transition from region 1 to region 2. Interestingly, the transition between regions 2 and 3 occurred at higher strains for creep than fatigue at 60% and 30% UTS.

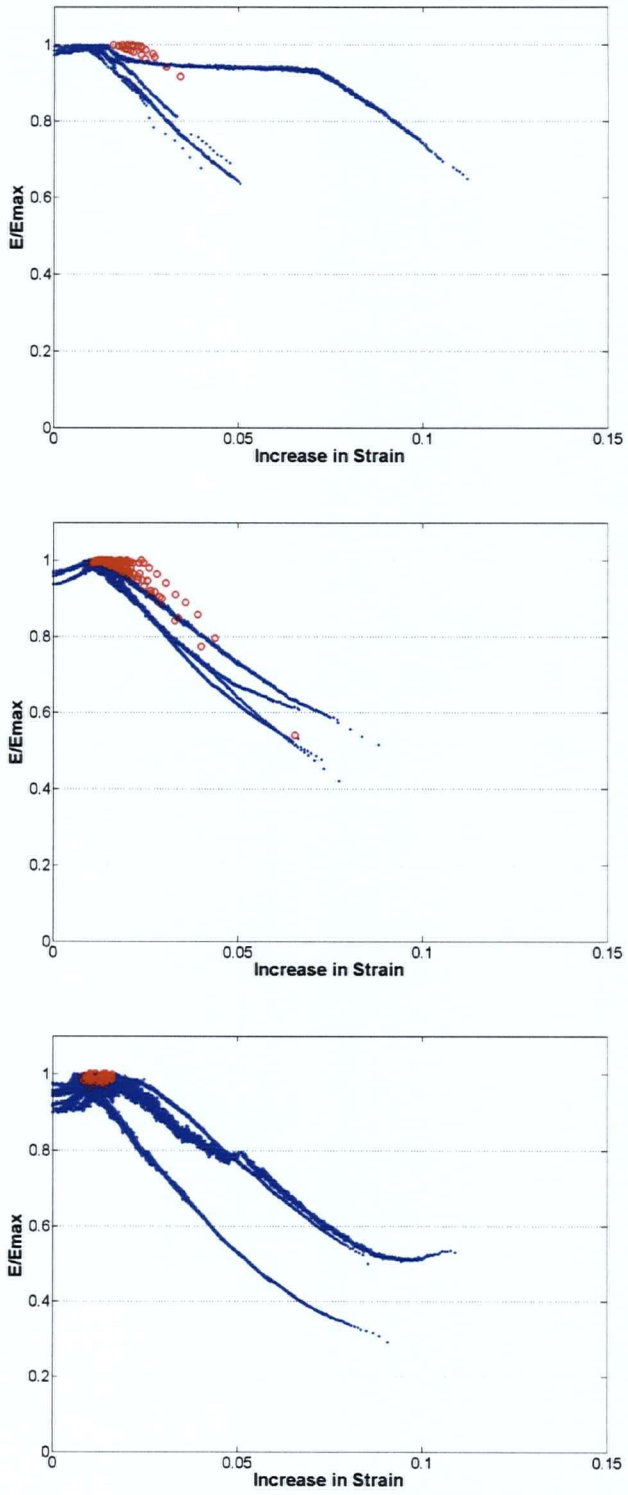

***Figure 29**: Modulus ratio versus increase in strain at (a) 60% UTS, (b) 30 % UTS, and (c) 15% UTS. Fatigue tests (blue dots) showed three distinct regions at all stresses: (1) region of increasing modulus ratio, (2) region of constant modulus ratio, and (3) region of decreasing modulus ratio. At 60%, one fatigue ligament had a discontinuity during region 3 (the same ligament is highlighted in Figure 22 above). Creep tests (red circles) showed regions 2 and 3 at 60% and 30% UTS, and region 2 at 15% UTS.*

At 60% and 30% UTS, the regions 1, 2 and 3 regions were evident for fatigue and regions 2 and 3 were evident for creep. At 15% UTS, the regions 1, 2 and 3 were present for fatigue but only region 2 was present for creep. Only one of the creep ligaments at 15% UTS ruptured during creep loading and it did not exhibit a clear modulus ratio reduction prior to rupture. As a result, none of the 15% creep ligaments showed the third region.

To understand how the three regions of the modulus ratio versus increase in strain translate to time of loading, three time points were selected (the end of the first region, the end of the second region and the end of the third region) and were plotted in Figure 30. The second region occurs over a large time, but appears compressed on a modulus ratio versus increase in strain graph.

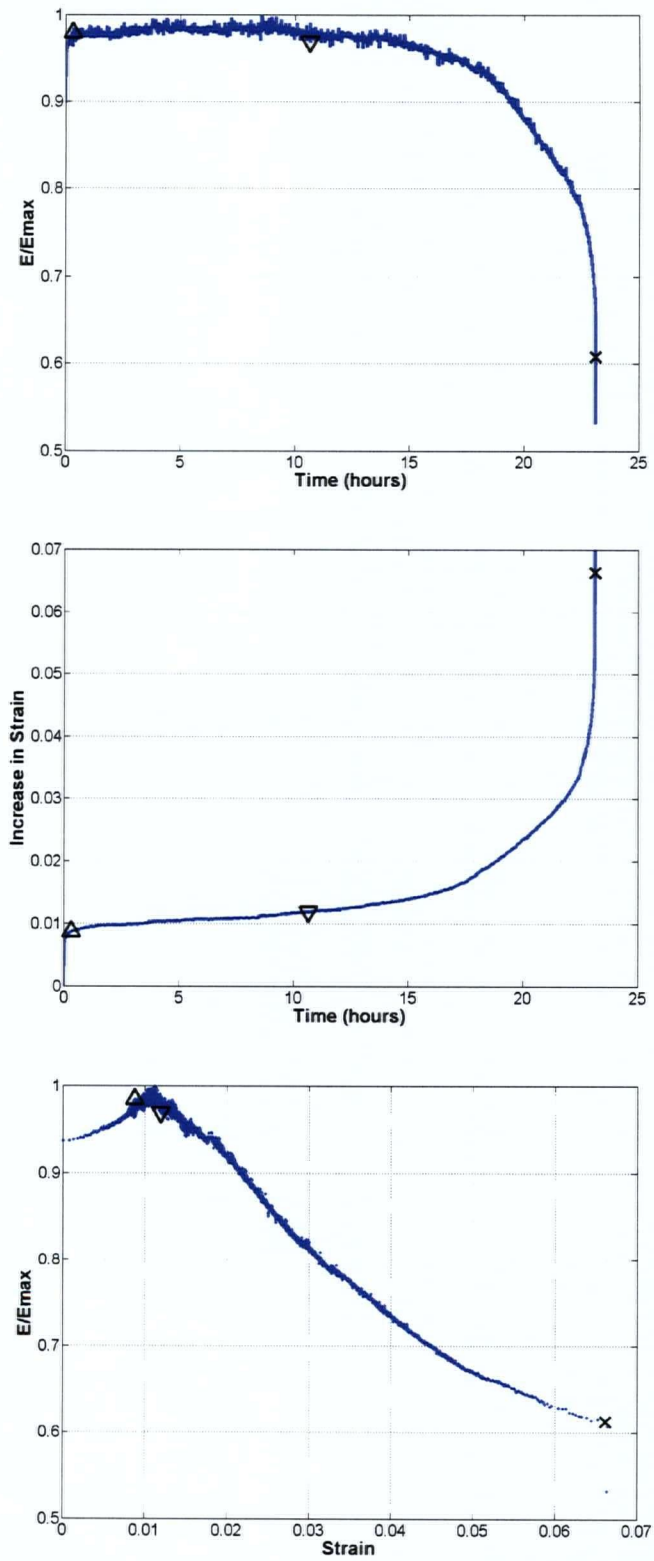

***Figure 30**: Modulus and strain behaviour of a typical fatigue ligament at 30% UTS shown with (a) modulus ratio as a function of time, (b) increase in strain as a function of time, and (c) modulus ratio as a function of increase in strain. The transition between region 1 and region 2 is marked with a triangle (△). The transition between region 2 and 3 is marked with an inverted triangle (▽). The end of region 3 (rupture) is marked with an X-mark (✖).*

3.4 Residual Strength and Strain

Residual strength and strain analysis consisted of three groups: (Group 1) ligaments without previous damage (those that had a modulus ratio greater than 0.97 at the end of creep or fatigue loading), (Group 2) ligaments with previous damage (those that had a modulus ratio less than 0.97 at the end of creep or fatigue loading), and (Group 3) single stretch to failure group. Figures 31 and 32 show the stress strain curves for the single stretch to failure group and the residual strength groups, respectively. Ligaments without previous damage were subjected to 30% creep (n = 3), 15% fatigue (n = 3) or 15% creep (n = 4). Three pairs (left and right MCLs) were nested between 15% fatigue and 15% creep. When all residual strength ligaments, including the nested pairs, were analyzed, the trends and significance did not change; however, the paired ligaments in the 15% UTS creep group were not used to obtain the following results. Ligaments with previous damage were subjected to 30% creep (n = 3) and 15% fatigue (n = 4). No trends were observed to indicate that fatigue and creep tests could not be grouped based on modulus reduction. In groups 1 and 2, the creep and fatigue stress-strain curves were evenly distributed across the range of values.

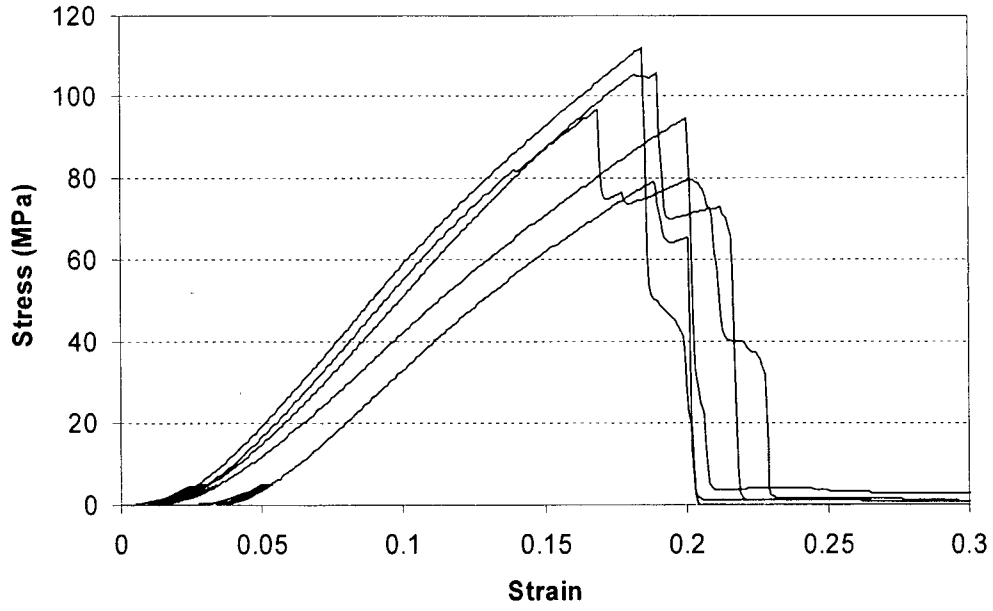

***Figure 31**: Stress-strain plots for the single stretch to failure group. Precondition cycles are included in the data. The mean UTS was determined to be 97.7 ± 12.6 MPa (n = 5).*

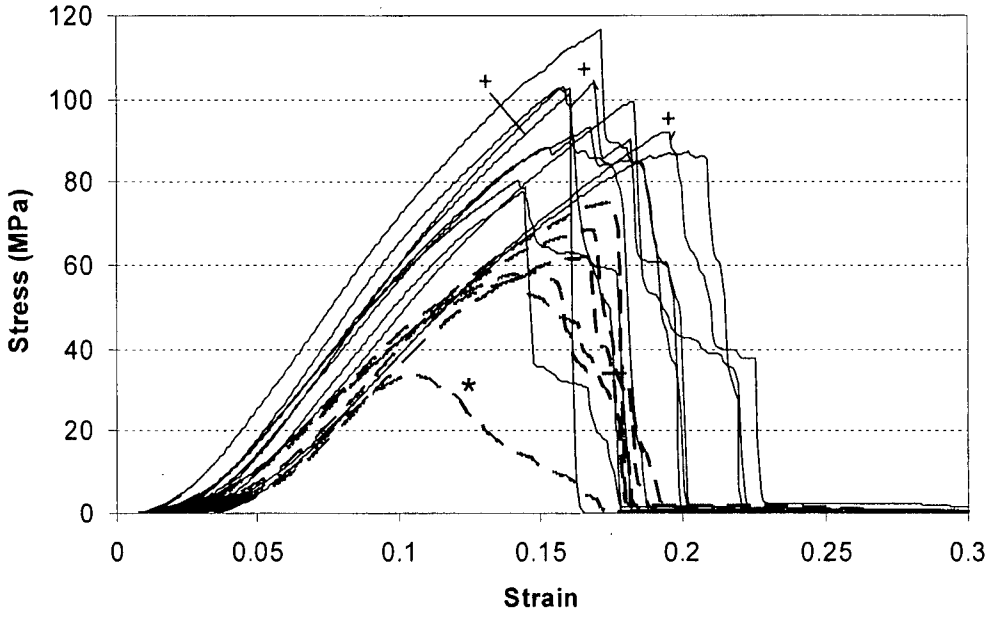

***Figure 32**: Stress-strain plots for the two residual strength groups: ligaments that had a modulus ratio less than 0.97 at the end of creep or fatigue loading (dashed lines, residual strength = 59.3 ± 14.2 MPa) and ligaments that had a modulus ratio greater than 0.97 at the end of creep or fatigue loading (solid lines, residual strength = 93.5 ± 12.6 MPa). The residual strength outlier is marked with an asterisk. Three pairs were nested in the ligaments with a modulus ratio greater than 0.97. One ligament from each pair was removed from the analysis. The excluded ligaments are mark with a plus sign (+).*

No differences were seen between the single stretch to failure group and the ligaments without damage for strength (comparing UTS to residual strength), failure strain, tangent modulus, and strain at 10 MPa. Therefore, the single stretch to failure group (Group 3) and the residual strength group without previous damage (Group 1) were combined to create one group: (Group 4) previously-undamaged group. This new group was then compared to the previously-damaged group (Group 2). Both previously-undamaged and previously-damaged groups were compared for strength, failure strain, tangent modulus and strain at 10 MPa. It is worthy to note the presence of one potential outlier in the previously-damaged group. The potential outlier is marked with an asterisk (*) in Figures 32 and 33. The ligament in question was cyclically loaded at 15% UTS until a point very close to rupture, and, as a result, its modulus ratio was much smaller than the other damaged specimens. In fact, the modulus ratio was closer to those that ruptured during 15% fatigue loading than those that did not. With that being the case, it could be that all damaged ligaments would behave this way if they were loaded to the same percentage of

their lifetime. As a result, the analysis involving residual strength was completed with and without this '*residual strength outlier*'. The results of the analysis with the *residual strength outlier* are presented in Table 7 and the results without the *residual strength outlier* are shown in Table 8.

***Table 7**: Comparison of previously-undamaged ligaments to previously-damaged ligaments including the residual strength outlier. Data presented as mean ± standard deviations followed by the p-value resulting from the comparison of both groups.*

	Strength (Peak Stress, MPa)	**Failure Strain (Strain at Peak Stress)**	**Tangent Modulus (MPa)**	**Strain at 10 MPa**
(2) Previously-Damaged	59.3 ± 14.2	0.1513 ± 0.0251	488.0 ± 64.6	0.0542 ± 0.0061
(4) Previously-Undamaged	87.7 ± 12.3	0.1627 ± 0.0185	613.2 ± 63.4	0.0444 ± 0.0085
p-value	< 0.001	0.041	0.001	0.022

***Table 8**: Comparison of previously-undamaged ligaments to previously-damaged ligaments excluding the residual strength outlier. Data presented as mean ± standard deviations followed by the p-value resulting from the comparison of both groups.*

	Strength (Peak Stress, MPa)	**Failure Strain (Strain at Peak Stress)**	**Tangent Modulus (MPa)**	**Strain at 10 MPa**
(2) Previously-Damaged	64.5 ± 7.4	0.1602 ± 0.0137	472.8 ± 59.0	0.0530 ± 0.0059
(4) Previously-Undamaged	87.7 ± 12.3	0.1627 ± 0.0185	613.2 ± 63.4	0.0444 ± 0.0085
p-value	< 0.001	0.156	0.006	0.057

Comparison of previously-undamaged and previously-damaged ligaments showed that damage resulted in decreased strength and modulus. The effect of damage on the failure strain was unclear because the inclusion or exclusion of the *residual strength outlier* affected the result. When the *residual strength outlier* was included, the failure strain of the previously-damaged group was significantly smaller than the previously-undamaged group; however, when the *residual strength outlier* was excluded, no significant difference was detected between the previously-damaged and previously-undamaged failure strains. Comparison of failure strains and strains-at-ruptures (during creep or fatigue loading, see Section 3.2.2 for strain-at-rupture data) indicated no significant differences between any group when the *residual strength outlier* is

removed (all $p > 0.3$). The outlier also had an effect on the strain at 10 MPa, but to a lesser extent. At the very least, strain at 10 MPa showed a trend towards being greater for previously-damaged ligaments when compared to previously-undamaged ligaments.

3.5 Theoretical results

The damage theory developed in section 2.3.3.1 relied on two experimental curve fits. First, the relation between residual strength and modulus reduction was determined (Figure 33), and, second, the initial rate of modulus ratio reduction was determined as a function of nominal stress (Figure 34).

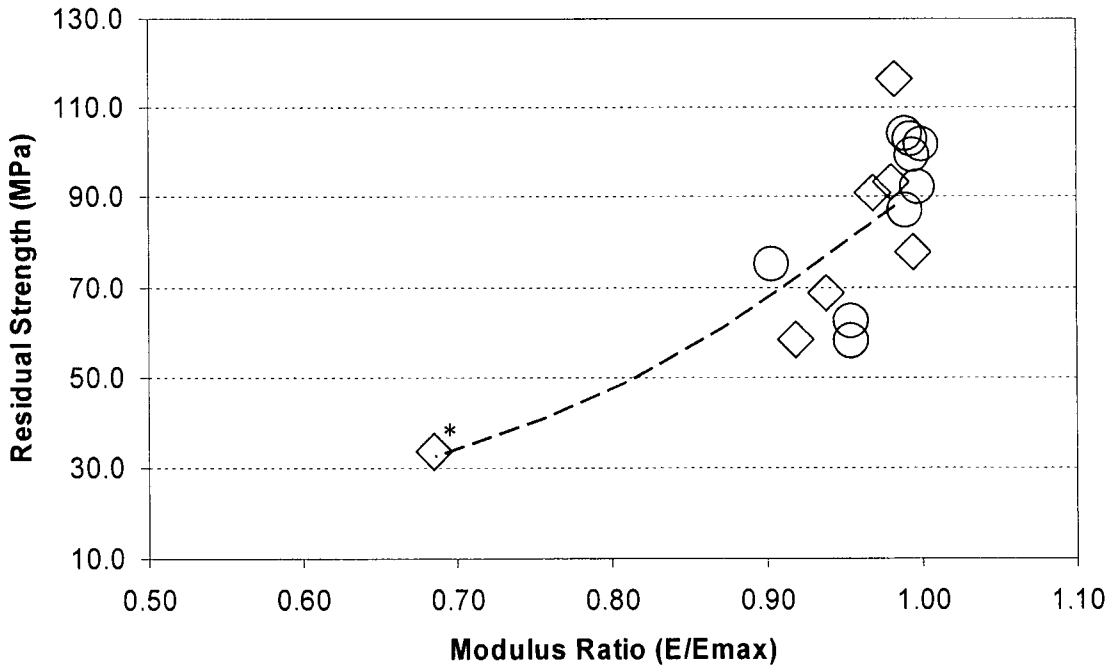

***Figure 33**: Residual strength versus modulus ratio at the end of the loading period. The figure includes data obtained from 15% fatigue (n = 7), 30% interrupted creep (n = 6) and 15% interrupted creep (n = 3) tests. Axes are shown in normal scale because the data collapses on a log-log scale. * indicates the residual strength outlier.*

The data in Figure 33, including the *residual strength outlier*, was fit with a power-law regression resulting in the following relation.

$$RS = B\left(\frac{E_{final}}{E_{\max}}\right)^{C} \tag{9}$$

$$RS = 92\left(\frac{E_{final}}{E_{\max}}\right)^{2.87} \tag{9'}$$

where the $r^2 = 0.71$. Without the *residual strength outlier*, the constants B and C were 97 and 4.87, respectively, and the r^2 value dropped to 0.48.

The second empirically-based part of the damage theory required that the initial damage rate be defined. Initial damage rate is related to the initial modulus ratio reduction. Figure 34 shows the power-law relation of initial modulus ratio reduction with nominal stress.

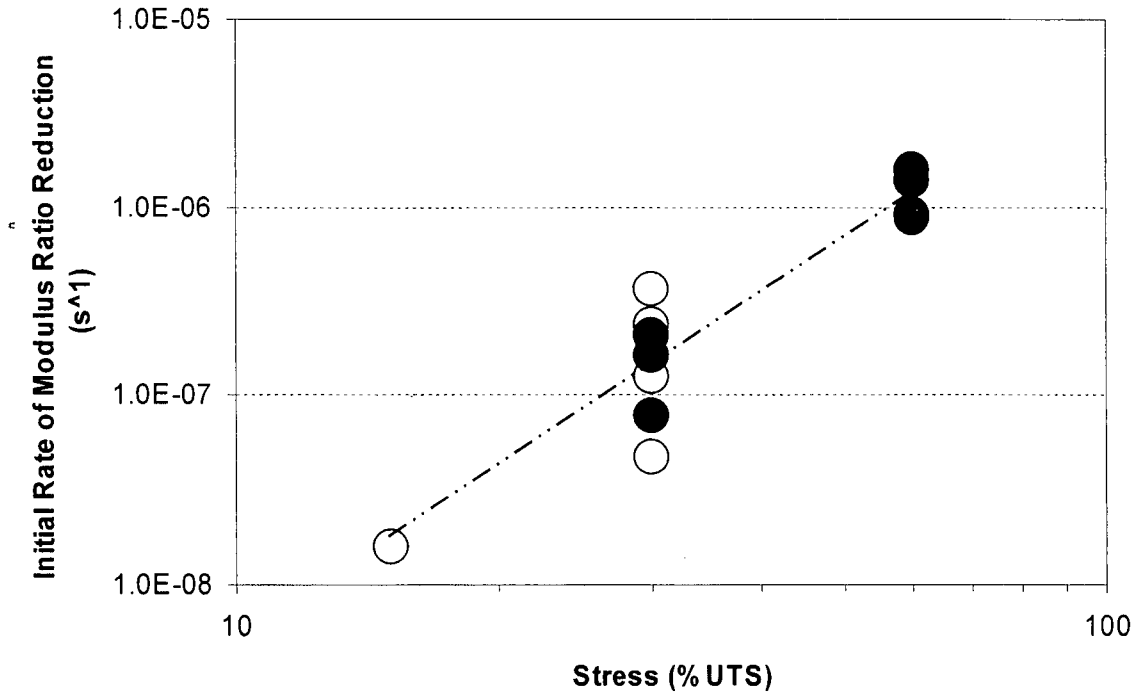

***Figure 34**: Initial rate of modulus ratio reduction as a function of stress (%UTS) for creep ligaments that had a modulus ratio less than 0.97 (open circle) and creep ligament that ruptured (solid circle). Power law regression was insensitive to the addition/removal of the one specimen at 15% UTS (this is not the residual strength outlier).*

The values generated from the regression follow were the following.

$$\frac{d\left(\frac{E}{E_{\max}}\right)}{dt} = F\sigma_o{}^{G} \tag{14}$$

$$\frac{d\left(\frac{E}{E_{\max}}\right)}{dt} = 5\cdot 10^{-12}\sigma_o{}^{3.04} \tag{14'}$$

The r^2 value for the regression was 0.86. The values determined for the constants in equation (9') and (14') were substituted into equation (18) to predict the time-to-rupture for creep loading as a function of nominal stress. Figure 35 shows the results of the theoretical model when compared to the experimental times-to-rupture.

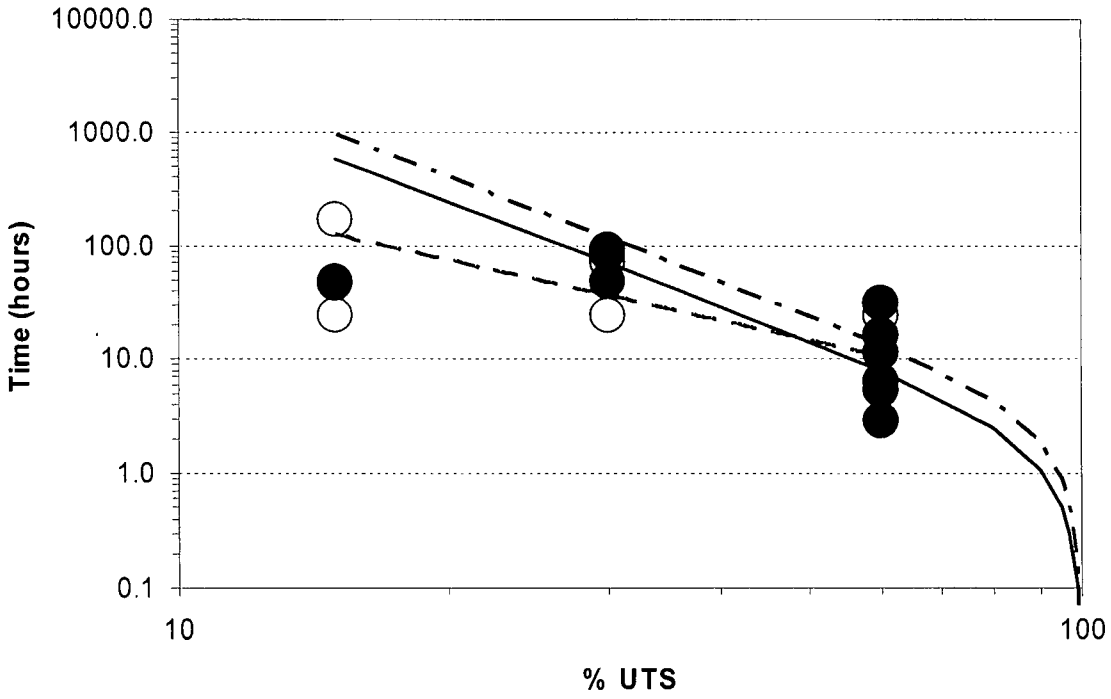

***Figure 35**: Time-to-rupture prediction as a function of nominal stress (%UTS) for interrupted creep. Figure shows the experimental results for interrupted creep tests (solid circle represents ruptured specimens and open circle represents an unruptured specimen), the power-law regression of the time-to-rupture for ruptured creep specimens (dashed line, from Section 3.1), time-to-rupture prediction using damage theory with the residual strength outlier (dot-dash line) and the time-to-rupture prediction developed using the damage theory without the residual strength outlier (solid line).*

The predicted creep time-to-rupture agreed with the experimental data as shown in the figure above. Inclusion or exclusion of the *residual strength outlier* changed the results of the damage theory, but both predictions were reasonable. The longest experimental loading duration at 15% UTS was well below the prediction of the damage theory at that stress.

The damage theory was also used to predict time-to-rupture of fatigue loading. Damage theory predictions based on time-dependent creep damage severely overestimated the fatigue time-to-rupture (Figure 36). The damage theory over-predicts the time-to-rupture by 19700%, 41200% and 66800% of the actual time-to-rupture (approximated using equation (19)) for 60%, 30% and 15% UTS, respectively.

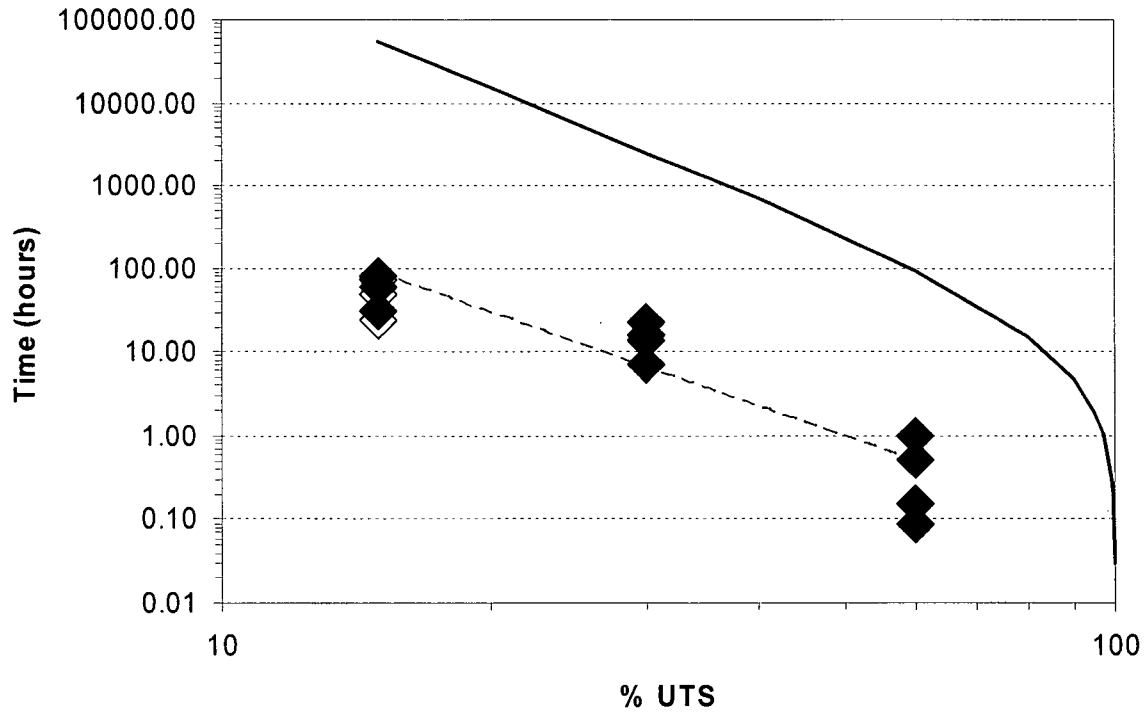

***Figure 36**: Time-to-rupture predictions as a function of nominal stress (%UTS) for fatigue. Figure shows the experimental results for fatigue tests (solid diamond represents ruptured specimens and open diamond represents an unruptured specimen), the power-law regression of the time-to-rupture for ruptured fatigue specimens (dashed line, from Section 3.1), and the time-to-rupture prediction developed using the damage theory without the residual strength outlier (solid line).*

3.5.1 Sensitivity Analysis

The CDM model relies on four empirically derived constants (B, C, F, and G) to predict time-to-rupture and potential errors in the constants can propagate through the theory and affect the predictions. As such, a sensitivity analysis was performed by individually varying the constants by 10% to see the effect of the creep time-to-rupture prediction for a 30% UTS nominal stress (Table 9). The base values of the constants were those fits including all relevant experimental data (B = 92, C = 2.87, F = $-5*10^{-12}$, and G =3.044), giving a creep time-to-rupture prediction of 117 hours.

***Table 9**: Creep time-to-rupture predictions for a 30% UTS nominal stress when empirical constants are varied up and down by 10%. An asterisk indicates multiplication.*

	Time-to-Rupture Prediction (hours)	Error (% of base prediction)
0.9*B	125	7
1.1*B	110	-6
0.9*C	127	9
1.1*C	108	-8
0.9*G	346	196
1.1*G	39	-66
0.9*F	130	11
0.9*F	106	-9

The sensitivity analysis revealed that the CDM model was most sensitive to errors in the constant G with a 10% error producing either a 200% increase or a 60% decrease in the time-to-rupture prediction.

To check what realistic errors could be associated with the constants B and C, one data point at a time was systematically removed from the residual strength data set. The extreme values were recorded and used to calculate the time-to-rupture for creep at 30% UTS (Table 10). Removal of the residual strength outlier caused the largest increase in B and C. Both B and C increased or decreased together, compounding error in the prediction. The same method was used on the initial rate of modulus ratio change data set to provide realistic errors in F and G (Table 10). The constant F and G changed in opposite directions when data was removed, minimizing the effect of error in both terms. The largest change in the time-to-rupture prediction arose from the

exclusion of the *residual strength outlier* (-40%). This error (shown as the difference between the solid and dot-dash lines in Figure 35) was much to small to account for the overestimation of fatigue time-to-rupture (Figure 36). Data at 60% UTS was used to show the relative values. The inclusion or exclusion of the *residual strength outlier* altered the fatigue time-to-rupture prediction by 7 hours. For comparison, the overestimation of the fatigue time-to-rupture prediction was 92 hours.

***Table 10**: Creep time-to-rupture predictions for a 30% UTS nominal stress given two realistic extremes of empirical constants B/C and F/G.*

	Time-to-Rupture Prediction (hours)	Error (% of base prediction)
B = 97, C = 4.87 F = $-5*10^{-12}$, G = 3.044	70	-40
B = 90, C = 2.79 F = $-5*10^{-12}$, G = 3.044	121	4
B = 92, C = 2.87 F = $-7*10^{-12}$, G = 2.94	121	4
B = 92, C = 2.87 F = $-3*10^{-12}$, G = 3.14	138	18

4.0 DISCUSSION

This experimental work answered two main questions. First, does loading condition (static creep or cyclic fatigue) alter damage accumulation in ligament as measured by changes in mechanical behaviour? Second, can fatigue time-to-rupture be predicted using a continuum damage model based on creep behaviour? The second question can, in fact, help to answer the first question. To facilitate analysis and discussion, the first major question was divided into four sub-questions. Each sub-question and applicable results are discussed in separate sections.

4.1 Does creep or fatigue result in an earlier time to rupture?

Simply stated, ligament damage accumulation is affected by loading conditions and cyclic loading causes more damage than static loading alone. Fatigue has two potential sources of damage: one resulting from the time at high load (creep-like, time-dependent damage) and one resulting from the varying load (cycle-dependent damage). This results from the constraint that ligaments can only resist tensile loads. As such, fatigue loading involves a non-zero mean stress; therefore, fatigue loading will include a creep response. In contrast, creep loading causes damage only by subjecting the ligament to a continual non-zero stress (time-dependent damage) and does not involve damage from a varying load (cycle-dependent damage) because the load is held constant. Evidence in support of this theory was provided by the time-to-rupture analysis.

Fatigue loading caused earlier rupture than creep loading in ligament. However, data from Wang and coworkers (66,67) did not find a similar relationship in tendon. They did not explicitly compare creep and fatigue times-to-rupture; however, they did provide graphs showing the times-to-rupture for creep (Figure 37) and fatigue (Figure 38). An informal, visual comparison of their data revealed that fatigue times-to-rupture at 1.1 Hz were very similar to creep times-to-rupture. Data was compared at maximum stresses corresponding to 55%, 30% and 15% yield stress (80, 43, and 22 MPa). For clarity, Wang and Ker (66) used yield stress in the same way other damage theories use UTS, so percent-yield of wallaby tail tendon should be comparable to

percent-UTS of rabbit MCL. They found that time-to-rupture decreased with increasing frequency, indicating that some cycle-dependent damage occurs in tendon.

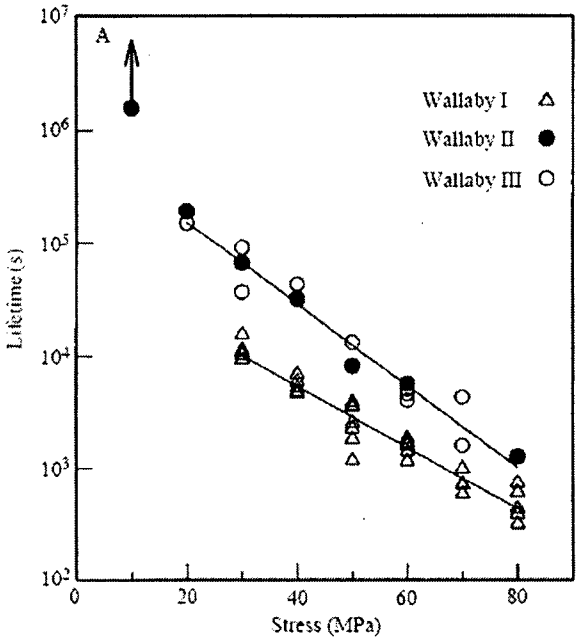

***Figure 37**: Time-to-rupture as a function of applied stress for wallaby tail tendons subjected to creep loading. From Wang and Ker (66).*

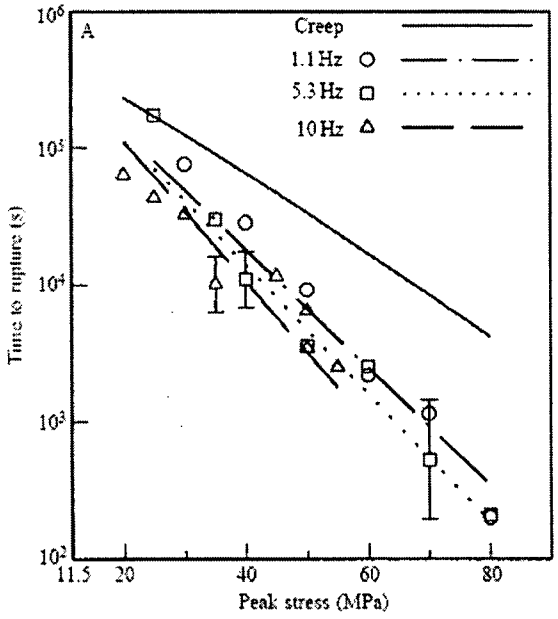

***Figure 38**: Time-to-rupture as a function of applied stress for wallaby tail tendons subjected to fatigue loading at 1.1, 5.3 and 10 Hz. The solid line is the prediction of fatigue time-to-rupture from Wang and Ker's damage model. From Wang et al. (67).*

Data collected by Wren et al.(75) with human Achilles tendon suggests that fatigue loading causes earlier rupture than creep loading, but, once again, no explicit comparison was made. Inspection of their data (Figures 39 and 40) suggests that fatigue times-to-rupture were less than those of creep at similar initial strains. Schechtman and Bader (48) varied both frequency and stress during their tendon fatigue tests so it is difficult to relate the influence of cycle-dependent damage. If they had not varied frequency and stress together, then the square wave loading would have provided insightful information about the contributions of time- and cycle-dependent damage because idealized square wave loading would not alter the time at high load. The tendons studies above do not provide a clear understanding if fatigue time-to-rupture is less than creep time-to-rupture. Results from the present study indicate that the additional cycle-dependent damage involved in fatigue loading causes a significant decrease in time-to-rupture (at 60% and 30% UTS) in ligament.

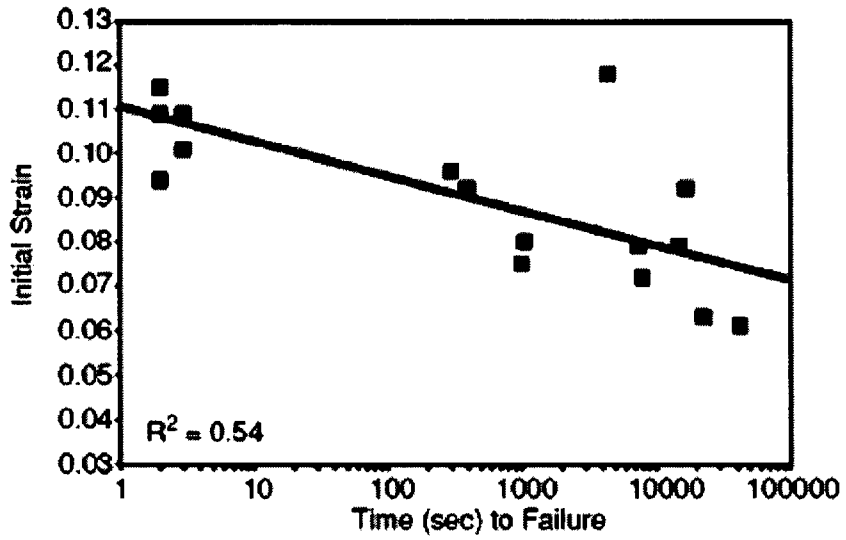

***Figure 39**: Time-to-rupture as a function of initial strain for human Achilles tendons subjected to creep loading. From Wren et al. (75).*

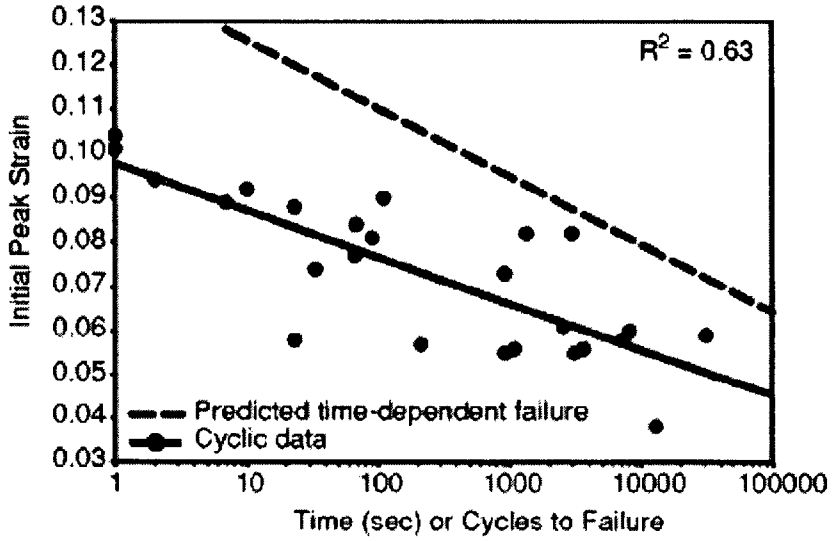

***Figure 40**: Time-to-rupture as a function of initial strain for human Achilles tendons subjected to fatigue loading at 1 Hz. The dashed line is the fatigue time-to-rupture prediction from Wren et al.'s damage model. From Wren et al. (75).*

The idea of additional cycle-dependent damage is further reinforced with the CDM model because the model over-predicts the time-to-rupture for fatigue loading. The model was based solely on time-dependent damage. Cyclically varying the nominal stress in the model did not predict enough damage accumulation to match experimental damage accumulation. The model is based solely on time-dependent damage, and therefore, should be able to predict time-dependent damage behaviour at a given nominal stress. This implies that either the model does not predict time-dependent damage correctly or, more likely, fatigue loading in ligaments involves both time- and cycle-dependent damage. Figure 35 shows good agreement between predicted and experimental time-to-rupture, so it seems that the continuum damage model does a fair job at predicting time-dependent damage. It is reasonable to assume that the over-prediction of time-to-rupture arises because the continuum damage model does not account for additional cycle-dependent damage caused by fatigue loading.

Time-dependent damage models also over-predict fatigue time-to-rupture in tendon. Both Wang and Ker (67) and Wren et al. (75) developed damage theories with differing damage accumulation rates and failure criteria. In both cases, the models over-predicted the time-to-rupture of fatigue loading, similar to the present study. Data presented by Wang and Ker (Figure 38) was used to estimate the percent difference between the experimental data and the predicted

time-to-rupture. At 55%, 30% and 15% yield stress (80, 43, and 22 MPa), their CDM model over-predicted the time-to-rupture by approximately 1200%, 375% and 67%, respectively. Wang and Ker (67) performed fatigue tests with a minimum stress of 11.5 MPa. This explains why the error between their damage theory and experimental results decreases at lower maximum stresses. As the maximum stress approached 11.5 MPa, the loading becomes more like a constant stress at 11.5 MPa (more like a creep test), so their model provided a better prediction. Direct comparison to the over-prediction of the model developed by Wren et al. is difficult because they use initial strain as an input to their damage theory.

The information above suggests that both tendon and ligament are affected by time- and cycle-dependent damage. Cycle-dependent damage may cause greater effects in ligament than in tendon, as highlighted by earlier times-to-rupture of fatigue tests and greater over-prediction of time-to-rupture of the time-dependent CDM model. However, these apparent ligament and tendon differences may result from the higher minimum stresses use to study tendon fatigue (11.5 and 10 MPa in tendon compared to 1 N (~0.3 MPa) in ligament). Higher minimum stresses cause a higher mean stress and more time-dependent damage; therefore, the tendon fatigue test may have higher relative contributions of time-dependent damage to the total damage because of the loading protocol. At the present time, it is unclear if the greater effect of cycle-dependent damage on ligament reflects loading protocol differences or true differences between tendon and ligament.

As stated above, ligament appears to be strongly affected by cycle-dependent damage, as highlighted by earlier ligament ruptures in fatigue than in creep. At linear-region stresses, all fatigue ligaments ruptured sooner than all creep ligaments at the same stress level. At the toe- to linear-region transition stress, one creep test ruptured before some of the fatigue ligaments, however, it ruptured later than its matched pair in fatigue loading. Comparison of interrupted and non-interrupted creep at 60% UTS provided further evidence to show that ligament is affected by cycle-dependent damage. Interrupted creep ligaments at 60% UTS were unloaded and reloaded a maximum of 10 unloading cycles before rupture. This caused a significant decrease in time-to-rupture. Clearly, cycle-dependent damage at high stresses accounts for a significant portion of the total ligament damage.

The evidence supporting the existence of both cycle-dependent and time-dependent damage has been established but nothing has been proposed to explain why or how these mechanisms work. Before speculation on specific damage mechanisms can be made, the results and significance of the recorded strain profiles need to be examined.

4.2 Do the strain profiles differ between creep and fatigue?

Strain in response to loading may be the most clinically relevant material behaviour. Greater strain for a given load will result in greater ligament/joint laxity which, in turn, may induce damage in other structures and cause further joint laxity (as previously depicted in Figure 4).

Insightful information can be gained by comparing ligament strain response to creep and fatigue loading. When comparing normalized time-points prior to rupture (Figures 21 and 24), creep resulted in greater increases in strain than fatigue. This interesting finding suggests that different loading conditions affect the microstructure of ligament in different ways, resulting in dissimilar behaviour. One major question arises in light of this finding: why would cyclically loaded ligaments strain less than statically loaded ligaments for a given normalized time-point? While the present study was not designed to answer this question, knowledge from the literature can be applied to help elucidate the behaviour.

The differences in strain profile may be partially explained by fibre recruitment (Figure 41). As explained in Section 1.1, unstressed fibres are crimped and straighten out when loaded (become recruited into load-bearing). For clarity, loading of individual fibres can be simplified with an off-on two step load-bearing. In an off-on model, crimped fibres do not support load, whereas recruited (straightened) fibres do support load and some fibres become recruited before others (Figure 42).

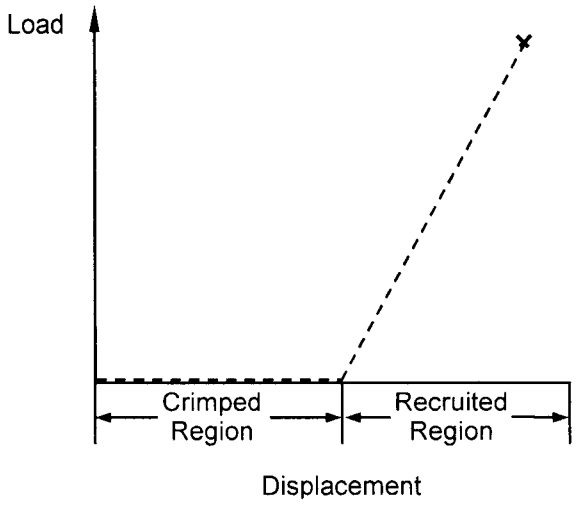

***Figure 41**: Simplified conceptual fibre recruitment for an individual fibre. Each fibre has a crimped region where load is near zero, followed by a recruited region where load and displacement are linear up to rupture (X mark). This model is a large simplification only used to explain concepts. In reality, fibres likely resist some load while still crimped and may not behave in a linear manner when straightened.*

Work by Thornton et al. (62) showed that fibre recruitment is a time-dependent phenomenon. In that study, the number of recruited fibres immediately following a ramp to a nominal stress (stress based on fully intact CSA) was less than the number of recruited fibres after the ligament was held at that same nominal stress for 20 minutes. Therefore, creep loading causes fibre recruitment, first, by the initial loading ramp, and second, by the sustained load (an additional time-dependent fibre recruitment). The concepts above are developed in Figures 42 and 43.

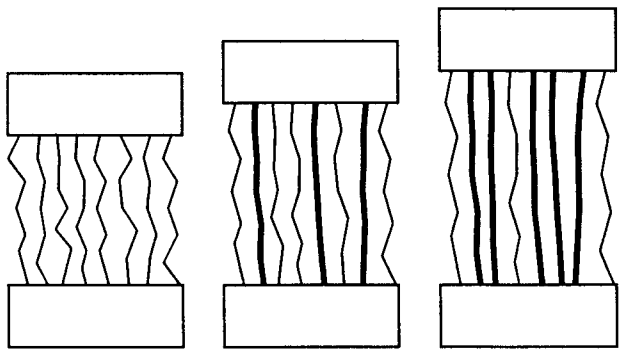

***Figure 42**: Simplified conceptual fibre recruitment for a theoretical eight fibre ligament. All fibres are crimped in the unstressed state (left). Some fibres become recruited into load bearing immediately following the application of a load (middle). Additional fibres are recruited into load bearing following a sustained load (right). Bold lines indicate recruited fibres.*

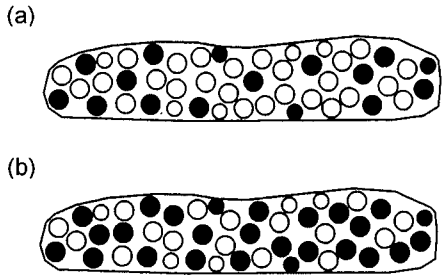

***Figure 43**: Schematic cross section of a ligament showing fibre recruitment (a) after the initial loading ramp and (b) after a sustained load at the same nominal stress. Each figure shows a ligament with both crimped (open circles) and recruited (solid circles) fibres. Sustained loading (b) causes additional fibre recruitment. In both cases, the recruited fibres are distributed throughout the cross-section.*

Thornton et al. saw this phenomenon in both the toe- and linear-region for creep tests. Fibres subjected to fatigue loading may not have the additional recruitment caused by sustained load because of continual unloading/reloading. This would result in a smaller increase in strain for fatigue loading.

The above explanation, by itself, implies that fatigue loading would be beneficial in a physiologic setting because the ligament would strain less at a given maximum load when compared to creep loading; however, the above explanation has not included the effects of damage on ligament strain. If fatigue loading results in less fibre recruitment, then the applied forces will be resisted by fewer fibres. For a given nominal stress, the effective stress on each recruited fibre during fatigue would be higher than the effective stress on each recruited fibre in creep. Fibres recruited during the initial loading ramp likely experience a decrease in load during the sustained loading because the load may be redistributed to fibres that are newly recruited during the sustained loading. The effective stress on the fibres will be a function of how many fibres are recruited. Fatigue loading may result in less fibre recruitment causing higher effective stresses on those fibres that are recruited. This will result in a faster damage rate in fatigue (as damage rate is dependent on effective stress – Equation (16)), which helps to explain the earlier time-to-rupture seen in fatigue loading. The faster damage rate means that fatigue loading will progress through the three strain stages (primary, secondary and tertiary) faster than creep loading. This is evident when comparing creep and fatigue increases in strain at specific, absolute time-points and steady-state strain rates.

At a high linear-region stress (60% UTS), fatigue increase in strain progressed through the three strain stages (and ruptured) earlier than creep. As such, fatigue increase in strain was greater than creep at early time-points (0.8 and 4.2 hours). At a late time-point (24 hours), creep ligaments had also progressed through the three strain stages (and ruptured) and the increase in strain of creep and fatigue were similar. At a low linear-region stress (30% UTS), neither creep nor fatigue had progressed to the tertiary strain stage at early time-points (0.8 and 4.2 hours), so creep increase in strain was greater than that of fatigue; however, all fatigue ligaments had progressed through the three strain stages (and ruptured) by a late time-point (24 hours). Only two creep ligaments had begun the tertiary strain and no creep ligaments had fully progressed though all three stages at the same time-point (24 hours). Fatigue increase in strain was greater than creep at this late time-point. At the toe- to linear-region transition stress, both fatigue and creep ligaments were in the primary or secondary strain stage at early time points (0.8 and 24 hours), so creep increase in strain was greater than fatigue. At a late time-point (24 hours), some fatigue ligaments had began tertiary strain resulting in similar increases in strain for fatigue and creep.

The strain results can be interpreted with the fibre recruitment theory. During fatigue, the effective stresses on recruited fibres will be higher, causing a faster damage rate. The faster damage rate causes the fatigue to progress through the three strain stages earlier, which increases ligament strain. This damage acceleration is magnified at higher nominal stresses because the effective stresses are higher, and damage rate is greater at higher stresses (see the CDM theory, Equation (16)). This explains why the relation of creep and fatigue increases in strain varied with nominal stress at a specific time-points (e.g. at 0.8 hours, fatigue increase in strain was greater than creep at 60% UTS, but less than creep at 30% and 15% UTS). Simply stated, higher nominal stress causes a greater acceleration of damage and ligaments progress through the strain stages and rupture at earlier times. Accelerated fatigue damage was also evident when comparing creep and fatigue steady-state strain rates. At all stresses, there was at least a trend for fatigue steady-state strain rates to be greater than creep steady-state strain rates. The strains recorded at specific time-points and the steady-state strain rates observed provide more evidence in support of the fibre recruitment theory described above.

Fibre recruitment is likely not the only factor contributing to the observed strain behaviour. Other factors affecting ligament strain may include fascicle rotation (50), or fibre sliding (50). In

the future, these factors could be included in the fibre recruitment theory to aid in explaining ligament strain behaviour.

The discussion above implies that strain is affected by damage. With strain being affected by damage, one might think that strain would be a good predictor of damage. The potential use of strain and stress-strain characteristics as damage indicators is discussed in the following section.

4.3 Does creep or fatigue cause changes in the stress-strain characteristics?

Mechanical evidence of damage has potential to manifest itself in numerous ways. Damage can affect the strain response, as previously discussed, but it can also affect the stress-strain relationship (Figure 44). There are two regions of the stress-strain curve that could show the effects of damage: the linear-region and toe-region. In the case of repeated loading in load control, the stress-strain curve can also be translated along the strain axis (strain translation). Strain translation can be quantified by the valley strain in each cycle. Peak strain in each cycle includes the combined effects of strain translation, toe-region changes and linear-region changes.

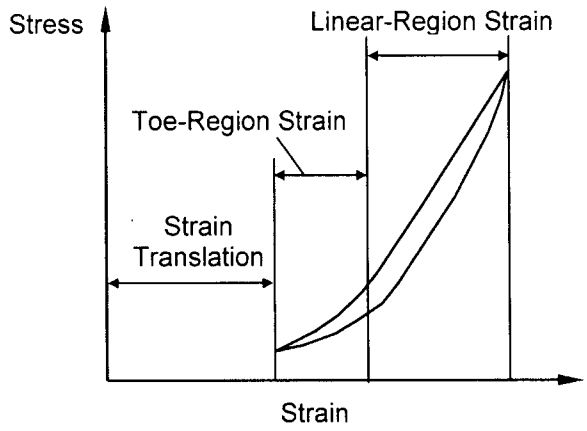

***Figure 44**: Schematic diagram showing the two regions of a ligament stress-strain curve: the toe-region and linear-region. In repetitive loading, the stress-strain curve can be displaced along the strain axis (strain translation).*

The way damage affects stress-strain behaviour depends on how ligament damage occurs. Collagen is the main load bearing structure in ligament (44,68), so fibre rupture (resulting from collagen molecule rupture or breaking crosslinks between molecules) should be the main form of mechanical damage. Shorter fibres are recruited first and likely rupture first as well. The resulting damage will affect both regions of the stress-strain curve, and, in the case of repeated loading, the strain translation. With shorter fibres ruptured, larger strains are required before load is supported, thus there will be increased strain translation and increased toe-region strain. At some point, enough fibres will rupture to cause a reduction in tangent modulus and a corresponding increase in linear-region strain.

Damage to the matrix could also affect the toe- and linear-regions. If proteogylcans are damaged and their ability to transmit shear forces (45,46,64) is compromised then fibre interactions may be altered. Matrix damage likely has less of an effect on the mechanical response of ligament than fibre rupture because the shear modulus of proteoglycans is much lower than the elastic modulus of collagen fibrils (44). Differentiating between fibre damage and matrix damage is very difficult without looking directly at the microstructure. The mechanical evidence of damage observed during creep and fatigue loading likely includes both fibre and matrix damage, but the proposed explanations have more emphasis on fibre damage because fibres are thought to be the main load-bearing structure in ligament.

The linear-region response was characterized by tangent modulus. Typically, modulus ratio (E/E_{max}) progressed through three regions during creep (interrupted) and fatigue loading: (1) a region of increasing modulus ratio, (2) a region of constant modulus ratio, and (3) a region of decreasing modulus ratio (Figure 27). These three regions can be explained using the ideas of fibre recruitment and effective cross-sectional area.

During the initial stage of loading (region 1), fibres are recruited into load-bearing and the effective cross-sectional area increases. In this region, not enough fibres are recruited to resist the applied loads, so additional strain and fibre recruitment occurs. Some fibre rupture can potentially occur during this region if the effective stress is high enough. Yahia et al. (76) found that some fibres ruptured when subjected to a single stretch greater than 10% strain. In the present study, a 10% strain (in the single stretch to failure group) corresponded to stresses between 30 and 60 MPa (Figure 31). In fact, a slight inflection point was observed around 10%

strain for ligaments subjected to the stretch to failure protocol. While work by Yahia involved a single stretch and not a repetitive or sustained load, it did show that fibre rupture can occur at nominal stresses below the UTS. In fact, Thornton et al. (62) observed some mechanical discontinuities during the first 30 cycles of repetitive loading with a maximum stress of 30 MPa. A temporary drop in modulus was observed as well as corresponding fibre recoiling. They suggested that the discontinuities and fibre recoiling resulted from fibre ruptures. Thirty cycles of loading at 30 MPa would be within region 1, and the modulus recovered following the fibre ruptures. At some point, enough fibres will be recruited to resist the applied load and the modulus ratio approaches unity.

Region 2 is a region where the modulus ratio maintains a value close to unity. In this region, the modulus ratio is at a maximum. Region 2 involves a maximum effective area of load-bearing fibres, which involve varied amounts of fibre stretch. For clarity, fibre load-bearing may involve two sequential stages. First, the fibre straightens out (becomes recruited), then the fibre stretches until rupture. Once again, an off-on model can be used to simplify this two stage loading (Figure 45), where crimped fibres do not contribute to load-bearing and only straightened fibres support load. From this perspective, a ligament with no visible crimp may still involve an uneven distribution of load because each fibre may be stretched to different amounts. Fibres subjected to greater stretch will likely be carrying more load than those subjected to less stretch (in both cases the load may still be less than when the fibre was initially recruited as discussed in Section 4.2). This becomes important at high stresses where very few crimped fibres can be observed (62). Throughout region 2, the applied forces are resisted by a certain number of fibres but there is continued, but limited, capacity for additional fibre loading (either through small amounts of fibre uncrimping or fibre stretching). Presumably some damage occurs during this region, but the modulus ratio is maintained around unity because additional fibres are available to support more load. At some point, virtually all remaining fibres will be fully loaded and additional damage will cause a decrease in modulus ratio (region 3), and eventually lead to rupture. Ligament fatigue data from Zec et al. (78) also showed that fatigue loading began with an initial stiffening period, followed by a relatively constant period. Most of their specimens did not fail during loading, so a region of decreasing modulus was not observed.

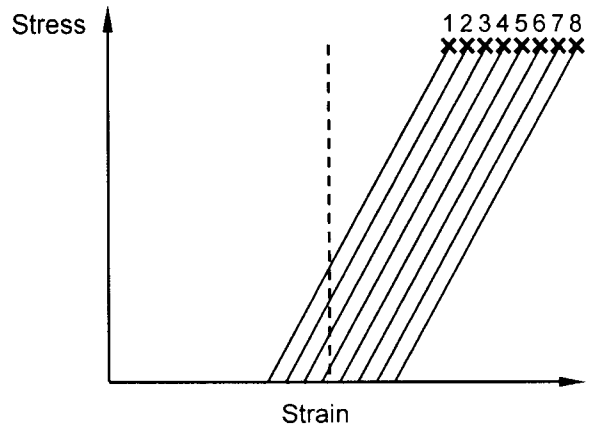

***Figure 45**: Theoretical simplification of fibre loading in ligament. Eight fibres are shown with variable amount of crimp (zero stress region), followed by a linear response. The dashed line shows a strain where fibres 1 to 4 are loaded and fibres 5 to 8 are still crimped and unloaded. Fibres 1 to 4 are subjected to variable amounts of stress because they become loaded at different strains.*

Current modulus results provide some interesting findings. First, initial modulus and maximum modulus were not different between creep and fatigue. No difference in initial modulus was expected because the initial loading curve for creep and fatigue had the same half-sinusoidal profile. The finding that the maximum modulus did not differ between creep and fatigue results from the fact that both groups were loaded to the same maximum stress. The amount of recruited fibres required to resist the load depends on the maximum stress. The modulus ratio prior to rupture was smaller for fatigue ligaments than it was for creep ligaments. The creep tests were periodically unloaded to determine modulus and each unloading was followed by long period of creep loading. Therefore, higher modulus ratio prior to failure arose from the inability of the creep protocol to capture the actual modulus ratio at rupture. One 30% UTS creep ligament that happened to undergo an unloading cycle immediately (10 seconds) before rupture had a final modulus ratio of 0.54, which was comparable to that of 30% fatigue ligaments prior to rupture.

Both toe-region changes (as shown by strain to 5 MPa) and linear-region changes (as shown by increasing linear strain resulting from a tangent modulus reduction) paralleled each other in progression after an initial period of non-linearity. The total cycle strain is a summation of strain in the toe- and linear-regions. Total cycle strain increased during loading, but the relative size of the toe- and linear-regions was fairly constant in the later stages of loading. An initial decrease

in the relative size of the toe-region was observed (Figure 28). This decrease corresponded to the initial region of increasing modulus ratio (Region 1) and may be affected by initial fibre recruitment or viscoelastic effects. This can be seen by comparison of the 168 hour creep test shown in Figure 27(c) and Figure 28. The constant proportion of toe-region strain to linear-region strain after region 1 (time of increasing modulus ratio) has implications for damage modeling because it means that only linear-region damage needs to be monitored without losing additional information.

As shown above, toe- and linear-region changes can be monitored with tangent modulus, but the other stress-strain characteristic, strain translation, has not been addressed. The strain translation mirrored the increase in strain (peak strain) during loading with minor deviation during the tertiary strain stage. Since peak cycle strain (analyzed as increase in strain) is more comparable to creep loading, so the relationship between strain translation and modulus was quantified using increase in strain (Figure 29). A clear relationship was seen between modulus ratio and increase in strain with an initial nonlinear region of increasing modulus ratio and increase in strain (corresponding to region 1 described above), followed by a region of constant modulus ratio where increase in strain extended (corresponding to region 2 described above), and finally a region of decreasing modulus ratio and increasing increase in strain (corresponding to region 3 described above). In fact, the transitions between regions 1-2 and 2-3 roughly corresponded to the transitions between the three stages of strain. These relationships can be explained with the fibre recruitment theory. As described above, the three regions are likely influenced by a strain-based fibre recruitment process; therefore, it is understandable that increase in strain and modulus ratio have a clear relationship. The nonlinearity observed in region 1, again, may be influenced by initial fibre recruitment or viscoelastic effects.

A rather puzzling finding was that the increase in strain change during region 2 was typically between 0.005 and 0.01 with no apparent dependency on stress (or total strain) level (no statistical analysis was completed). At the present time, no complete explanation can be offered concerning this behaviour. Region 3 showed a clear linear relation between modulus ratio and increase in strain. A similar relationship was observed by Wang and Ker (66) in wallaby tail tendon. The tendons underwent primary, then tertiary strain without secondary strain. Also, they interrupted their creep tests based on increase in strain (so-called 'extra strain'). As a result, they

did not capture the initial nonlinear region between modulus and strain and only observed the final linear region (region 3).

Other researchers have speculated on the interactions of strain and damage. Wren et al. (75) suggested that strain is the major determinant of damage. They made this suggestion because they found that initial strain was the best predictor for time-to-rupture for Achilles tendon. In the present study, no appreciable increase in r^2 value is observed when initial strain is used instead of nominal stress. Theoretically, nominal stress and initial strain should be fairly interchangeable if the modulus is similar, from a mechanics point of view. They may have found better correlation between initial strain and time-to-rupture because their specimens had a very large range of UTS (based on their Figure 5a). Another possible factor could have been error in their CSA measurement. In contrast to Wren et al, Schechtman and Bader (49) propose that strain is not a reliable indicator of damage in tendon because rupture is a strain-based process governed by a limiting value of strain. However, a damage process based on a limiting value of strain may actually imply that strain could be a reliable indicator of damage, but it should be noted that the present study related increase in strain (or valley strain) to a modulus reduction, not total strain. Provenzano et al. (43) suggest that strain can be used to define ligament damage. They stretched ligaments to a certain strain then measured the permanent strain after unloading. Viscoelastic effects were eliminated by allowing the ligament to recover for a period longer than 10 times the loading duration. Obviously this technique could not be applied to the present study because of the long durations of loading. The ratio of loading to recovery duration may deviate from the value of 10 for longer tests, but it is unknown what the ratio would be for longer tests. Clearly using strain as a damage indicator for tendon is controversial. For the present study, strain is not the best candidate to indicate damage in ligament because of viscoelastic complications. In composites research, Smith and Weitsman (57) developed a combined viscoelastic-damage model to describe the strain behaviour of swirl mat composites. Such a theory could be applied to ligament, but the influence of initial fibre recruitment may complicate modeling.

In summary, tangent modulus was used to track damage in this study. As discussed above, tangent modulus changes can represent damage in both toe- and linear-regions of the stress-strain curve. In addition, tangent modulus changes can also be related to increase in strain. Other researchers tracked damage progression with modulus as well (42,66,82), but confirmation of this technique for use with ligament was required.

4.4 Can residual strength and strain be used to confirm damage from creep and fatigue?

Damage, as determined by tangent modulus changes, was confirmed with residual strength tests following both creep and fatigue loading. Damage from creep and fatigue loading was assumed to occur in the same way, either fibre rupture or matrix degradation or both. Realizing the differences in *why and when* damage occurs in creep and fatigue is important, but it is speculated that the end result of damage (changes to the stress-strain relationship) are the same for both creep and fatigue loading. No discernable trends were observed to indicate that the end result of damage was different for creep and fatigue.

Ligaments with a reduced modulus ratio, and inferred damage, resulting from creep or fatigue loading differed in stress-strain behaviour when compared to previously-undamaged ligaments. Strength and tangent modulus were decreased for previously-damaged ligaments. Tangent modulus findings are not surprising because the criterion to determine previous damage was based on a modulus reduction. A strength reduction confirms that damage is present. Fibre rupture, matrix degradation or some combination of the two could cause a strength decrease because both mechanisms would damage some of the load-bearing components in ligament. As stated previously, damage from these mechanisms would likely affect the toe-region response as well. A trend showing an increased toe-region for damaged specimens was observed, which fits with the proposed damage mechanisms.

The inclusion or exclusion of the potential outlier greatly alters the conclusions about failure strain. Admittedly, there could be a trend where previously induced damage lowers the failure strain, but some evidence suggests that failure strain is constant in similar material, tendon. A strain limiting phenomenon was previously seen in tendon (48). In a later paper (49), it was suggested that a fibre (and therefore a tendon) could only strain a certain amount before rupture. This theory may also be true in ligament. Without the *residual strength outlier*, no differences were detected between failure strains and strains at rupture. This is not conclusive proof about a strain limiting failure mechanism in ligament, but it does suggest that it is possible.

For comparison, Panjabi and coworkers (39-41) looked at the effects of damage induced by low-speed and high-speed single stretch to 80% failure displacement on ACL stress-strain behaviour.

They found that a low-speed partial failure increased toe-region strain, modulus at 50% failure force and relaxation. Failure displacement and force were not affected by a low-speed subfailure stretch. Following a high-speed subfailure stretch, the ACL showed increased displacements in both the toe- and linear-regions, an increase in failure displacement, a decrease in energy absorbed to failure and a trend for decreased failure load. Comparison of residual strength tests of low-speed subfailure stretch, high-speed subfailure stretch, and creep/fatigue (present study) are difficult because the severity of damage may be different in all three cases. Toe-region elongation was observed in all three damage scenarios. Difference in modulus findings between the subfailure stretch work and the present study may arise from computational methods. The present study calculated modulus with a linear regression of the upper 50% of the loading curve, while Panjabi and coworkers calculated modulus (stiffness) as the tangent to the force-displacement curve at 50% failure force. Strength (or failure force) was decreased by creep and fatigue, was not changed by a slow subfailure stretch, and showed decreasing trend following a high-speed subfailure. Perhaps the slow subfailure stretch caused damage in the matrix and minor damage to the fibres. Initially recruited fibres may have ruptured, but enough intact fibres remained to maintain strength at failure strain. Since the fibres are the main load-bearing component, it would make sense that the residual strength was not altered. Failure strain (or failure displacement) are even more complicated to compare. Failure strains were observed to increase (following high-speed subfailure), stay the same (low-speed subfailure and the present study, excluding the *residual strength outlier*) and perhaps even decrease (present study, including the *residual strength outlier*). There is no clear pattern in the findings, which suggests that failure strains may indeed remain constant after partial damage.

In summary, damage indicated by a modulus reduction was related to decreased strength and tangent modulus, and a trend for increasing toe-region strain. The relation between damage and failure strain was unclear. The analysis confirmed that a modulus reduction can be used as an indicator of damage in ligament. Modulus reduction was a critical part of the continuum damage theory.

4.5 Continuum Damage Theory

Modulus reduction indicated damage in the continuum damage theory. Modulus (or stiffness) ratio has been used by previous investigators to model damage in bone (82) tendon (49,66) and composites (42). The damage model developed in the present study was inspired by work of Wang and Ker (66), Ker and Zioupos (30) and Poursartip et al. (42). It also utilized some of the basic concepts outline in Lemaitre's book on damage mechanics.

A novel aspect of the theory was the addition of term explicitly relating modulus ratio to a cross-sectional area reduction via residual strength in Figure 33. Previous tendon and bone studies assumed that damaged material does not contribute to load-bearing, and therefore, the modulus ratio was used as a direct indicator of an area reduction. In ligament and tendon, this is not necessarily the case. A ruptured fibre may still have the ability to support some load by transferring shear forces through the proteogylcan matrix. The current state of knowledge made it difficult to directly measure the effective area as determined by ruptured fibres and shear-induced loads, so an approximation was made using residual strength data. In composites, effective area was directly measured using C-scans to relate a modulus reduction to an CSA reduction (42). In the composites, the relation between area and modulus was linear. There is no guarantee that this relationship is linear in ligament due to potential partial loading of ruptured fibres, so the best empirical fit was used to describe the relationship (power law).

Another difficulty arises in the definition of the undamaged reference modulus. The majority of researchers in tendon and bone used the modulus of the first loading curve to determine damage. This technique works well for bone, but it does not work as well for ligament and tendon. Ligaments and tendons have the ability to recruit fibres during the initial stages of loading, which causes a stiffening of the material. If the first loading cycle is used to determine the undamaged stiffness, then the damage level for a significant portion of loading would exceed unity. Damage exceeding unity was acknowledged by previous tendon researchers (49,66). This implies a negative damage level, which is likely not the case.

A better undamaged reference modulus is the maximum modulus recorded during loading. Maximum modulus was previously used for this purpose in composites modeling (42). In ligament, the initial modulus was typically between 90 and 95% of the maximum modulus

(modulus ratio between 0.9 and 0.95). It was shown in Section 3.4 that a modulus ratio (E/E_{max}) below 0.97 indicated some damaged was sustained. If initial modulus was used as the undamaged reference point, then a damaged state would actually be described by a damage level exceeding unity. Therefore, maximum modulus was used as the undamaged reference modulus. For clarification, the modulus ratios during the initial stages of loading were also below 0.97. However, this is more an effect of fibre recruitment and viscoelasticity than damage. Effectively, the damage theory does not apply to this initial stage of loading (typically complete within 1 hour). The theory can be applied at any point after the maximum modulus is attained. This corresponded to the point where the modulus ratio first increased to 0.98 because there was about a 2% noise in the modulus recordings and changes less than 0.02 were difficult to reliably identify. The relationship between modulus and toe-region changes and the relationship between modulus and increase in strain after this point have been previously explained (Section 4.4); the damage theory (after modulus ratio increased to 0.98) can be used to indicate changes in toe-region strain and increase in strain. The initial damage rate was determined after the point where modulus ratio first increased to 0.98.

Initial damage rate was determined by the most direct method, by measuring the initial rate of modulus ratio change. Once the initial rate of modulus ratio change was found, it was a simple matter to determine the damage rate by substitution of the values into the damage rate equation. Wang and Ker (66) determined the initial rate of modulus change by creating a relation between modulus ratio and increase in strain ('extra strain'). They combined the derivative of this relation and the minimum strain rate to estimate the initial rate of modulus change. They acknowledged that their less direct technique probably underestimated the initial damage rate, but they could not use their modulus data because they had "difficulty achieving the required accuracy." This technique worked because of the approximately linear relation between modulus ratio and increase in strain observed in region 3 (decreasing modulus ratio roughly corresponding to tertiary strain). In fact, it is possible to define damage with respect to tertiary strain rate (32). Some researchers (10,48,75) have avoided the difficulties associated with determining the damage rate by assuming a constant damage rate that is inversely proportional with time-to-rupture. This technique simplifies the computations, but it may not reflect what is actually happening in the material. Ligaments and tendons have an increasing damage rate. This is reflected by the existence of the tertiary strain stage. Wang and colleagues (66,67) state that wallaby tail tendon did not exhibit a secondary creep stage, and suggested that damage rate was

always increasing. As a result, they used a non-constant damage rate in their damage model. The present study also found that damage was not constant, although ligaments did progress though all three stages of creep.

Results shown in Figure 35 indicate that the application of basic damage mechanics principles provided a good estimation of time-dependent damage behaviour. Fatigue damage behaviour could not be predicted by oscillating nominal stress in the time-dependent damage model developed with creep data (Figure 36). This is most likely due to the additional cycle-dependent damage mechanism present in fatigue loading. Theoretically, the principles used to develop the time-dependent model could be applied to experimental fatigue data to create a time- and cycle-dependent damage model, but further experimental data is required before the relative contributions of time- and cycle-dependent damage can be quantified for fatigue loading.

4.6 Strengths and Limitations

As with any scientific investigation it is important to recognize both the strengths and limitations. Strengths highlight new knowledge, novel techniques, and important findings, while limitations offer insight into potential improvements in experimental techniques or new topics for study.

4.6.1 Strengths

To the author's knowledge, this is the first study to investigate the interactions of time-dependent and cycle-dependent damage in ligament. Previous studies have considered damage in tendon. While the structure of ligament is similar to tendon, tendons are thought to experience higher *in vivo* stresses than ligaments. Results from this study suggest that ligament may be more susceptible to cycle-dependent damage than tendon, but further investigation is required to verify this proposition.

Several strengths arise from the experimental design of the current study. First, the inclusion of periodic unloading/reloading of creep tests allowed information to be gathered about the stress-strain characteristics for both fatigue and creep. Without periodically unloading ligaments subjected to creep, only strain profile and time-to-rupture can be used to assess damage. In this study, stress-strain information for both loading conditions was interpreted to show the progression of damage and theorize reasons for the observed differences in creep and fatigue.

Second, stress levels were selected to cover different ranges of tissue response. The behaviour of ligament is non-linearly dependent on stress. Ligament subjected to stresses up to the toe- to linear-region transition stress behave differently (as a result of fibre recruitment) than linear-region stresses (62). In addition, within the linear-region, their may be differences in behaviour when comparing high-linear and low-linear stresses. Without examining different regions in the stress-strain relationship, a full understanding of damage and behaviour could not be determined.

Third, residual strength tests confirmed the presence of damage indicated by a decreased modulus ratio and the continuum damage theory. Damage was shown to affect both toe- and linear-regions of the stress-strain behaviour. Residual strength testing provided confirmation that the damage theory, and its accompanying assumptions, was valid.

The damage theory developed in the study made some advances to previous biologic tissue damage models. The inclusion of an explicit relation between modulus ratio and cross-sectional area reduction eliminated the need to assume that damaged material does not contribute to load-bearing, which may not be a valid assumption in ligament and tendon. Also, the non-constant damage rate was defined using modulus ratio change and was more direct than previous tendon work (66).

In addition, loading condition was clearly shown to affect ligament behaviour and damage at elevated stresses. This information may have clinical significance for ligaments that are subjected to high *in vivo* loads, such as those ligaments whose complementary supporting structures have been previously injured. An example could be an ACL deficient knee. The MCL will likely be subjected to higher than normal stresses because it has to resist anterior tibial translation (primary ACL role) as well as resist valgus bending and external tibial rotation (primary MCL role). Subjecting a ligament to high stresses, either static or cyclic, causes a

higher damage rate than lower stresses. This puts the ligament at risk of damage accumulation and increased laxity, which in turn will cause increased joint laxity, and may create an unstable joint. Interpretation of this clinically relevant finding should recognize the study limitations as well.

4.6.2 Limitations

The largest limitations of the study arise from the fact that it was an *in vitro* experiment. Fibroblasts may respond to mechanical stimulus and invoke a healing response if damage is present *in vivo* (11). Caution must be used when extrapolating the lifetimes determined from this experiment to the lifetimes *in vivo*. The extent that active healing will change ligament lifetimes will depend on the healing rate. Schechtman and Bader (48) provided a simple model using the Palmgren-Minor rule to show the interaction of damage and healing. They suggest that tendon could be damaged by a period of cyclic loading, but throughout the course of a day, active healing could counteract that damage. Specific details of the interaction of damage and healing are not presently known, so direct *in vivo* application of experimental data should be done with prudence.

Also, the loading histories *in vivo* are more complex than those tested. *In vivo* loads are both static and cyclic, and cyclic loading is not necessarily at a constant frequency. Loading histories will affect the damage rate and render a Palmgren-Minor analysis inapplicable. Researchers in bone have attempted to understand damage accumulation under variable loading using equi-damage plots (79).

In vitro testing requires maintenance of ligament hydration. Ligaments submerged in saline baths have abnormally increased water content and correspondingly altered mechanical behaviour (61). In this study, an environment chamber was used to maintain water content without altering mechanical properties (61), but it prohibited the use of antibacterial agents. After more than 90 hours of loading, deposition of a foreign substance on bone was observed for 2 of the 46 specimens tested. One of the ligaments (creep at 30% UTS) was loaded to rupture, but the other (creep at 15% UTS, loaded for 168 hours) showed no evidence of damage in its

stress-strain behaviour. In addition, Wang and Ker (66) loaded a wallaby tail tendon for 360 hours and found little strain change and no indication of rupture.

The experimental design also has some limitations. The intention was to study damage in creep and fatigue using mechanical evidence of damage. Mechanical evidence of damage highlights the effects of damage on the macroscopic behaviour of ligament, but it does not provide explicit information about what is happening to the microstructure. The proposed microstructural response can only be verified with a microstructural investigation.

In addition, the current study design made it difficult to determine the relative contributions of time- and cycle-dependent damage. Also, all cyclic loading was completed using a sine wave. This provided a continually changing loading rate. It is currently unknown what effects are caused by changing the loading profile to a constant ramp or a square wave. A more detailed fatigue investigation showing the effects of mean stress, stress amplitude, frequency and loading profile is required to determine the contributions of different damage mechanisms to the overall damage.

4.7 Future Work

The two study design limitations noted in the preceding section lead to some recommendations for future work. As stated above, the relative contributions of time- and cycle-dependent damage are currently unknown. This question could be answered by completing more fatigue test with varied mean stresses, frequencies, stress amplitudes (amplitude of oscillation) and loading profile (sine, triangle or square). Altering the mean stress may affect the time-dependent damage. Increasing frequency will likely increase the cycle-dependent damage (some pilot tests were completed at 10Hz - see Appendix I). Decreasing the stress amplitude would cause the fatigue test to behave more 'creep-like' and reduce the cycle-dependent damage. Different loading profiles may highlight the effects of loading rate on cycle-dependent damage. Given a proper experimental design, these parameters could be used to quantify which damage mechanism causes the majority of damage in fatigue for a given loading condition.

An investigation into the microstructural influences on creep-fatigue damage interactions is required before a complete understanding of creep and fatigue damage is established. A possible aspect for investigation is the fibre recruitment differences between creep and fatigue. Findings from this potential study would either validate or further refine the microstructural theory suggested above.

Further development of the CDM model could involve the incorporation of strain or strain rate as a damage indicator. Figure 29 suggests a clear relationship between modulus and increase in strain and Figure 35 confirms that modulus can be used to predict damage. These two relationships suggest that strain has potential as a damage indicator in ligament. Tertiary strain response was suggested as a possible damage indicator by Lemaitre (32).

Knowledge and understanding gained from this study can be applied to further research involving the effects of repair on damage accumulation. An *in vivo* (or perhaps even *ex vivo*, with viable cells) model could be used to study the influence of active healing on damage accumulation. The interactions of both damage and repair can be applied to a healing ligament mechanics. Understanding gained from studying damage and repair in healing ligaments can be used to help eliminate increase ligament laxity that occurs after traumatic injury.

5.0 SUMMARY

In summary, the present study investigated damage accumulation in ligaments subjected to both creep and fatigue loading. Fatigue loading was found to be more damaging than creep. In addition, fatigue and creep loading resulted in different strain profiles, indicating that the microstructure responds differently to both loading conditions.

Tangent modulus was used as a damage indicator for a continuum damage mechanics model and was shown to be an acceptable method for tracking damage through residual strength testing. Additional modeling of toe-region changes resulting from damage did not add additional information because toe-region changes paralleled linear-region changes (modeled with tangent modulus) at times when the CDM model was applied. Experimental data also suggested that increase in strain could be used as a damage indicator instead of modulus. Strain may be a more clinically relevant measure than tangent modulus.

The current study investigated damage resulting from creep and fatigue at stresses above the normal physiologic range. Results can be applied to ligaments subjected to elevated stresses resulting from injury to complementary joint structures. In addition, a partially injured ligament or a healing ligament may experience higher effective stress in intact fibres and the behaviour examined in the present study will be applicable.

REFERENCES

1. Adeeb SM, Zec ML, Thornton GM, Frank CB, Shrive NG: A novel application of the principles of linear elastic fracture mechanics (LEFM) to the fatigue behavior of tendon tissue. *J Biomech Eng* 126:641-50, 2004

2. Anderson A: Knee laxity and function after conservative treatment of anterior cruciate ligament injuries: a prospective study. *Int J Sports Med* 14:150-3, 1993

3. Arnoczky SP: Animal models for knee ligament research. In: *Knee ligaments: structure, function, injury and repair* pp 401-17. Ed by WH Akeson, D Daniel, and JJ O'Connor. New York, Raven Press, 1990

4. Aydog ST, Korkusuz P, Doral MN, Tetik O, Demirel HA: Decrease in the numbers of mechanoreceptors in rabbit ACL: the effects of ageing. *Knee Surg Sports Traumatol Arthrosc* 2005

5. Azangwe G, Fraser K, Mathias KJ, Siddiqui AM: In vitro monitoring of rabbit anterior cruciate ligament damage by acoustic emission. *Med Eng Phys* 22:279-83, 2000

6. Bertram JE: Constrained optimization in human walking: cost minimization and gait plasticity. *J Exp Biol* 208:979-91, 2005

7. Bowman SM, Guo XE, Cheng DW, Keaveny TM, Gibson LJ, Hayes WC, McMahon TA: Creep contributes to the fatigue behavior of bovine trabecular bone. *J Biomech Eng* 120:647-54, 1998

8. Caler WE, Carter DR: Bone creep-fatigue damage accumulation. *J Biomech* 22:625-35, 1989

9. Callister WD: *Materials science and engineering: An introduction,* Toronto, John Wiley & Sons, Inc., 2000

10. Carter DR, Caler WE: A cumulative damage model for bone fracture. *J Orthop Res* 3:84-90, 1985

11. Cool SM, Snyman CP, Nurcombe V, Forwood M: Temporal expression of fibroblast

growth factor receptors during primary ligament repair. *Knee Surg Sports Traumatol Arthrosc* 12:490-6, 2004

12. Cotton JR, Winwood K, Zioupos P, Taylor M: Damage rate is a predictor of fatigue life and creep strain rate in tensile fatigue of human cortical bone samples. *J Biomech Eng* 127:213-9, 2005

13. Cotton JR, Zioupos P, Winwood K, Taylor M: Analysis of creep strain during tensile fatigue of cortical bone. *J Biomech* 36:943-9, 2003

14. Crisco JJ, Moore DC, McGovern RD: Strain-rate sensitivity of the rabbit MCL diminishes at traumatic loading rates. *J Biomech* 35:1379-85, 2002

15. Diamant J, Keller A, Baer E, Litt M, Arridge RG: Collagen; ultrastructure and its relation to mechanical properties as a function of ageing. *Proc R Soc Lond B Biol Sci* 180:293-315, 1972

16. Findley W, Lai J, Onaran K: *Creep and relaxation of nonlinear visoelastic material: with an introduction to linear viscoelasticity,* New York, North-Holland Publishing Company, 1976

17. Fleming BC, Beynnon BD: In vivo measurement of ligament/tendon strains and forces: a review. *Ann Biomed Eng* 32:318-28, 2004

18. Fondrk M, Bahniuk E, Davy DT, Michaels C: Some viscoplastic characteristics of bovine and human cortical bone. *J Biomech* 21:623-30, 1988

19. Frank C, MacFarlane B, Edwards P, Rangayyan R, Liu ZQ, Walsh S, Bray R: A quantitative analysis of matrix alignment in ligament scars: a comparison of movement versus immobilization in an immature rabbit model. *J Orthop Res* 9:219-27, 1991

20. Frank C, McDonald D, Bray D, Bray R, Rangayyan R, Chimich D, Shrive N: Collagen fibril diameters in the healing adult rabbit medial collateral ligament. *Connect Tissue Res* 27:251-63, 1992

21. Frank CB , Shrive NG: Ligament. In: *Biomechanics of the Musculo-skeletal System* pp 107-126. Ed by Nigg B. and Herzog W. Toronto, John Wiley & Sons, 1999

22. Fruensgaard S, Johannsen HV: Incomplete ruptures of the anterior cruciate ligament. *J Bone Joint Surg Br* 71:526-30, 1989

23. Gushue DL, Houck J, Lerner AL: Rabbit knee joint biomechanics: motion analysis and modeling of forces during hopping. *J Orthop Res* 23:735-42, 2005

24. Haut RC, Little RW: Rheologic properties of canine anterior cruciate ligaments. *J Biomech* 2:289-98, 1969

25. Hingorani RV, Provenzano PP, Lakes RS, Escarcega A, Vanderby R Jr: Nonlinear viscoelasticity in rabbit medial collateral ligament. *Ann Biomed Eng* 32:306-12, 2004

26. Holden JP, Grood ES, Korvick DL, Cummings JF, Butler DL, Bylski-Austrow DI: In vivo forces in the anterior cruciate ligament: direct measurements during walking and trotting in a quadruped. *J Biomech* 27:517-26, 1994

27. Kastelic J, Galeski A, Baer E: The multicomposite structure of tendon. *Connect Tissue Res* 6:11-23, 1978

28. Kastelic J, Palley I, Baer E: A structural mechanical model for tendon crimping. *J Biomech* 13:887-93, 1980

29. Ker RF, Wang XT, Pike AV: Fatigue quality of mammalian tendons. *J Exp Biol* 203 Pt 8:1317-27, 2000

30. Ker RF, Zioupos P: Creep and fatigue damage in mammalian tendon and bone. *Comments. Theor. Biol.* 4:151-181, 1997

31. Lam TC, Thomas CG, Shrive NG, Frank CB, Sabiston CP: The effects of temperature on the viscoelastic properties of the rabbit medial collateral ligament. *J Biomech Eng* 112:147-52, 1990

32. Lemaitre J: *A course on damage mechanics,* New York, Springer, 1996

33. Lo I, Thornton G, Miniaci A, Frank C, Ratter J, Bray R: Structure and function of diarthodial joints. pp 41-126. Ed by J McGinty, S Burkhart, R Jackson, D Johnson, and J Richmond. Philadelphia, Lippincott Williams & Wilkins, 2003

34. Maganaris CN: Tensile properties of in vivo human tendinous tissue. *J Biomech* 35:1019-27, 2002

35. Moore TL, O'Brien FJ, Gibson LJ: Creep does not contribute to fatigue in bovine trabecular bone. *J Biomech Eng* 126:321-9, 2004

36. Noyes FR, Butler DL, Grood ES, Zernicke RF, Hefzy MS: Biomechanical analysis of human ligament grafts used in knee-ligament repairs and reconstructions. *J Bone Joint Surg Am* 66:344-52, 1984

37. Noyes FR, Grood ES: The strength of the anterior cruciate ligament in humans and Rhesus monkeys. *J Bone Joint Surg Am* 58:1074-82, 1976

38. Ohara W , Paxton E , Fithian D: Epidemiology of knee ligament injuries. In: *Daniel's Knee Injuries: Ligament and cartilage structure, function, injury and repair* pp 311-344. Ed by Pedowitz R , O'Connor J , and Akeson W. Philadelphia, Lippincott Willian & Wilkins, 2003

39. Panjabi MM, Courtney TW: High-speed subfailure stretch of rabbit anterior cruciate ligament: changes in elastic, failure and viscoelastic characteristics. *Clin Biomech (Bristol, Avon)* 16:334-40, 2001

40. Panjabi MM, Moy P, Oxland TR, Cholewicki J: Subfailure injury affects the relaxation behavior of rabbit ACL. *Clin Biomech (Bristol, Avon)* 14:24-31, 1999

41. Panjabi MM, Yoldas E, Oxland TR, Crisco JJ 3rd: Subfailure injury of the rabbit anterior cruciate ligament. *J Orthop Res* 14:216-22, 1996

42. Poursartip A , Ashby M, Beaumont P: The fatigue damamge mechanics pf a carbon fibre laminate: I - development of the model. *Composites Sci and Tech* 25:193-218, 1986

43. Provenzano PP, Heisey D, Hayashi K, Lakes R, Vanderby R Jr: Subfailure damage in ligament: a structural and cellular evaluation. *J Appl Physiol* 92:362-71, 2002

44. Provenzano PP, Vanderby R Jr: Collagen fibril morphology and organization: Implications for force transmission in ligament and tendon. *Matrix Biol* 2005

45. Puxkandl R, Zizak I, Paris O, Keckes J, Tesch W, Bernstorff S, Purslow P, Fratzl P:

Viscoelastic properties of collagen: synchrotron radiation investigations and structural model. *Philos Trans R Soc Lond B Biol Sci* 357:191-7, 2002

46. Redaelli A, Vesentini S, Soncini M, Vena P, Mantero S, Montevecchi FM: Possible role of decorin glycosaminoglycans in fibril to fibril force transfer in relative mature tendons--a computational study from molecular to microstructural level. *J Biomech* 36:1555-69, 2003

47. Rigby JB, Hirai N, Spikes HD, Eyring H: The mechanical porperties of rat tail tendon. *J Gen Physiol* 43:265-83, 1959

48. Schechtman H, Bader DL: In vitro fatigue of human tendons. *J Biomech* 30:829-35, 1997

49. Schechtman H, Bader DL: Fatigue damage of human tendons. *J Biomech* 35:347-53, 2002

50. Screen HR, Lee DA, Bader DL, Shelton JC: An investigation into the effects of the hierarchical structure of tendon fascicles on micromechanical properties. *Proc Inst Mech Eng [H]* 218:109-19, 2004

51. Shelburne KB, Pandy MG, Anderson FC, Torry MR: Pattern of anterior cruciate ligament force in normal walking. *J Biomech* 37:797-805, 2004

52. Shelburne KB, Pandy MG, Torry MR: Comparison of shear forces and ligament loading in the healthy and ACL-deficient knee during gait. *J Biomech* 37:313-9, 2004

53. Shrive N, Chimich D, Marchuk L, Wilson J, Brant R, Frank C: Soft-tissue "flaws" are associated with the material properties of the healing rabbit medial collateral ligament. *J Orthop Res* 13:923-9, 1995

54. Shrive NG, Lam TC, Damson E, Frank CB: A new method of measuring the cross-sectional area of connective tissue structures. *J Biomech Eng* 110:104-9, 1988

55. Shrive N, Thornton G, Hart D, Frank C: Ligament Mechanics. pp 97-112. Ed by R Pedowitz, J O'Connor, and W Akeson. Philadelphia, Lippincott Williams & Wilkins, 2003

56. Smith L, Weitsman YJ: Inelastic behavior of randomly reinforced polymeric composites under cyclic loading. *Mech of Time-Dependent Materials* 1:293-305, 1998

57. Smith L, Weitsman YJ: The visco-damage mechanical response of swirl-mat composites.

Inter'l J Fracture Mech 97:301-319, 1999

58. Terrier P, Schutz Y: Variability of gait patterns during unconstrained walking assessed by satellite positioning (GPS). *Eur J Appl Physiol* 90:554-61, 2003

59. Thornton GM, Leask GP, Shrive NG, Frank CB: Early medial collateral ligament scars have inferior creep behaviour. *J Orthop Res* 18:238-46, 2000

60. Thornton GM, Oliynyk A, Frank CB, Shrive NG: Ligament creep cannot be predicted from stress relaxation at low stress: a biomechanical study of the rabbit medial collateral ligament. *J Orthop Res* 15:652-6, 1997

61. Thornton GM, Shrive NG, Frank CB: Altering ligament water content affects ligament pre-stress and creep behaviour. *J Orthop Res* 19:845-51, 2001

62. Thornton GM, Shrive NG, Frank CB: Ligament creep recruits fibres at low stresses and can lead to modulus-reducing fibre damage at higher creep stresses: a study in rabbit medial collateral ligament model. *J Orthop Res* 20:967-74, 2002

63. Thornton GM, Shrive NG, Frank CB: Healing ligaments have decreased cyclic modulus compared to normal ligaments and immobilization further compromises healing ligament response to cyclic loading. *J Orthop Res* 21:716-22, 2003

64. Vesentini S, Redaelli A, Montevecchi FM: Estimation of the binding force of the collagen molecule-decorin core protein complex in collagen fibril. *J Biomech* 38:433-43, 2005

65. Wang XT, DeRuijter MR, Alexander RM: The effect of temperature on the tensile stiffness of mammalian tail tendons. *Zool. Lond.* 223:491-97, 1991

66. Wang XT, Ker RF: Creep rupture of wallaby tail tendons. *J Exp Biol* 198:831-45, 1995

67. Wang XT, Ker RF, Alexander RM: Fatigue rupture of wallaby tail tendons. *J Exp Biol* 198:847-52, 1995

68. Weiss JA, Gardiner JC: Computational modeling of ligament mechanics. *Crit Rev Biomed Eng* 29:303-71, 2001

69. Wilson A. , Shrive NG, Damson E. , Frank CB, Leask G. , Mikalson I. , Kraus V.: An

environment chamber for soft tissue testing. *Proc. 1995 BioEng. Conf.* 29:255-6, 1995

70. Woo SL, Danto MI, Ohland KJ, Lee TQ, Newton PO: The use of a laser micrometer system to determine the cross-sectional shape and area of ligaments: a comparative study with two existing methods. *J Biomech Eng* 112:426-31, 1990

71. Woo SL, Lee TQ, Gomez MA, Sato S, Field FP: Temperature dependent behavior of the canine medial collateral ligament. *J Biomech Eng* 109:68-71, 1987

72. Woo SL, Newton PO, MacKenna DA, Lyon RM: A comparative evaluation of the mechanical properties of the rabbit medial collateral and anterior cruciate ligaments. *J Biomech* 25:377-86, 1992

73. Woo SL, Orlando CA, Camp JF, Akeson WH: Effects of postmortem storage by freezing on ligament tensile behavior. *J Biomech* 19:399-404, 1986

74. Woo SL, Young EP, Ohland KJ, Marcin JP, Horibe S, Lin HC: The effects of transection of the anterior cruciate ligament on healing of the medial collateral ligament. A biomechanical study of the knee in dogs. *J Bone Joint Surg Am* 72:382-92, 1990

75. Wren TA, Lindsey DP, Beaupre GS, Carter DR: Effects of creep and cyclic loading on the mechanical properties and failure of human Achilles tendons. *Ann Biomed Eng* 31:710-7, 2003

76. Yahia L, Brunet J, Labelle S, Rivard CH: A scanning electron microscopic study of rabbit ligaments under strain. *Matrix* 10:58-64, 1990

77. Yahia LH, Drouin G: Microscopical investigation of canine anterior cruciate ligament and patellar tendon: collagen fascicle morphology and architecture. *J Orthop Res* 7:243-51, 1989

78. Zec ML, Frank CB, Shrive NG. The accumulation of damage under cyclic loading is not altered following traumatic strain in the rabbit MCL. ASME Summer BioEng Conf. 2003.

79. Zioupos P, Casinos A: Cumulative damage and the response of human bone in two-step loading fatigue. *J Biomech* 31:825-33, 1998

80. Zioupos P, Currey JD, Casinos A: Tensile fatigue in bone: are cycles-, or time to failure, or

both, important? *J Theor Biol* 210:389-99, 2001

81. Zioupos P, Currey JD, Sedman AJ: An examination of the micromechanics of failure of bone and antler by acoustic emission tests and Laser Scanning Confocal Microscopy. *Med Eng Phys* 16:203-12, 1994

82. Zioupos P, Wang XT, Currey JD: Experimental and theoretical quantification of the development of damage in fatigue tests of bone and antler. *J Biomech* 29:989-1002, 1996

APPENDIX A: LOAD CELL CALIBRATION

Load cell calibration was verified by Instron Corporation. The certificate of calibration follows.

CERTIFICATE OF CALIBRATION

ISSUED BY: INSTRON CALIBRATION LABORATORY

DATE OF ISSUE: 22-Jul-05 CERTIFICATE NUMBER: **695044-03**

NVLAP
Lab code: 200301-0

Instron Corporation
825 University Avenue
Norwood, MA 02062-2643
Telephone:(800) 473-7838
Fax: (781) 575-5755
Email: service_requests@instron.com

Customer UNIVERSITY OF BRITISH COLUMBIA
Room 500, 828W 10th Ave,
Vancouver, B.C. V5Z 1L8

Contact: Chad Larson

Date of Verification: 22-Jul-05
Ambient Temperature: 22 °C

Machine		**Transducer**	
Manufacturer:	Instron	Manufacturer:	SENSOTEC
Model:	8841	Model:	75/C863-01
Serial No.:	C6176	Serial No.:	721070
Type:	Electromechanical Extended Range	Capacity:	1 kN
		Type:	Tension/Compression
Capacity:	1 kN		
Year of Mfg:			

Classification

1. GPIB (kN) - PASSED**

Certification Statement

This certifies that the forces verified with machine indicator 1 (listed above) are WITHIN ± 1 % accuracy, 1% repeatability, and zero return tolerance. All machine indicators were verified by Instron Corporation in accordance with ASTM E4-02.

** within ± .5% accuracy and .5% repeatability.

CERTIFICATE OF CALIBRATION

NVLAP ACCREDITED CALIBRATION LABORATORY No. 200301-0

CERTIFICATE NUMBER:
695044-03

Method of Verification

The testing machine was verified in the 'as found' condition with no adjustments carried out.

The verification and equipment used conform to a controlled Quality Assurance program which meets the specifications outlined in ANSI/NCSL Z540-1, ISO 10012-1, ISO 9001, and ISO/IEC 17025 (formerly ISO/IEC Guide 25).

The certification is based on runs 1 and 2 only. A third run is taken to satisfy uncertainty requirements according to ISO 17025 specifications.

Summary of Results

Indicator 1. - GPIB (kN)

Range F/S (%)	Tested Force Range (kN)	Mode	Max Error	Max Repeat Error (%)	Zero Return	Resolution (kN)	ASTM Lower Limit (kN)
100	0.02 - 1	T	.43	.13	Pass	.000005	0.001
	0.02 - 1	C	.49	.08	Pass	.000005	0.001

Instron Calpro Version 5.2

CERTIFICATE OF CALIBRATION

NVLAP ACCREDITED CALIBRATION LABORATORY No. 200301-0

CERTIFICATE NUMBER:
695044-03

Datapoint Summary - Indicator 1. - GPIB (kN)

TENSION

% of Range	Run 1 Error (%)	Run 2 Error (%)	Run 3 Error (%)	ASTME4 Repeat Error (%)	Uncertainty Repeat Error (%)	Relative Uncertainty * (%)	Uncertainty of Measurement * (kN)
100% Range (Full Scale: 1 kN)							
2	-.15	-.05	-.14	.10	.032	.066	± .000
4	.07	.20	.18	.13	.040	.082	± .000
8	.20	.25	.29	.05	.026	.053	± .000
14	.28	.29	.33	.01	.015	.032	± .000
20	.31	.32	.29	.01	.009	.019	± .000
40	.36	.34	.36	.02	.007	.015	± .000
60	.43	.43	.40	.00	.010	.021	± .000
80	.40	.43	.40	.03	.010	.021	± .000
100	.38	.43	.43	.05	.017	.034	± .000
0 Return							

Datapoint Summary - Indicator 1. - GPIB (kN)

COMPRESSION

% of Range	Run 1 Error (%)	Run 2 Error (%)	Run 3 Error (%)	ASTME4 Repeat Error (%)	Uncertainty Repeat Error (%)	Relative Uncertainty * (%)	Uncertainty of Measurement * (kN)
100% Range (Full Scale: 1 kN)							
2	.41	.49	.45	.08	.023	.049	± .000
4	.30	.23	.30	.07	.023	.048	± .000
8	.34	.37	.14	.03	.072	.145	± .000
14	.38	.41	.39	.03	.009	.019	± .000
20	.34	.41	.37	.07	.020	.041	± .000
40	.31	.35	.37	.04	.018	.036	± .000
60	.34	.36	.34	.02	.007	.015	± .000
80	.38	.36	.36	.02	.007	.015	± .000
100	.35	.34	.30	.01	.015	.031	± .000
0 Return							

** The reported expanded uncertainty is based on a standard uncertainty multiplied by a coverage factor k=2, providing a level of confidence of approximately 95 %.*

Instron Calpro Version 5.2

CERTIFICATE OF CALIBRATION

NVLAP ACCREDITED CALIBRATION LABORATORY No. 200301-0

CERTIFICATE NUMBER:
695044-03

Data - Indicator 1. - GPIB (kN)

TENSION

	Run 1		Run 2		Run 3	
% of Range	Indicated (kN)	Applied (kN)	Indicated (kN)	Applied (kN)	Indicated (kN)	Applied (kN)
100% Range (Full Scale: 1 kN)						
2	.01975	.01978	.01987	.01988	.02104	.02107
4	.04052	.04049	.04021	.04013	.04004	.03997
8	.07972	.07956	.07984	.07964	.08020	.07997
14	.14098	.14058	.13971	.13931	.14135	.14089
20	.19997	.19936	.20141	.20077	.19975	.19917
40	.40001	.39858	.40038	.39902	.39826	.39685
60	.59776	.59523	.60009	.59754	.80496	.80173
80	.79773	.79455	.79976	.79637	.80444	.80124
100	.98433	.98063	.99005	.98581	1.00055	.99631
0 Return	.00005		.00010		.00006	

Data - Indicator 1. - GPIB (kN)

COMPRESSION

	Run 1		Run 2		Run 3	
% of Range	Indicated (kN)	Applied (kN)	Indicated (kN)	Applied (kN)	Indicated (kN)	Applied (kN)
100% Range (Full Scale: 1 kN)						
2	.02207	.02198	.02063	.02053	.02014	.02005
4	.04031	.04019	.03987	.03978	.04041	.04029
8	.08013	.07986	.05957	.05935	.08003	.07992
14	.14081	.14028	.14294	.14235	.13982	.13928
20	.20114	.20045	.20047	.19966	.19957	.19883
40	.39945	.39823	.40210	.40071	.39956	.39808
60	.60345	.60141	.60123	.59906	.60049	.59846
80	.79927	.79626	.80227	.79937	.80333	.80048
100	1.00120	.99769	.99655	.99313	.99657	.99357
0 Return	.00002		.00003		.00006	

Instron Calpro Version 5.2

CERTIFICATE OF CALIBRATION

NVLAP ACCREDITED CALIBRATION LABORATORY No. 200301-0

CERTIFICATE NUMBER:
695044-03

The Return to Zero tolerance is = the indicator resolution, 0.1 % of the maximum force verified in the range, or 1% of the lowest force verified in the range, whichever is greater.

Graphical Data - Indicator 1. - GPIB (kN)

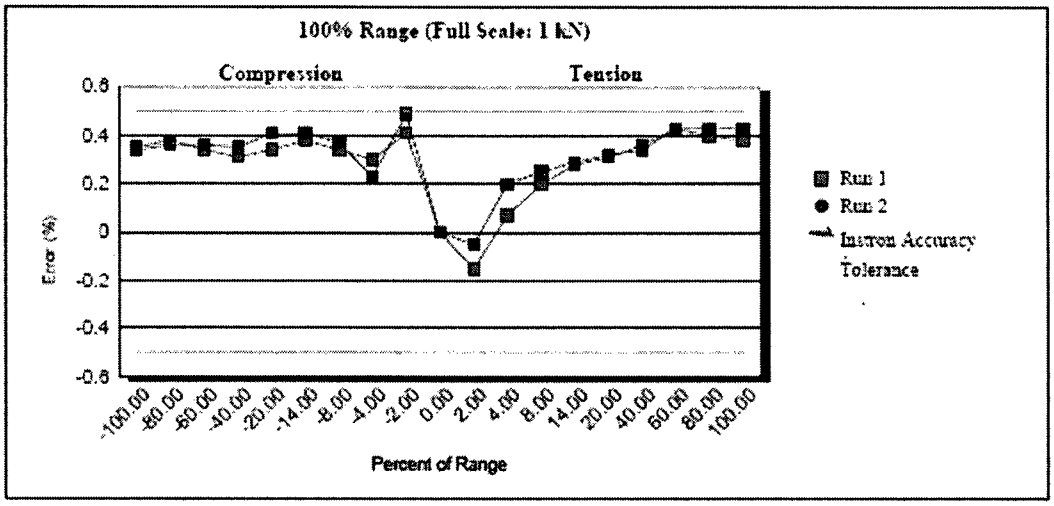

Verification Equipment

Make/Model	S/N	Description	Calibration Agency	Capacity	Cal Date	Cal Due
INTERFACE	D56202	Load Cell	Instron Corp.	120 lbf	18-Feb-04	18-Feb-06
FLINTEC	466644	Load Cell	Instron Corp.	1200 lbf	07-May-04	07-May-06
HBM ML38	884300	Load Cell Indicator	Instron Corp.	N/A	09-Dec-04	09-Dec-06

Verification Equipment Usage

Range F. S. (kN)	Standard S/N	Mode	Percent(s) of Range	Uncertainty of Calibration (% of capacity)	Lower Limit (kN) Standard Class A / A1
1	466644	T	40, 60, 80, 100	.005	.089 / .1646
	466644	C	60, 80, 100	.005	.089 / .1201
	D56202	T	2, 4, 8, 14, 20, 40	.005	.0133 / .0178

Instron Calpro Version 5.2

CERTIFICATE OF CALIBRATION

NVLAP ACCREDITED CALIBRATION LABORATORY No. 200301-0

CERTIFICATE NUMBER:
695044-03

Verification Equipment Usage

Range F. S. (kN)	Standard S/N	Mode	Percent(s) of Range	Uncertainty of Calibration (% of capacity)	Lower Limit (kN) Standard Class A / A1
1	D56202	C	2, 4, 8, 14, 20, 40	.005	.0133 / .0133

Instron standards certified to ASTM Standard E74-02 and traceable to NIST.

Standard Class A is used for machine accuracy errors greater than 0.5% and Standard Class A1 is used for machine accuracy errors that are less than or equal to 0.5%.

Comments:

Verified by: W.S. Kim
Senior Field Service Rep.

NOTE: Clause 20 of ASTM E-4: 2003 states: It is recommended that testing machines be verified annually or more frequently if required. In no case shall the time interval between verifications exceed 18 months (except for machines in which long term test runs beyond the 18 month period). Testing machines shall be verified immediately after repairs that may in any way affect the operation of the weighing system or values displayed. Verification is required immediately after a testing machine is relocated and where there is a reason to doubt the accuracy of the force indicating system, regardless of the time interval since the last verification.

Instron Calpro Version 5.2

APPENDIX B: ACTUATOR STRAIN VALIDATION

Position measurements were verified with an Optotrak 3020 system (accuracy of 0.1 mm, resolution of 0.01 mm; Northern Digital Inc, Waterloo, ONT), but the use of the environment chamber prohibited Optotrak position measurements during testing. An MCL was prepared and mounting following standardized techniques (Figure B-1). Optotrak markers were fixed on the femur, tibia, crosshead, and base.

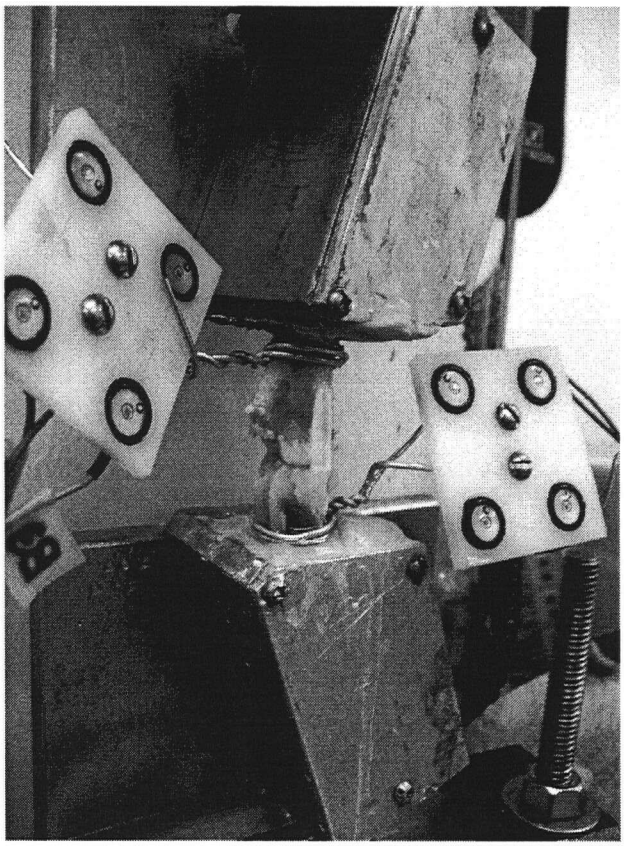

***Figure B-1**: MCL mounted on the testing machine using the steel grips. Optotrak markers were fixed to the tibia and femur to track MCL stretch for comparison with crosshead displacement data.*

Two virtual points (the MCL origin and insertion) were digitized to track motion. Comparison of markers on the crosshead to the markers on the tibia and the markers on the base to the markers on the femur showed no movement induced from the grips. Relative motion of the MCL insertion to the origin was compared to the motion recorded by the crosshead (Figure B-2). The

difference between the two measurements was greatest at forces corresponding to 60% UTS (0.155 mm) and smallest at forces corresponding to 15% UTS (0.01 mm). The differences have two possible sources: inherent errors in both measurement systems or bone flexion. The error of 0.16 mm is close to the accuracy of both the Optotrak and the Instron systems. As the testing configuration also involved sections of the femur and tibia, bone flexion is also a potential source of error. A comparison of the Instron crosshead measurements and the Optotrack system (without an MCL) is shown in Figure B-3.

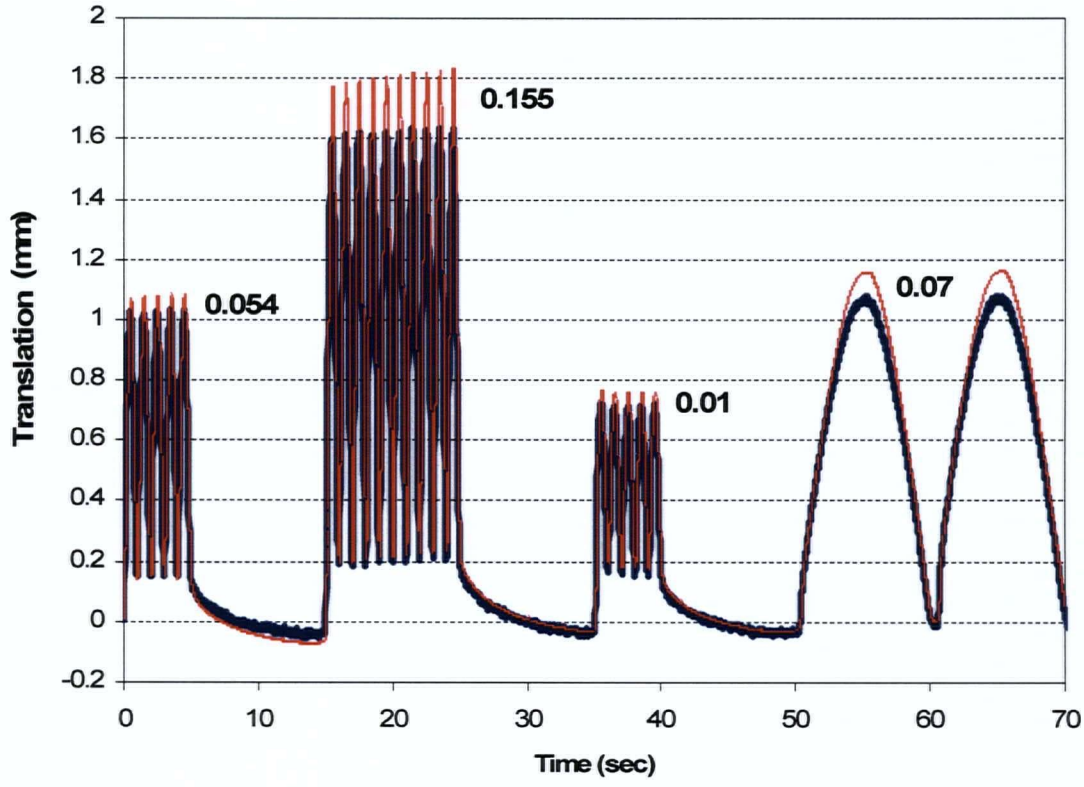

***Figure B-2**: Comparison of crosshead displacement (red, thin line) and Optotrak (blue, bold line) measurements. Motion was recorded for 30% UTS at 1 Hz, 60% UTS at 1 Hz, 15% UTS at 1 Hz and 30% UTS at 0.1 Hz. The amplitude difference recorded by the crosshead and the Optotrak is noted after each waveform.*

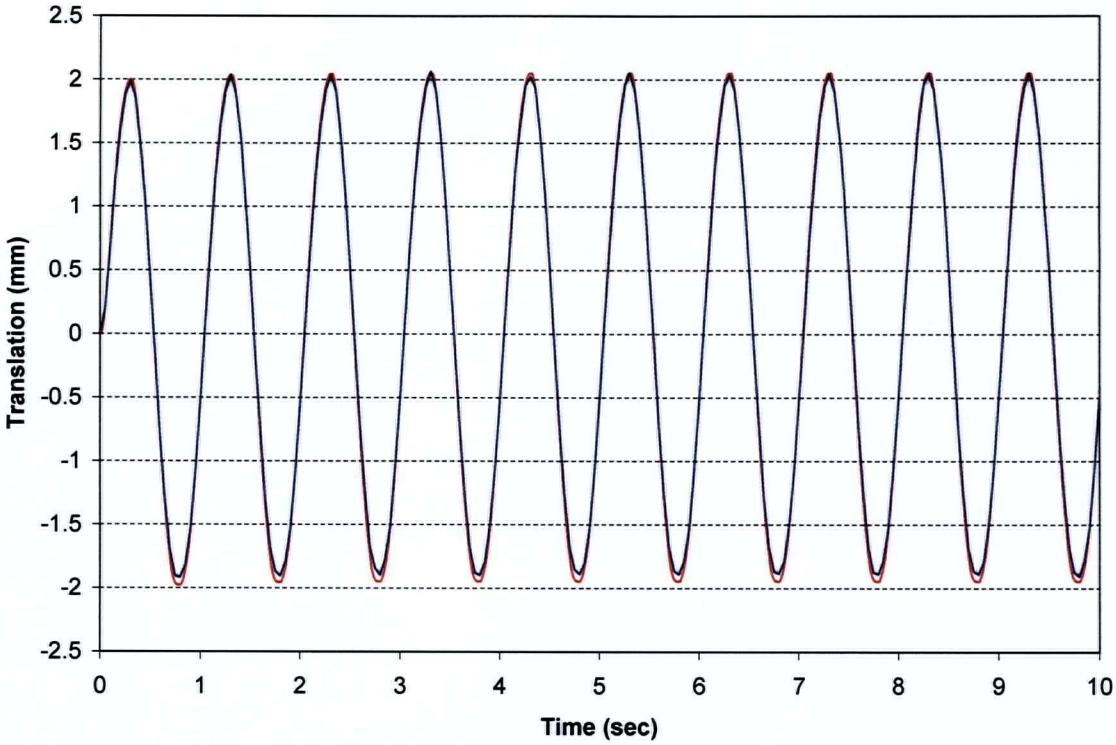

***Figure B-3**: Comparison of crosshead displacement (red line) and Optotrak (blue line) without an MCL. An amplitude difference of 0.05mm was recorded.*

APPENDIX C: ENVIRONMENTAL CHAMBER

The environmental system was composed of five main parts: a two part chamber, a connector tube, a heating system and a humidifier. The chamber was composed of two parts, a base and a removable casing (Figures C1 – C5). Humidified air (99% RH) was pumped from the humidifier (HM 485, Holmes Group, Mississauga, ONT) through the connector tube (Figure C6) to the chamber. The heating system consisted of a cable heater (62H56A4X, Watlow Electric Manufacturing Company, Burnaby BC), a RTD sensor (Valax Manufacturing Inc, Delta, BC) and control panel (Valax Manufacturing Inc, Delta, BC).

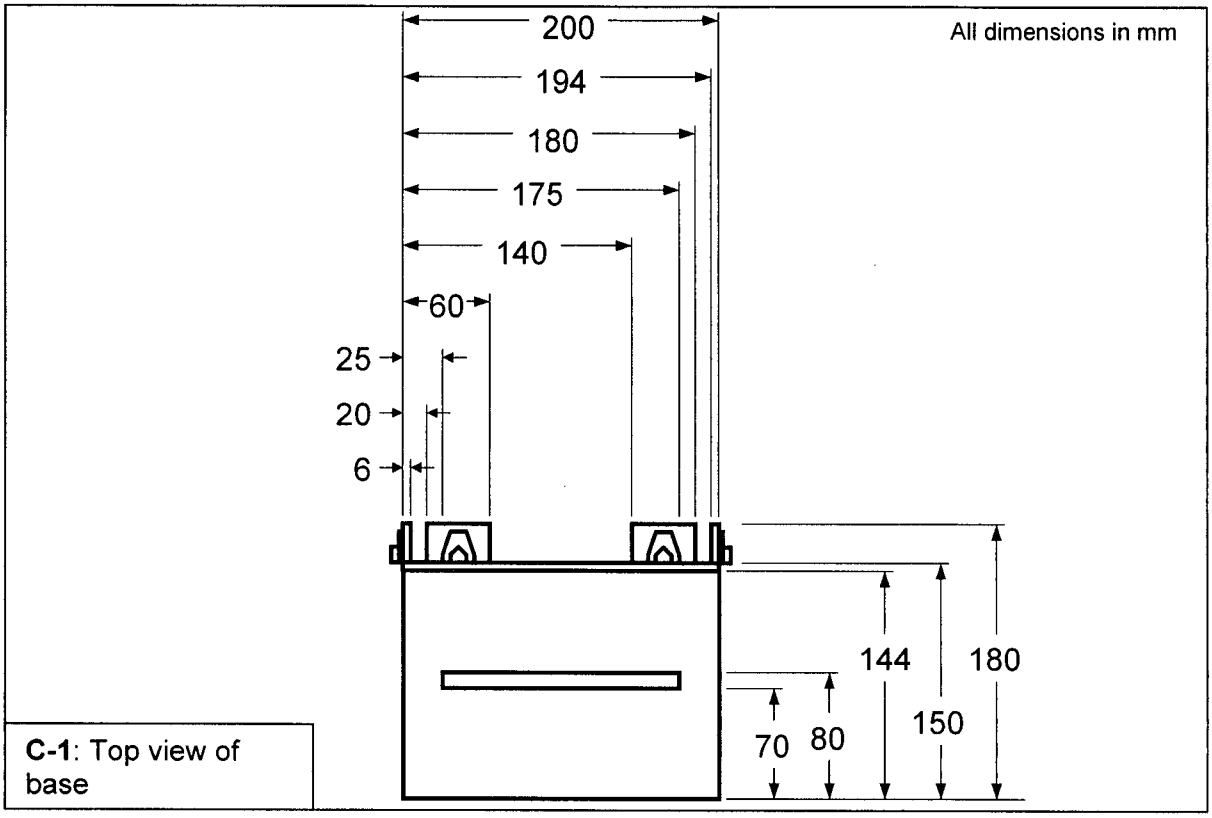

C-1: Top view of base

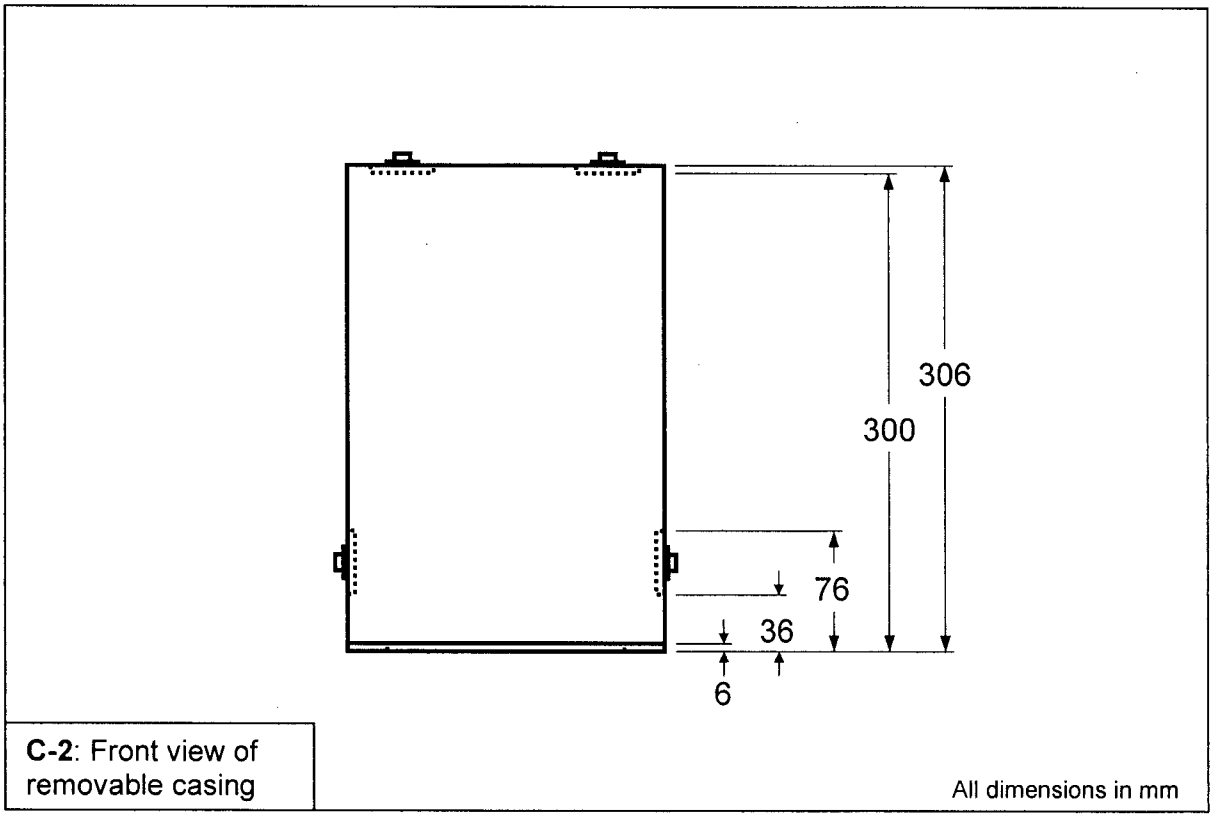

C-2: Front view of removable casing

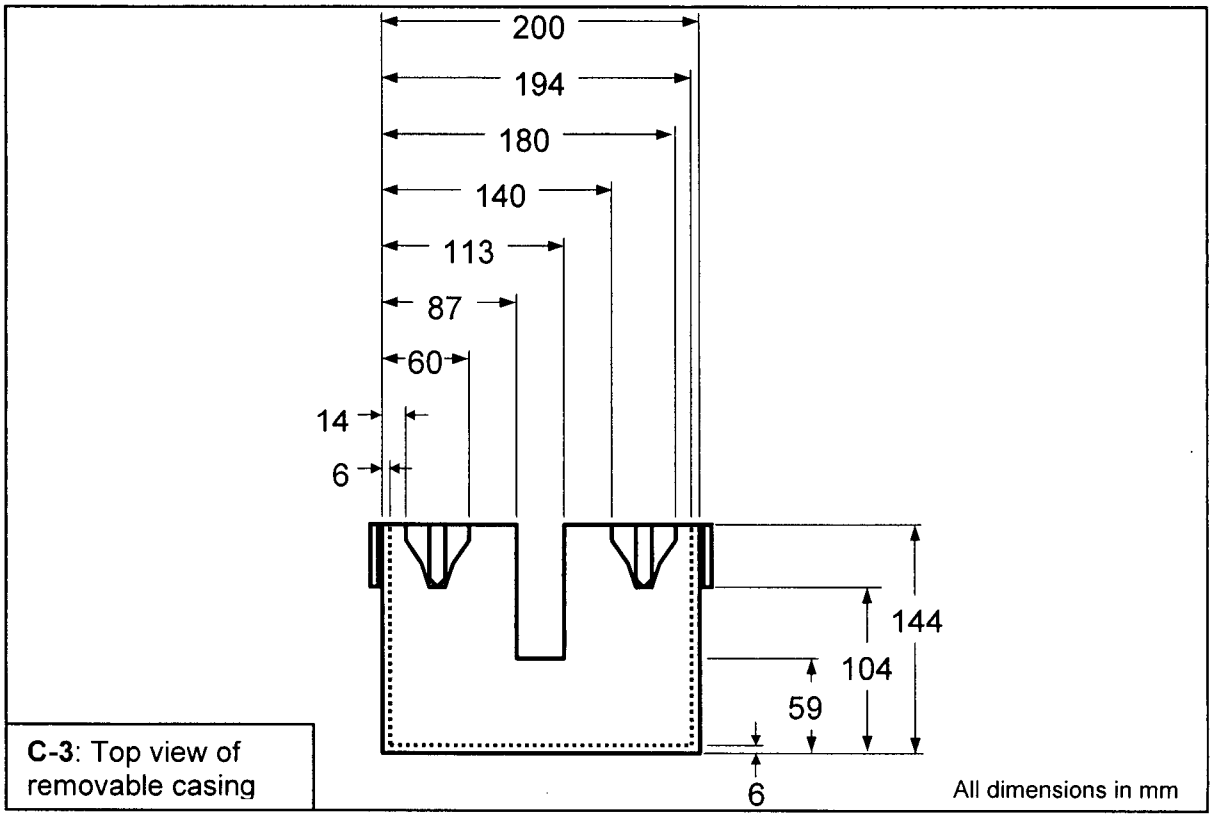

C-3: Top view of removable casing

All dimensions in mm

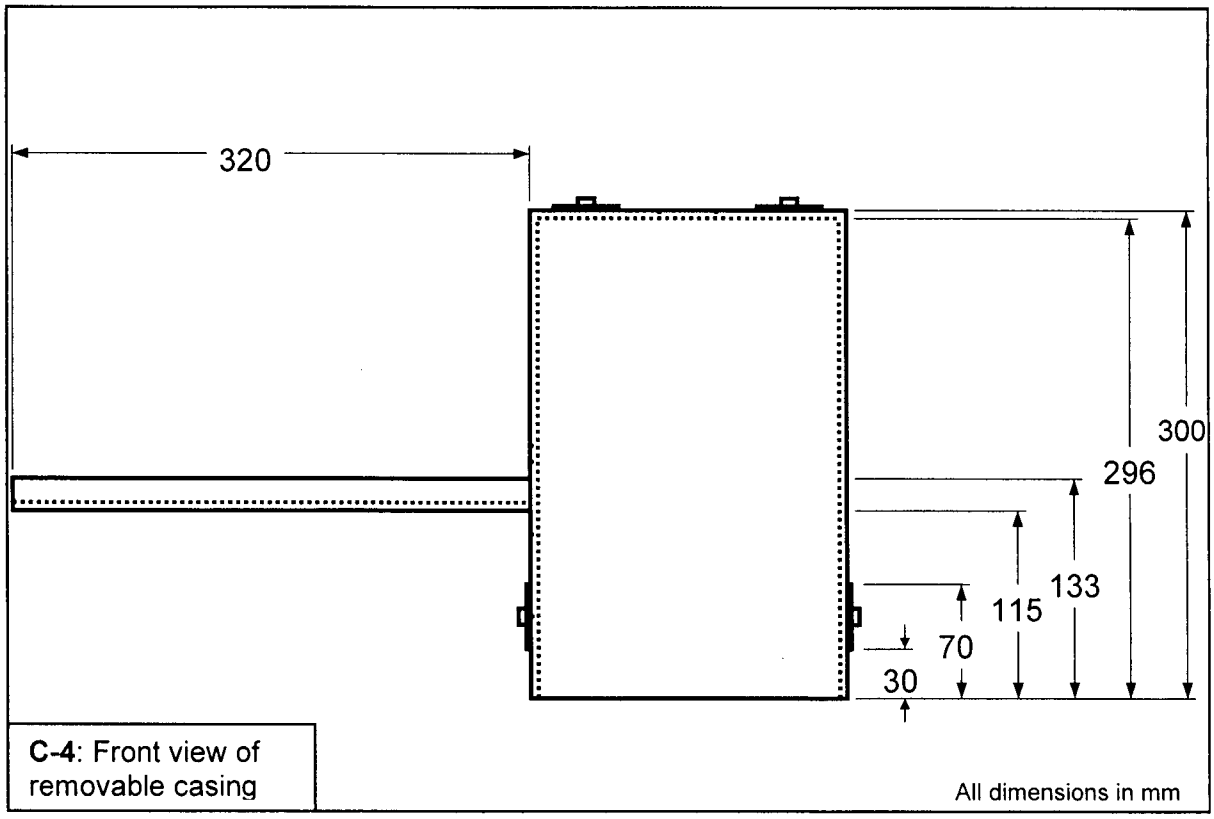

C-4: Front view of removable casing

All dimensions in mm

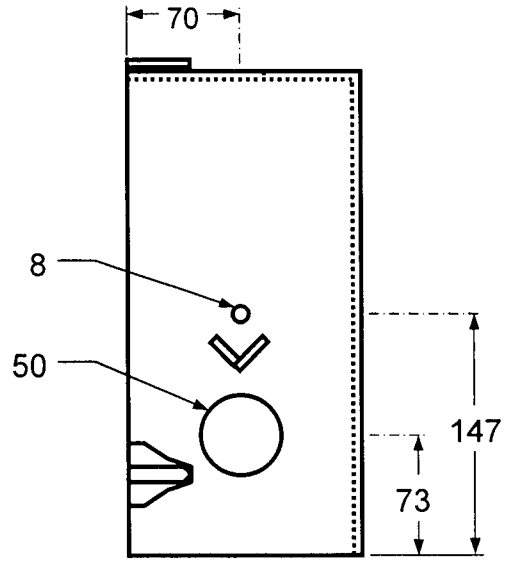

C-5: Left side view of removable casing

All dimensions in mm

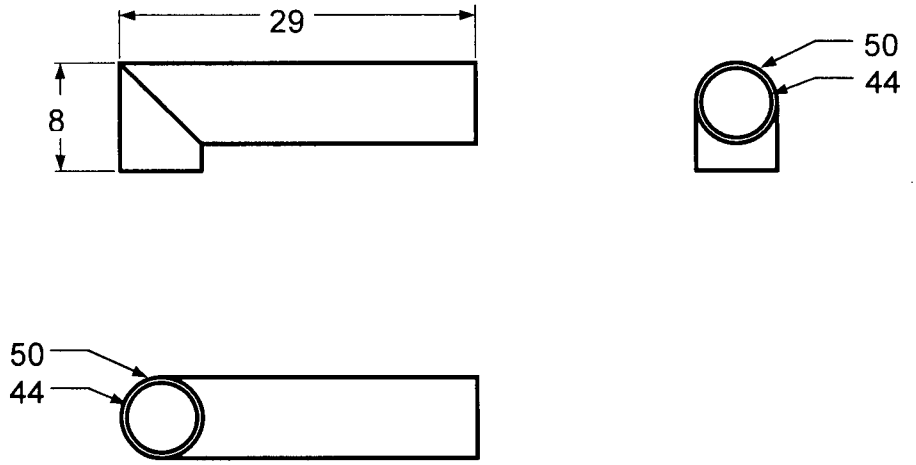

C-6: Connector tube

All dimensions in mm

APPENDIX D: SUMMARY OF STATISTICAL PROCEDURES

The following tables summarize the statistical procedures used for each test reported in the results section.

	Normal Distribution?	Nested Pairs?	Test
Time-to-rupture			
60% Non-Interrupted Creep and Interrupted Creep	No (n too small)	No	Wilcoxon
60% Creep and Fatigue	Yes	No	Student's t-test
30% Creep and Fatigue	Yes	No	Student's t-test
Initial Strain			
60% Creep and Fatigue	Yes	No	Student's t-test
30% Creep and Fatigue	Yes	Yes	Mixed Model
15% Creep and Fatigue	Yes	Yes	Mixed Model
Increase in Strain (0.8 hour)			
60% Creep and Fatigue	No	No	Wilcoxon
30% Creep and Fatigue	Yes	Yes	Mixed Model
15% Creep and Fatigue	Yes	Yes	Mixed Model
Increase in Strain (4.2 hour)			
60% Creep and Fatigue	No	No	Wilcoxon
30% Creep and Fatigue	Yes	Yes	Mixed Model
15% Creep and Fatigue	Yes	Yes	Mixed Model
Increase in Strain (24 hour)			
60% Creep and Fatigue	No	No	Wilcoxon
30% Creep and Fatigue	Yes	Yes	Mixed Model
15% Creep and Fatigue	Yes	Yes	Mixed Model
Increase in Strain (20% Time-to-Rupture)			
60% Non-Interrupted Creep and Interrupted Creep	No (n too small)	No	Wilcoxon
60% Creep and Fatigue	Yes	No	Student's t-test
30% Creep and Fatigue	Yes	No	Student's t-test
Increase in Strain (70% Time-to-Rupture)			
60% Non-Interrupted Creep and Interrupted Creep	No (n too small)	No	Wilcoxon
60% Creep and Fatigue	No	No	Wilcoxon
30% Creep and Fatigue	No	No	Wilcoxon

	Normal Distribution?	Nested Pairs?	Test
Increase in Strain (100% Time-to-Rupture)			
60% Non-Interrupted Creep and Interrupted Creep	No (n too small)	No	Wilcoxon
60% Creep and Fatigue	No	No	Wilcoxon
30% Creep and Fatigue	Yes	No	Student's t-test
15% Creep and Fatigue			
Steady State Strain Rate			
60% Creep and Fatigue	No	No	Wilcoxon
30% Creep and Fatigue	Yes	Yes	Mixed Model
15% Creep and Fatigue			
Strain-at-Rupture	Yes	No	Student's t-test
Initial Modulus			
60% Creep and Fatigue	Yes	No	Student's t-test
30% Creep and Fatigue	Yes	Yes	Mixed Model
15% Creep and Fatigue	Yes	Yes	Mixed Model
Maximum Modulus			
60% Creep and Fatigue	Yes	No	Student's t-test
30% Creep and Fatigue	Yes	Yes	Mixed Model
15% Creep and Fatigue	Yes	Yes	Mixed Model
Modulus Ratio Prior to Rupture			
60% Creep and Fatigue	Yes	No	Student's t-test
30% Creep and Fatigue	Yes	Yes	Mixed Model
Strain to 5 MPa (0% Time-to-Rupture)			
60% Creep and Fatigue	Yes	No	Repeated Measures
30% Creep and Fatigue	Yes	No	Repeated Measures
15% Fatigue	Yes	No	Repeated Measures
Strain to 5 MPa (20% Time-to-Rupture)			
60% Creep and Fatigue	Yes	No	Repeated Measures
30% Creep and Fatigue	Yes	No	Repeated Measures
15% Fatigue	Yes	No	Repeated Measures
Strain to 5 MPa (70% Time-to-Rupture)			
60% Creep and Fatigue	Yes	No	Repeated Measures
30% Creep and Fatigue	Yes	No	Repeated Measures
15% Fatigue	Yes	No	Repeated Measures
Strain At Failure	Yes	Yes	Mixed Model

APPENDIX E: INCREASE IN STRAIN PLOTS

Increase in strain versus time is shown for 60% fatigue (Figure E-1), 60% creep (Figure E-2), 30% fatigue (Figure E-3), 30% creep (Figure E-4), 15% fatigue (Figure E-5), and 15% creep (Figure E-6). The figures are plotted on different time scales to show more detail in each data set.

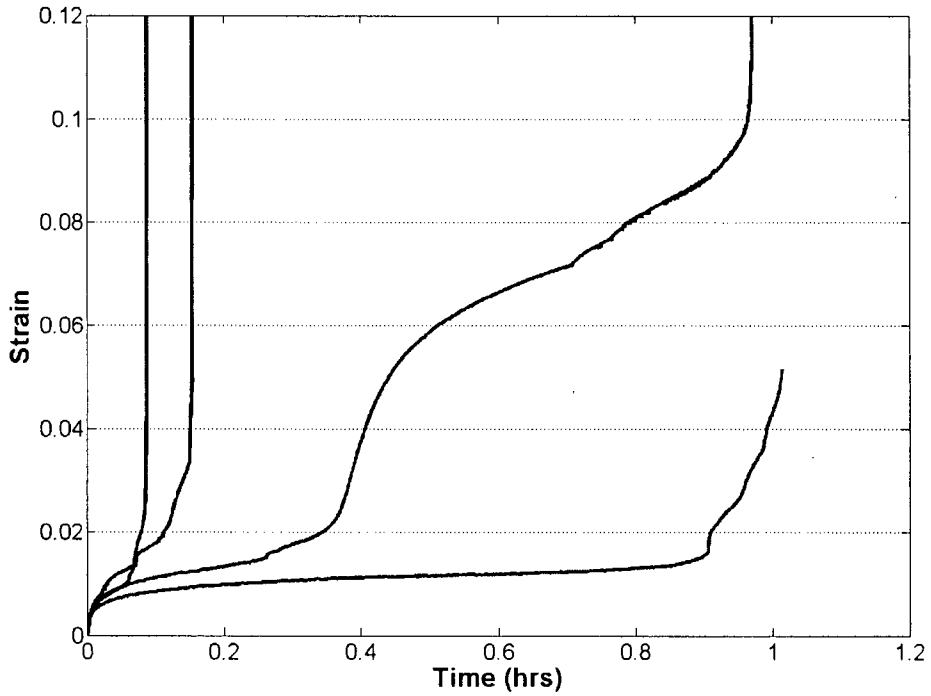

***Figure E-1**: 60% UTS fatigue increase in strain as a function of time.*

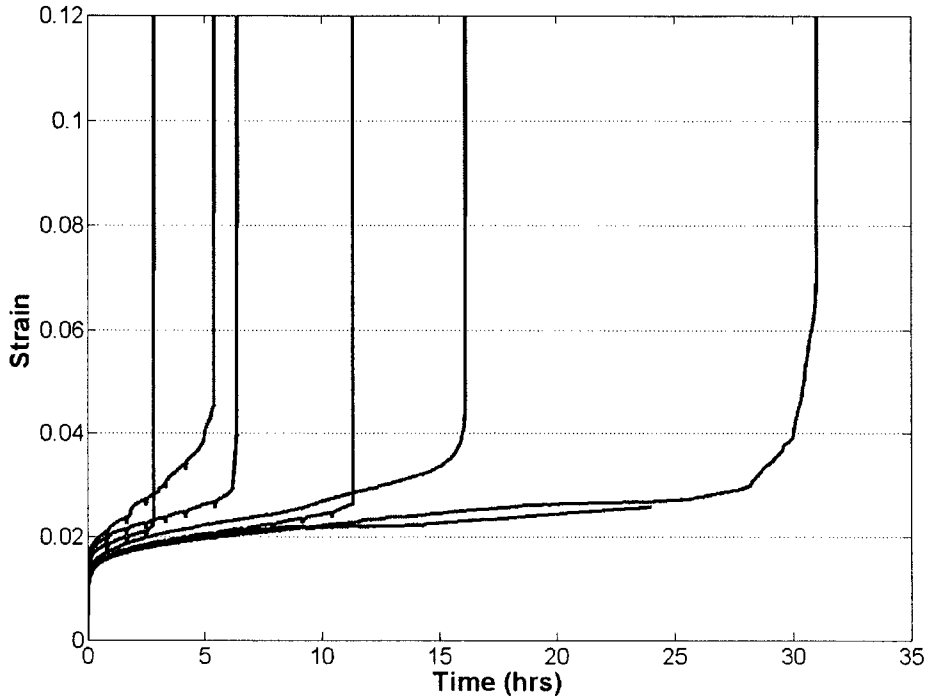

***Figure E-2**: 60% UTS creep increase in strain as a function of time.*

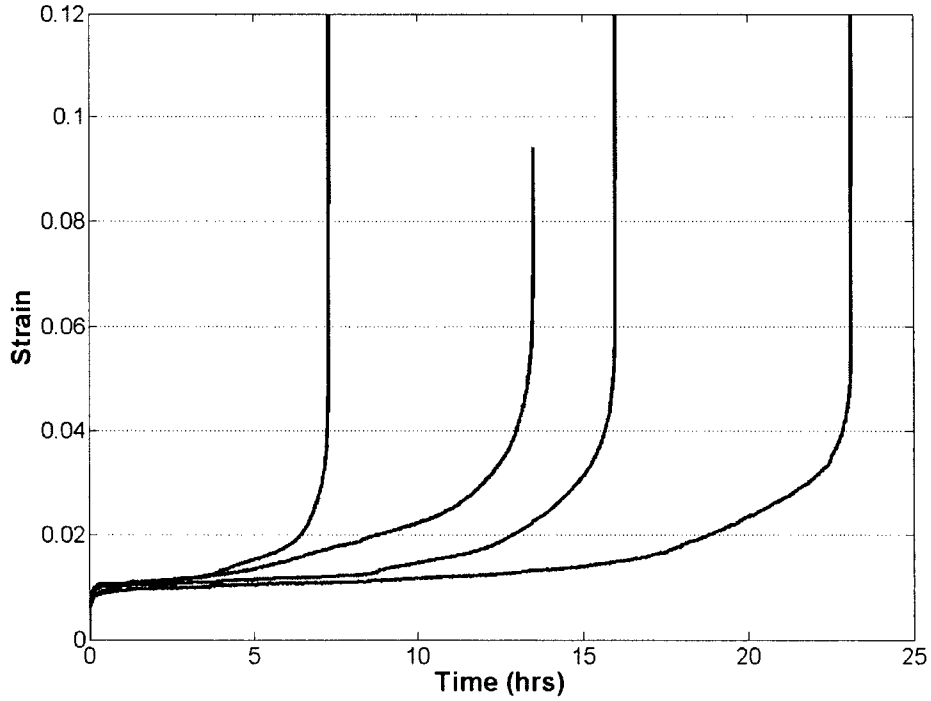

***Figure E-3**: 30% UTS fatigue increase in strain as a function of time.*

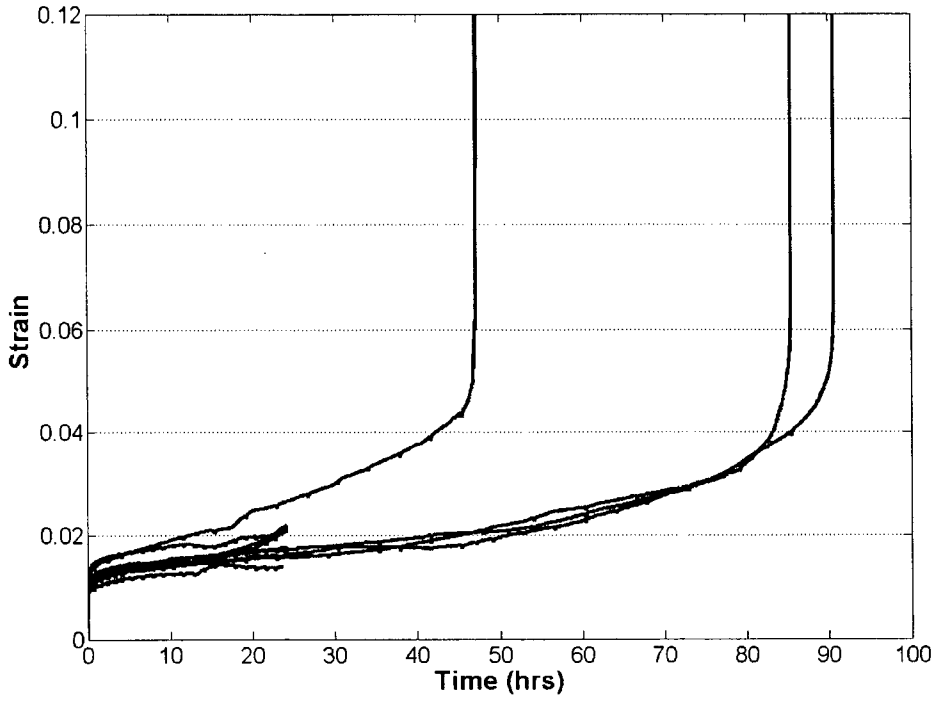

***Figure E-4**: 30% UTS creep increase in strain as a function of time.*

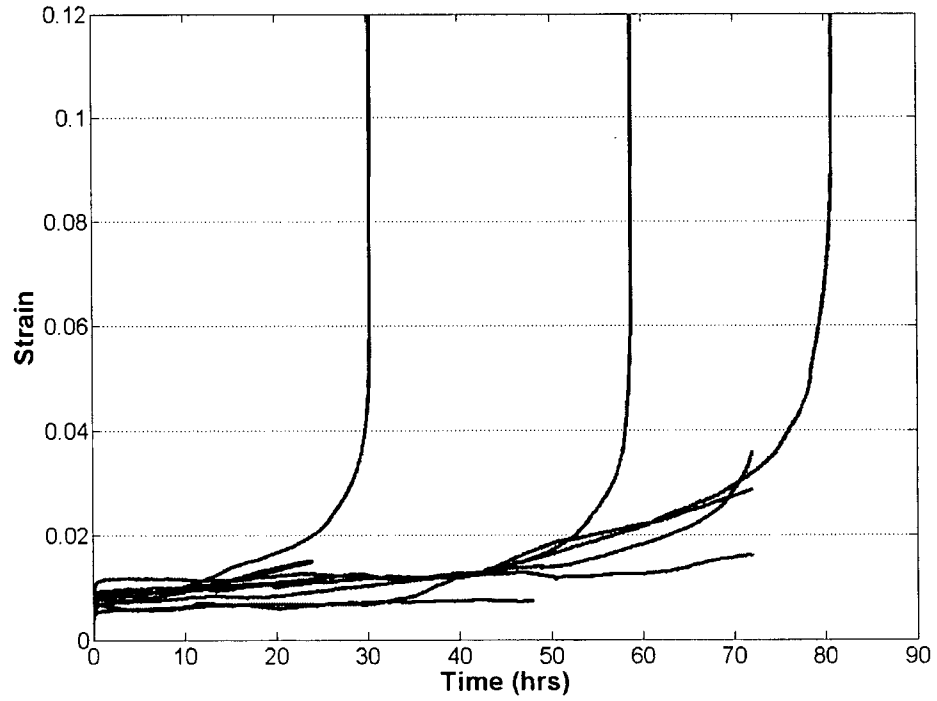

***Figure E-5**: 15% UTS fatigue increase in strain as a function of time.*

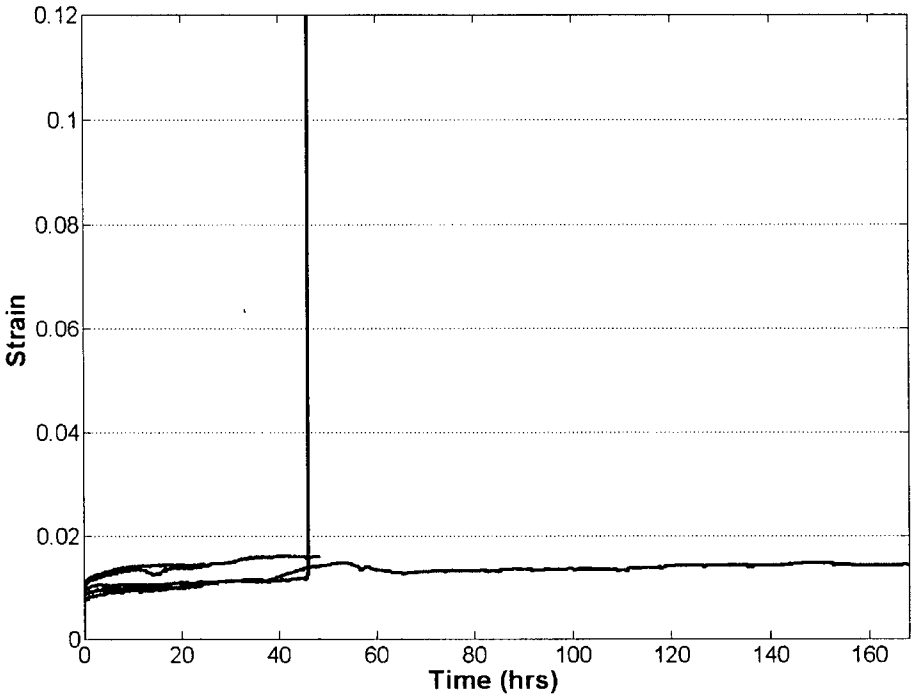

***Figure E-6**: 15% UTS creep increase in strain as a function of time.*

APPENDIX F: DISCONTINUITY DURING 60% UTS FATIGUE

One ligament tested in fatigue at 60% UTS experienced a discontinuity in strain without a corresponding change in stress. The discontinuity may result from a large group of fibres rupturing at the same time. The stress and strain data is shown in Figures F-1 and F-2, respectively.

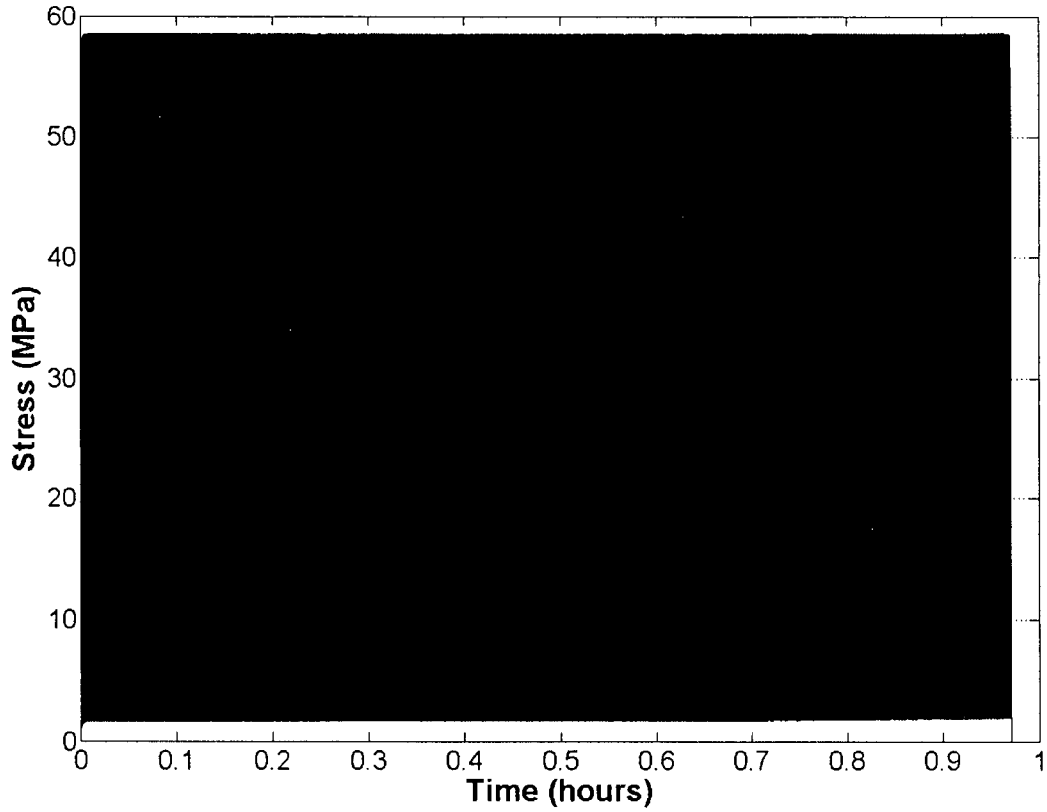

***Figure F-1**: Stress as a function of time*

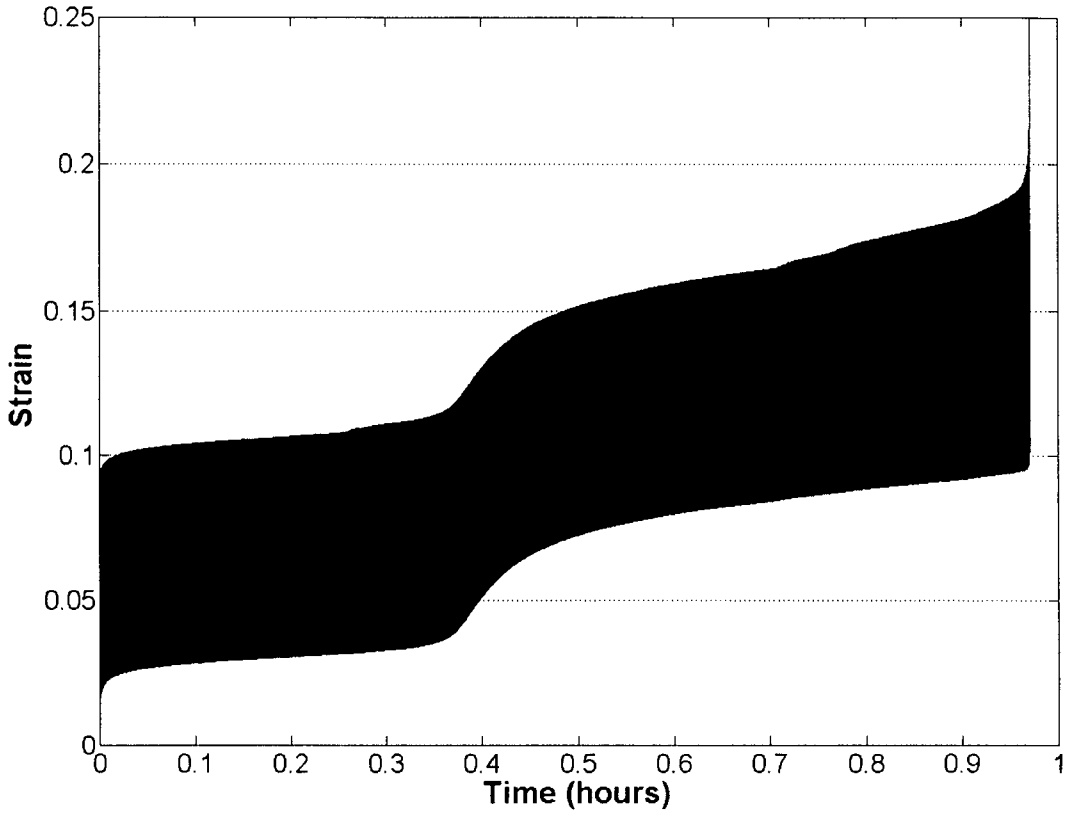

***Figure F-2**: Strain as a function of time showing a discontinuity around 0.35 hours.*

APPENDIX G: EXCLUDED DATA

Five fatigue specimens tested at 60% UTS were excluded from the data set because of equipment loosening. The malfunction resulted in very high strain values. Increase in strain values are plotted in Figure G-1.

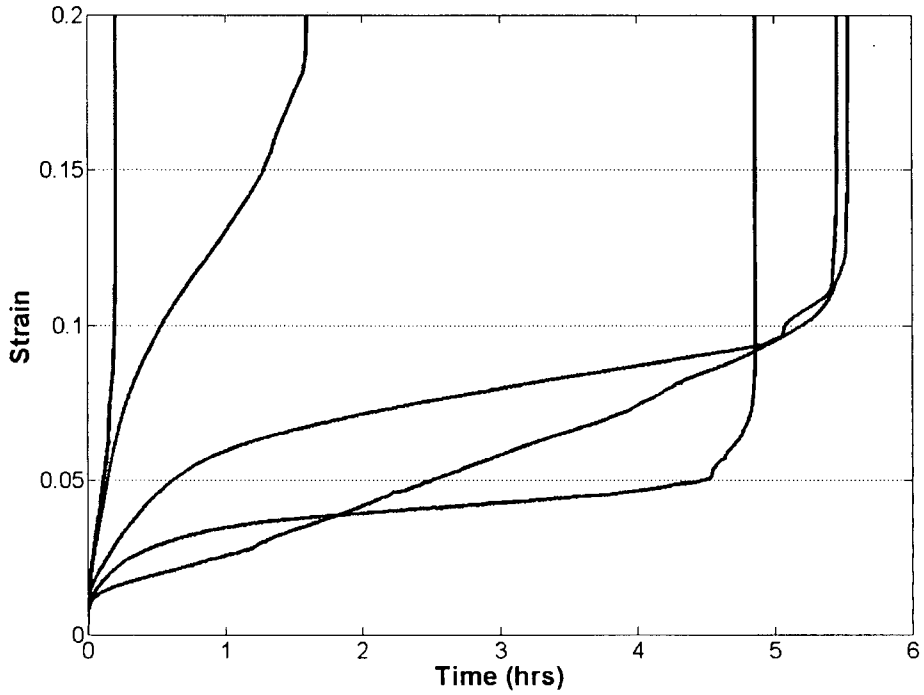

***Figure G-1**: Increase in strain for the excluded 60% UTS fatigue tests.*

APPENDIX H: MODULUS RATIO PLOTS

Modulus ratio versus time is shown for 60% fatigue (Figure H-1), 60% creep (Figure H-2), 30% fatigue (Figure H-3), 30% creep (Figure H-4), 15% fatigue (Figure H-5), and 15% creep (Figure H-6). The figures are plotted on different time scales to show more detail in each data set.

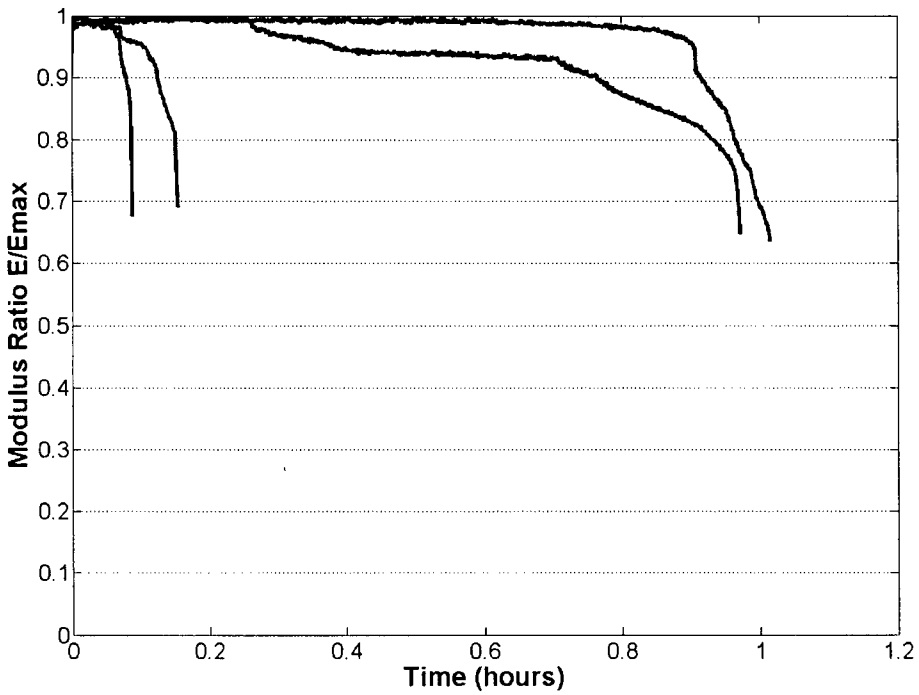

***Figure H-1**: 60% UTS fatigue modulus ratio as a function of time.*

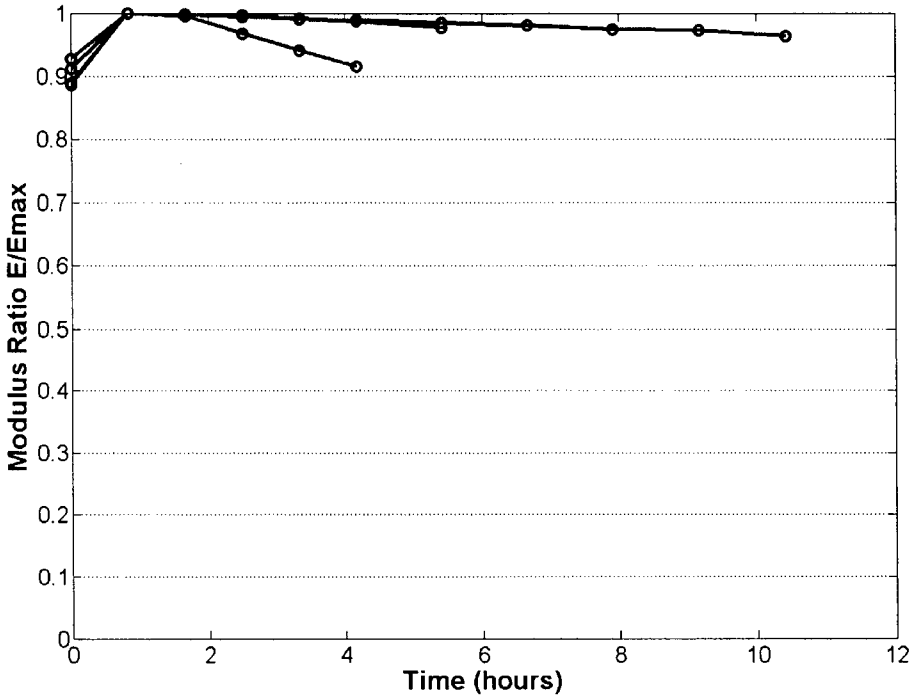

***Figure H-2**: 60% UTS creep modulus ratio as a function of time.*

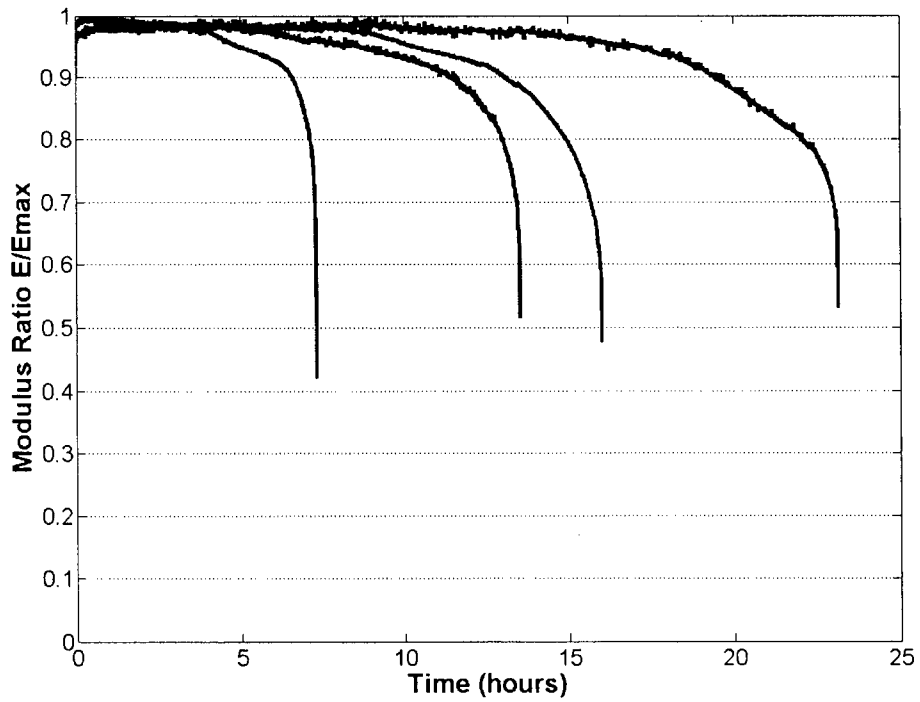

***Figure H-3**: 30% UTS fatigue modulus ratio as a function of time.*

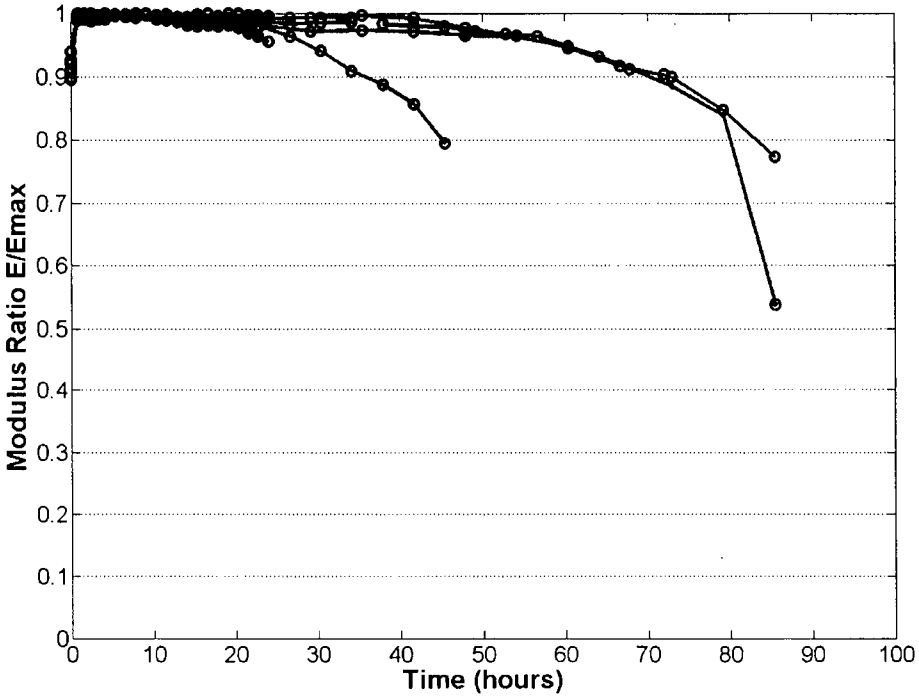

***Figure H-4**: 30% UTS creep modulus ratio as a function of time.*

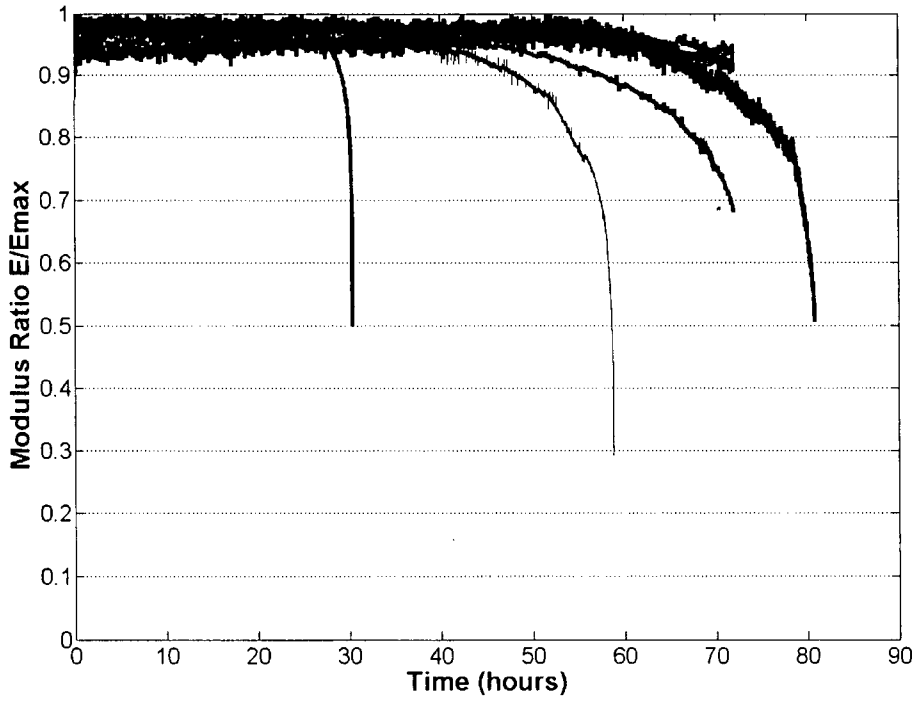

***Figure H-5**: 15% UTS fatigue modulus ratio as a function of time.*

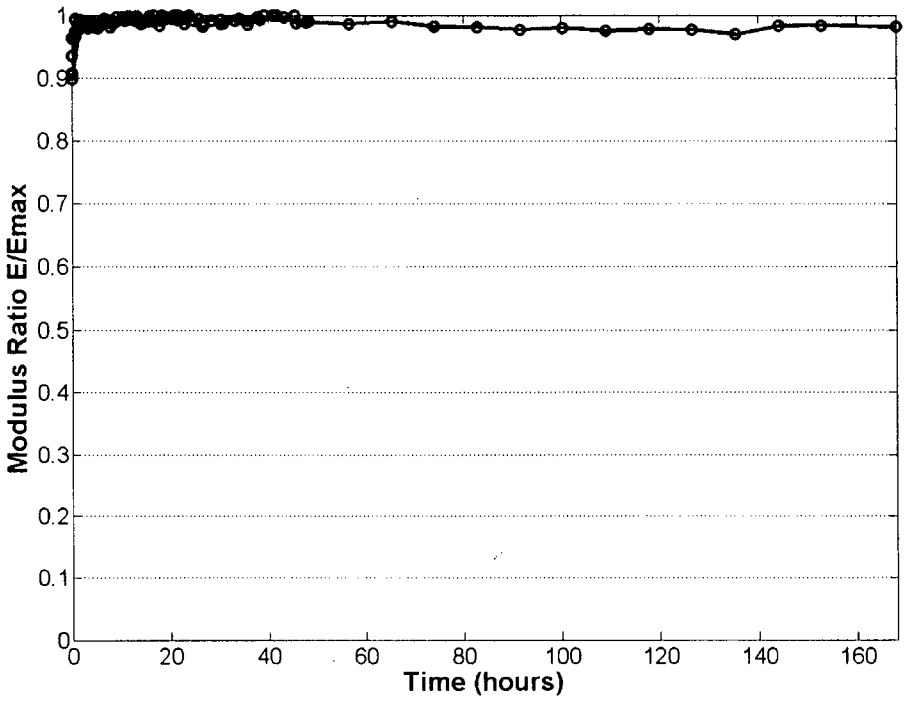

***Figure H-6**: 15% UTS creep modulus ratio as a function of time.*

APPENDIX I: PILOT TESTS

Three additional test where completed to assess the future direction of testing. Two MCLs were tested at 7.5% UTS, one in creep and one in fatigue. Both tests ran for 72 hours without signs of damage.

Another fatigue test was completed at 30% UTS. This test had a frequency of 10 Hz and loading was discontinued after approximately 26 hours of loading.